PNL-3064
UC-78

ThO_2-Based Pellet Fuels—Their Properties, Methods of Fabrication, and Irradiation Performance

A Critical Assessment of the State of the Technology and Recommendations for Further Work

September 1979

Prepared for the U.S. Department of Energy
under Contract EY-76-C-06-1830

Pacific Northwest Laboratory
Operated for the U.S. Department of Energy
by Battelle Memorial Institute

Battelle

PNL-3064

NOTICE

PACIFIC NORTHWEST LABORATORY
operated by
BATTELLE
for the
UNITED STATES DEPARTMENT OF ENERGY
Under Contract EY-76-C-06-1830

Printed in the United States of America
Available from
National Technical Information Service
United States Department of Commerce
5285 Port Royal Road
Springfield, Virginia 22151

Price: Printed Copy $____*; Microfiche $3.00

*Pages	NTIS Selling Price
001-025	$4.00
026-050	$4.50
051-075	$5.25
076-100	$6.00
101-125	$6.50
126-150	$7.25
151-175	$8.00
176-200	$9.00
201-225	$9.25
226-250	$9.50
251-275	$10.75
276-300	$11.00

PNL-3064
UC-78

ThO_2-BASED PELLET FUELS - THEIR PROPERTIES, METHODS OF FABRICATION, AND IRRADIATION PERFORMANCE

A CRITICAL ASSESSMENT OF THE STATE OF THE TECHNOLOGY AND RECOMMENDATIONS FOR FURTHER WORK

SEPTEMBER 1979

by
P. E. Hart
C. W. Griffin
K. A. Hsieh
R. B. Matthews
G. D. White

Prepared for
the U.S. Department of Energy
under Contract EY-76-C-06-1830

Pacific Northwest Laboratory
Richland, Washington 99352

ABSTRACT

This critical assessment of the ThO_2-UO_2 pellet fuel technology was conducted in support of the Fuels Refabrication and Development Program (FRAD). Included in this critical review are the following areas: powder preparation; pellet fabrication; fuel chemical, physical, and mechanical properties; and fuel irradiation performance. The authors identify 1) areas where data are either deficient or lacking and 2) requirements for additional development and experimental work.

CONTENTS

FIGURES

TABLES

ThO_2-BASED PELLET FUELS - THEIR PROPERTIES, METHODS OF FABRICATION, AND IRRADIATION PERFORMANCE

A CRITICAL ASSESSMENT OF THE STATE OF THE TECHNOLOGY AND RECOMMENDATIONS FOR FURTHER WORK

1.0 INTRODUCTION

Since early 1977, a renewed interest has developed in ThO_2-based fuel cycles for light water reactors. These fuel cycles are of interest because of the need for development of a proliferation-resistant nuclear technology.

In this light, this critical assessment of ThO_2 pellet fuel technology was sponsored by the Fuels Refabrication and Development (FRAD) Program to serve as a technical basis for defining a development program that will ultimately lead to licensable, proliferation-resistant fuel form(s). Included in this assessment are powder production and processing, pellet fabrication and sintering, fuel mechanical, physical, and chemical properties, and irradiation performance.

Much of the information reported in the literature relative to these areas of interest was generated 10 to 20 years ago. While fuel property data have been assembled previously, recent assessments relative to ThO_2-based fuel fabrication technology and irradiation performance have not been performed. The purpose of the present document is to critically assess these areas and to define deficiencies in the technology base.

Of primary interest to the FRAD program are ThO_2 fuels that contain 20 to 30 wt% UO_2. Prior experience with ThO_2-based fuels is primarily limited to those systems that contain less than 10 wt% UO_2. Therefore either through extrapolation or by additional experimental work, the ThO_2-based fuel technology must be extended to compositions containing more than 10 wt% UO_2. Prior experience with powder processing and fuel fabrication will be judged in

terms of establishing a fuel processing technology that is amenable to remote fuel refabrication in hot cell facilities. On this basis, the appropriateness of novel processing operations, such as freeze-drying of powders, which may replace more commonly used processes like precipitation, will be analyzed in terms of remote operations.

This review does not cite all references dealing with ThO_2 fuels. The references cited here are illustrative of the type of work that has been conducted with ThO_2 fuels.

Some pages of this report are marked in the outside margin with a dot array to call attention to the most important summaries and conclusions.

2.0 PRODUCTION OF ThO_2-BASED FUELS

This report section reviews the following topics: the occurrence and beneficiation of thorium-bearing ores, the production of ThO_2 powder, and the fabrication of ThO_2-based fuel pellets. The state of ThO_2 pellet production technology is reviewed in terms of the FRAD goal of developing a proliferation-resistant, remote refabrication process.

The discussion identifies some processes that have not previously been used in the fabrication of ThO_2-based fuel pellets but which may aid in reaching the FRAD refabrication goal.

2.1 THORIUM OCCURRENCE AND BENEFICIATION

Overall knowledge of world thorium resources is considerably less than the knowledge of uranium resources. Reasonably assured resources recoverable at costs less than \$30/lb ThO_2 are estimated at 630,000 metric tons (Foster 1978, p. 177). In the United States, low-grade resources such as the Conway Granites of New Hampshire contain an estimated 15 million metric tons of thorium recoverable at \$60/lb ThO_2 (Young 1979). Worldwide, many locations have been identified as having the potential to contain thorium. Few attempts, however, have been made to develop estimates of the world's undiscovered resources (Foster 1978).

There are four major types of thorium deposits: 1) veins and lodes, 2) residual deposits and placers, 3) sedimentary deposits, and 4) igneous metamorphic concentrations (i.e., carbonatite fenite, alkalic dikes, plugs and sills, granites, and pegmatites). Eighty-seven percent of the total thorium reserves and probable potential reserves are vein deposits location in Lemhi Pass, Idaho and the Wet Mountains of Colorado (Staatz 1978, p. 109).

Since vein deposits are the highest-grade resource of thorium in the United States, any large-scale production of thorium would result in their exploitation. Mining and beneficiation facilities are presently nonexistent. However, conceptual studies indicate the deposits would be mined by underground methods and submitted directly to a dilute sulfuric acid leach (Young 1980).

Monazite from placers is currently the world's primary source of thorium. The deposits are mined by suction dredging or excavation and concentrated by gravity and magnetic separation. The resulting monazite concentrate is then processed by digestion with caustic soda or sulfuric acid and step-wise precipitation of thorium and rare earths using ammonium hydroxide (Enderlin 1978).

After thorium has been extracted and concentrated by a method appropriate to the source of thorium, the concentrate is subjected to solvent extraction to obtain a purified thorium nitrate solution. The nitrate is then converted to the oxide, thoria, which can be used in the production of thoria fuel pellets. Processes for conversion of the thorium nitrate solution to a thoria powder are discussed in the following section.

2.2 CONVERSION OF THORIUM NITRATE TO THORIUM OXIDE POWDER

Since the ultimate goal of the Fuel Refabrication and Development Program is the remote refabrication of reprocessed spent fuel, a fabrication process must be developed that requires the fewest operations possible and the simplest and most easily maintained equipment. In the fabrication of fuel pellets from a powder, the most important task in achieving this goal is the production of powder with properties that will minimize the difficulty of fabrication and sintering operations. The ideal oxide powder production process would convert the nitrate directly to a dustless, free-flowing, and highly sinterable press feed. If the initial oxide product is unsuitable for use as press feed, a simple and remotely operable process of feed preparation will be required. The oxide production process will also need to be adaptable to remote operation and thus will require the same operational simplicity as the pellet fabrication.

Five thoria (ThO_2) powder production methods are reported in the literature:

1) thermal decomposition of oxalate precipitate
2) formation and comminution of dried sol-gel shards
3) thermal decomposition of hydroxide precipitate
4) hydrothermal denitration of the nitrate solution
5) thermal decomposition of the nitrate solution in a fluidized bed.

All of these production methods have one thing in common: they convert thorium nitrate solution into ThO_2 powder. Of the five methods, only the oxalate precipitation process has been used extensively for commercial ThO_2 production. The thermal decomposition of the hydroxide precipitate and the hydrothermal denitration of the nitrate solution were used primarily in the preparation of an oxide sol for the sol-gel process.

Two other oxide production methods described in the literature are worthy of consideration for producing ThO_2; both methods produce oxides by direct conversion of a salt solution:

6) the freeze-dry or cryochemical process (used primarily for the production of alumina and ferrite powders)

7) the evaporative decomposition of solutions or "spray calcine" process (used for the production of alumina, ferrite, and spinel powders).

Both processes could be adapted to the direct conversion of thorium nitrate solution to the oxide. The following sections discuss the various thorium nitrate conversion processes.

2.2.1 Thorium Oxalate Precipitation Process

The oxalate precipitation process consists of the following operations:

1) precipitation of thorium oxalate by reaction of the nitrate with oxalic acid

2) digestion

3) filtration

4) thermal decomposition of the thorium oxalate to form the oxide.

The literature includes numerous reports on fabrication studies of oxalate-derived ThO_2, both singly and combined with urania; however, these studies did not include in their experimental design the precipitation and decomposition of the oxalate. Investigations of thorium oxalate precipitation reported in the literature have been directed towards developing oxide powder properties related to catalysis or slurry formation, the latter as part of the development of the slurry blanket for the Homogeneous Reactor Experiment at Oak Ridge National Laboratory (Pearson et al. 1958).

Control parameters for the process, all of which can affect the physical properties of the product powder, are:

- molarity of the reactants
- H^+ molarity of the nitrate solution
- rate and sequence of combining the reactants
- reaction temperature
- degree of agitation during precipitation
- digestion time
- decomposition temperature profile versus time
- decomposition atmosphere.

Oxide powder properties have been found to differ, depending on various control parameters during the main steps of precipitation and decomposition. Only one investigation of this process, Kantan et al. (1958) related precipitation and decomposition parameters for oxalate to the sinterability of the powder produced. They showed that the precipitation and decomposition temperatures had a great influence on the final sintered density of oxalate-derived ThO_2. With a range of precipitation temperatures from 1° to 60°C and a range of decomposition temperatures from 800°C to 1200°C, the density of the sintered product varied from 86.7 to 94.7% of theoretical density. The maximum density of 94.7% was accomplished using oxide powder derived from oxalate precipitated at 20°C and decomposed at 900°C; compaction pressure was 414 MPa (60,000 psi) for powder sintered at 1500°C in air.

Effects of Precipitation Parameters on Powder Properties

Breysse et al. (1965) investigated the effect of various oxalate precipitation parameters on the surface area of the final oxide powder. Table 1 shows the Breysse data, relating several precipitation parameters to oxide powder surface area. The range of surface areas produced by the variation of a specific precipitation parameter suggests the significance of the parameter with respect to surface area.

Allred and co-workers (1957) determined that oxide powder particles, which are relics of the original oxalate particles, increased in size with increasing oxalate precipitation temperature. The particles increased from 1-μm cubes at

TABLE 1. Effects of Oxalate Precipitation Parameters on ThO_2 Powder Surface Area (oxalate decomposed at 350°C)

Precipitation Parameter	Surface Area, m^2/g
pH of initial nitrate solution	
2.2 to 0.7	33 to 36
Rate of addition	
2.5 mL/min to 0.833 mL/min	12 to 25
Sequence of addition	
$H_2C_2O_4$ to $Th(NO_3)_4$ (direct strike)	40
$Th(NO_3)_4$ to $H_2C_2O_4$ (reverse strike)	34
Concentration of $Th(NO_3)_4$ solution	
1.0 M (570 g nitrate/liter)	40
0.1 M	27
0.2 M	18
Excess of oxalic acid	
0	28
20%	24
100%	19
Precipitation temperature	
34°C	17
75°C	24
boiling	33
Time of digestion	
0 h	24
1 h	28
4 h	30

a precipitation temperature of 10°C to platelets ranging from 4 to 7 μm at 100°C. The cubes had an edge-to-depth ratio of 3:2, whereas the platelets had a ratio of 6:1.

Effects of Decomposition Parameters on Powder Properties

The thermal decomposition mechanism for thorium oxalate has been extensively investigated (Becket and Winfield 1951; D'Eye and Sellman 1955;

Wendlandt et al. 1961; Moorehead and McCartney 1976). The amount of water, both chemically combined and adsorbed, varies depending upon the age and storage condition of the oxalate. However, upon heating in air the oxalate loses water and forms the dihydrate below 200°C; the dihydrate decomposes at 270°C to form the anhydrous oxalate. D'Eye and Sellman (1955) reported that their investigation showed that the anhydrous thorium oxalate decomposed to thoria either simultaneously by two different reactions or solely by the carbonate route:

$$Th(C_2O_4)_2 \xrightarrow{330^\circ C} \begin{cases} ThO_2 + 2CO_2 + 2CO \\ Th(CO_3)_2 + 2CO \rightarrow ThO_2 + 2CO_2 \end{cases}$$

There was also evidence of CO disproportionating to form carbon and CO_2 in ThO_2 formed below 400°C.

Allred et al. (1957) found that increasing the oxalate decomposition temperature from 400°C to 900°C had practically no effect on the size or shape of the oxide particles for powders from the same precipitation batch. However, ThO_2 crystallite size was found to increase with increasing decomposition temperature in all cases, as shown in Figure 1. At a decomposition temperature of 900°C, the crystallite size was proportional to the final ThO_2 particle size, which increased with precipation temperature.

The effect of decomposition temperature on oxide powder surface area is shown in Figure 2 for oxalates precipitated at four different temperatures. Overall, powder surface area decreased with increasing decomposition temperature. Maximum rates of change in surface area occurred between 500° and 700°C.

With a decomposition temperature of 350°C, the results of Breysse et al. (1965) showed that the larger the particle size of the ThO_2 powder, the larger the surface area. Although this result seems a paradox, it is compatible with the oxalate decomposition work done by Becket and Winfield (1951) in which they showed the larger ThO_2 particles to be composed of laminae of oxide crystallites

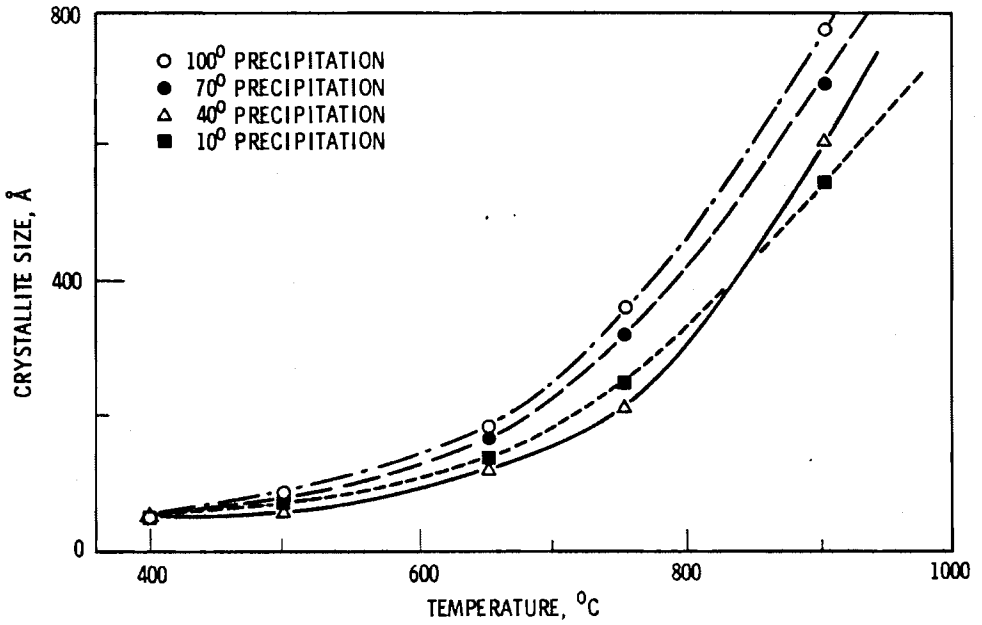

FIGURE 1. Effect of Decomposition Temperature on the Crystallite Size of ThO_2 for Four Precipation Temperatures

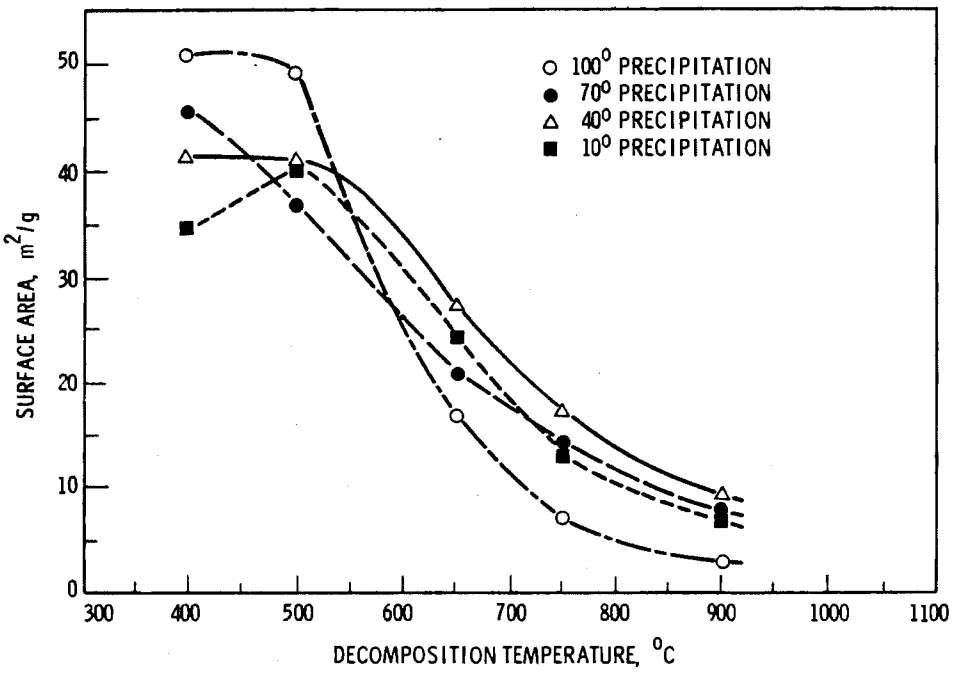

FIGURE 2. Effect of Decomposition Temperature on the Surface Area of ThO_2 Powder

with a central hole whose surface is not smooth like the exterior but is broken by very thin projecting laminae. In the work of Allred et al. (1957), the crystallite sizes measured by x-ray diffraction line broadening agreed closely with the particle sizes estimated from the specific surface areas. The interpretation of the data is that the particles are porous and that the surface area measured by the B.E.T. method is primarily the area of internal crystallite surfaces.

Foex (1949) investigated the rate of change of particle density as a function of decomposition temperature for thoria derived from the decomposition of the hydrous oxide. He observed that no sintering between particles occurred below 1000°C and from this inferred that crystal growth occurred only among closely joined crystallites. This is in accord with the low heat of activation for crystal growth, 4596 J/g-mole, determined by Allred et al. (1957) for ThO_2 derived from the oxalate.

Evaluation of the Thorium Oxalate Precipitation Process

For a more complete characterization of the oxalate precipitation process, parameters of oxalate precipitation and decomposition should be correlated with not only ThO_2 pellet density, but also ease of powder fabrication and sintered pellet microstructure. Although the as-received powders produced by this process have had poor fabrication and sintering properties, it may be possible through process modification to produce powders which do not require milling before pellet fabrication.

Development of the oxalate precipitation process as a completely remote operation is certainly feasible. A semi-remote facility for the production of plutonium oxide by the oxalate precipitation process (Crocker and Hopkins 1963) has been operated for many years in Building 234-5, 200W Area, Hanford. However, use of the process in a remote facility would depend upon the successful modification of the process to produce ThO_2 powder with excellent fabrication and sintering properties.

Depending on the recycle process used, coprecipitation of the mixed oxalates to form mixed ThO_2-UO_2 powders may be desired. Therefore, coprecipitation work should be done as part of the oxalate precipitation development.

2.2.2 Sol-Gel Process

The sol-gel process has been used for the fabrication of fuel particles for gas-cooled reactors and for vibratory compaction into fuel rods for LWRs. As discussed in detail in section 2.2.3, the sol-gel process has also been considered as a conversion step to prepare feed material for pelletized fuel. A recent review by Lackey and Selle (1978) describes the various sol-gel processes that have been developed for ThO_2, UO_2, PuO_2, and mixed-oxide sphere production. The reviewers note only limited production experience with the high U/Th ratios needed for denatured fuel cycles. To date, the sol-gel processes have been designed to produce ultra-high-density spheres; modifications to these processes will be needed to produce spheres with high UO_2 content and with properties suitable for fabricating pellet fuels.

2.2.3 Freeze-Dry Process

The freeze-dry method of producing an oxide powder directly from the salt solution shows potential for the production of mixed ThO_2-UO_2 powders with controlled physical and chemical properties. The primary investigative work on this process has been done at Bell Laboratory on the production of aluminum oxide powder from aluminum sulfate solution for use in the fabrication of alumina substrates with carefully controlled microstructures (Johnson and Schnettler 1970; Jaeger and Miller 1974). This application requires careful control of the powder production process, and the freeze-dry process has provided the necessary degree of control.

The freeze-drying process for powder production requires four basic operations: mixing of salt solutions, flash freezing of the solution, sublimation of the ice phase, and decomposition of the anhydrous salt. Solution chemistry assures mixing of two or more salt solutions on an atomic scale but does require the components to be mutually soluble salts. The mixed nitrates of thorium and uranium (iv) would be ideally suited for producing powders composed of mixed ThO_2-UO_2 crystallites by the freeze-dry process. Absolute control of the composition would be exercised since no material is added and no material is lost in the process. The composition of the final product would be that of the starting mixture.

The freezing and sublimation operations can best be explained using a pressure-temperature diagram. Figure 3 is an equilibrium diagram showing phase regions as a function of pressure and temperature. At state A, the initially prepared solution is present in liquid form. The solution is flash-frozen by spraying the salt solution into an immiscible cryogenic liquid, thereby taking the solution from state A to state B.

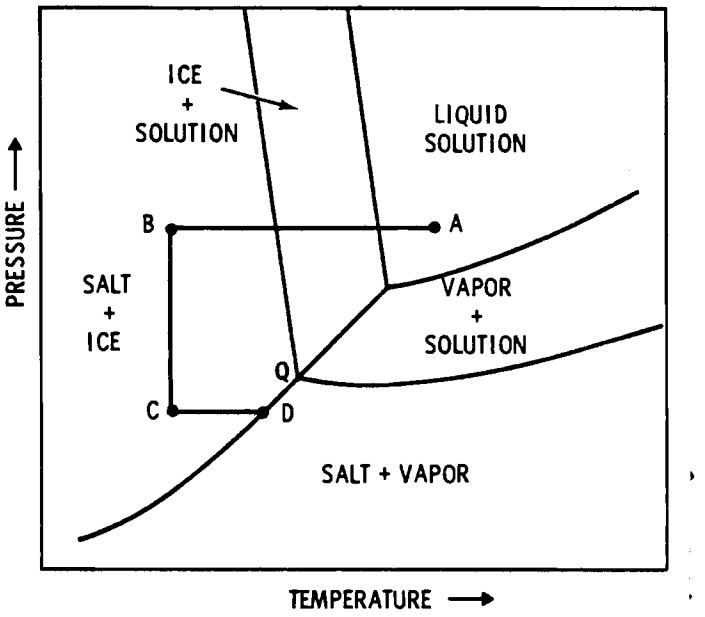

FIGURE 3. Pressure-Temperature Diagram Showing the Freeze-Drying Cycle

The solution freezes in the form of microspheres. The frozen microspheres, separated from the cryogenic liquid, are placed in a vacuum chamber, and the pressure is reduced in the transition from state B to state C below the quadruple point, Q. The frozen microspheres may now be heated to state D, where the ice sublimes, leaving the anhydrous salt. To greatly accelerate the process, the water vapor is condensed out of the vacuum system continuously.

The anhydrous salt may now be heated in air or other suitable atmospheres to form the oxide powder. The temperature, time, and atmosphere are chosen to produce complete decomposition of the salt, but at the same time to leave a residual oxide of high reactivity and sinterability.

The process for making an oxide powder by the freeze-drying method contains six positive control parameters for determining the physical properties of the powder:

- nozzle orifice diameter for spraying solution
- feed rate of solution through orifice
- temperature of cryogenic liquid
- molarity of the salt solution
- decomposition temperature profile versus time
- decomposition atmosphere

The first four parameters determine the microsphere sizes and density and the crystallite size of the salt. The last two parameters determine the oxide surface area and crystallite size during decomposition of the salt.

Freeze-dried microspheres of aluminum oxide and ferric oxide have been characterized with respect to crystallite size and aggregate structure (Johnson and Schnettler 1970). The crystallites nucleated and grew in the form of chainlike aggregates whose orientation was determined by the ice structure formed during the freezing of the solution; in these instances the chains were oriented radially. The crystallite size was relatively uniform and could be controlled over an order of magnitude by proper decomposition heat treatment. For alumina crystallites the size varied from less than 140 Å (γ-Al_2O_3) at a decomposition temperature of 860°C to 1000 Å (α-Al_2O_3) for alumina formed at 1200°C (Johnson and Schnettler 1970). After calcination, the spherical particles were free-flowing and dust-free. The radial porosity was impregnated with binder-lubricant, thus preparing a free-flowing press feed which was pressed into shapes as required.

In sintering studies of freeze-dried alumina powders, isostatically pressed specimens containing up to 0.65 wt% magnesia were heated at 1700°C for 1 hour in a dynamic wet hydrogen atmosphere (Kim and Monforte 1971). The sulfate precursor had been calcined at 1100°C and 1400°C for 2 hours in air. At magnesia additions of 0.25 wt%, specimens attained a density 99.9% of theoretical with grain sizes ranging from 2 to 10 μm.

Evaluation of the Freeze-Dry Process

There are two aspects of the freeze-dry process that make it an attractive candidate for remote operation:

- The technology is already well developed with highly reliable compressor and vacuum pumping systems.
- The powder product is granular, requiring only a small addition of binder/lubricant to become a press feed.

Mechanization of the freeze-dry process for production of press feed should not be difficult. If freeze-dried actinide oxide powders behave in a manner similar to freeze-dried alumina and ferrite powders, they should be highly sinterable and thus, amenable to a simple fabrication process.

2.2.4 Spray Calcine Process

The spray calcine process is the direct thermal conversion of a salt solution to an oxide powder by spraying the solution into a hot furnace with a collector at the bottom; it is also referred to as evaporative decomposition of solution. The process has been used in the laboratory (Roy et al. 1977; O'Holleran et al. 1978) and to a limited extent industrially (Ruthner 1973) to prepare reactive ceramic powders: MgO, Al_2O_3, Fe_2O_3, $MgAl_2O_4$, $MgCr_2O_4$, and $CaAl_2O_4$. Recently, the process has been used at the Pacific Northwest Laboratory (Bonner et al. 1976) to prepare oxide powder from solutions containing salts of nuclear waste elements for inclusion in the formulation and production of glass for the nuclear waste vitrification program. Actinide oxide powders, both singly and mixed, could be prepared in a similar manner using actinide nitrate solutions as feed.

The spray calcine process is uncomplicated and requires rather simple equipment. A laboratory-size conversion unit as described by Roy et al. (1977) consisted of a vertical, two heat-zone furnace with an atomizer unit mounted on top to introduce the salt solution into the heat zone as a fine mist mixed with air.

This apparatus was used to study the production of powders of Al_2O_3, Fe_2O_3, and $CaAl_2O_4$ using the nitrate solutions as feed. Powders had average particle

sizes from 0.1 μm to 10 μm when the feed solution concentration was varied from 0.05 M to saturation, respectively, at constant air-jet pressure 2 MPa (15 psi), feed rate (4 mL/min), and temperature (900°C). High air-jet pressure caused turbulence that resulted in particle agglomeration. The powder collection method was considered inefficient, and the apparatus was subsequently equipped with an electrostatic precipitator for more efficient powder collection.

Evaluation of the Spray Calcine Process

Conversion of the spray calcine process to a completely remote operation would require some highly creative engineering. A closed system would be required with provisions for recovering the very fine powder particles from the exhaust. The system must be maintained remotely, also. Under the most favorable conditions, the control of a production-size system for producing ceramic-grade oxide power would be difficult. Remote operation would not make it easier. Therefore, prospects for producing oxide powder remotely using the spray calcine process are not considered promising.

2.2.5 CONVERSION PROCESSES SUMMARY

Several processes to convert thorium nitrate to ThO_2 are described in the process literature. The two principal processes are the thorium oxalate precipitation process and the sol-gel process, which have been discussed here in detail. Also included in this discussion were two processes for oxide production, freeze drying and spray calcining, which have not been used to produce thorium oxide. Each process was evaluated with respect to its adaptability to remote operation and with respect to the ease of fabrication of pellets from the product oxide. Of the processes reviewed, the sol-gel and freeze-dry processes are judged to have the most potential for remote operation development. This conclusion is based upon the desirability of producing a granular oxide product, rather than a powder which would require granulation. Both the sol-gel and freeze-dry processes may be used to produce spherical particles that are free-flowing. If the particles can be produced having the necessary compactibility and sinterability, the oxide product would make an excellent press feed. These desirable oxide properties would permit the use of simplified pellet fabrication operations in a remotely operated facility.

2.3 PELLET FUEL FABRICATION

The ultimate goal of the FRAD program is to develop pellet fuel refabrication processes that can be used in a remotely operated facility. The ThO_2-based pellet fuels under consideration in the FRAD program will contain more than 20 wt% UO_2. Past experience with the fabrication of ThO_2-based fuels has been with hands-on operations largely limited to compositions containing less than 10 wt% UO_2. Early fabrication flow sheets included steps such as extensive milling, binder additions, and lengthy sintering cycles, all of which would be undesirable in a remotely operated facility. Nevertheless, past experience can serve as a basis for defining the direction of future ThO_2-based pellet fuel development.

Experience in the development of UO_2 pellet fuels is also pertinent to the development of ThO_2 fuel technology. The UO_2 fabrication technology in the 1950s and early 1960s required wet powder processing with the addition of organic binders at levels of 1 to 2 wt%. With the development of free-flowing UO_2 powders, pellet production was greatly simplified by the elimination of wet binder addition, powder drying, and binder removal steps. The ThO_2 fabrication technology of today is much like the UO_2 technology of 10 to 20 years ago and is not amenable to fuel fabrication in a remotely operated facility. As with UO_2 fuels, the key to the development of an acceptable ThO_2-based fuel technology is the production of a free-flowing, highly sinterable ThO_2 powder. The powder when mixed with UO_2 must result in a homogeneous fuel with a theoretical density of 92 to 95%.

In the following discussion, major ThO_2 and ThO_2-UO_2 pellet fabrication campaigns and laboratory-scale studies are described and assessed from the standpoint of simplifying the fabrication technology for ThO_2-based fuels. Advances in UO_2 fabrication technology will be cited when they may aid in defining future ThO_2 fuel development work.

2.3.1 Major ThO_2 and ThO_2-UO_2 Pellet Fabrication Experience

Major ThO_2 and ThO_2-UO_2 pellet fuel fabrication campaigns were carried out in the late 1950s and early 1970s. Two of the larger efforts were

conducted by Nuclear Materials and Equipment Corporation (NUMEC) and the Bettis Atomic Power Laboratory. The Bettis work culminated in a mixed ThO_2-UO_2 core loading for the Shippingport Light Water Breeding Reactor (LWBR). Other major efforts included the fabrication of ThO_2-UO_2 core loadings for the Borax IV, Elk River, and Indian Point reactors.

ThO_2 Experience

In 1965 NUMEC fabricated 13,000 kg of ThO_2 pellets for a critical mass facility (Beltram et al. 1965). The NUMEC flow sheet used the oxalate precipitation process to convert thorium nitrate to ThO_2. The oxalate precipitate was calcined at 800 to 900°C to achieve a specified residual carbon impurity level of less than 300 ppm in the ThO_2 powder. An attempt to use a dry binderless method for pellet fabrication was unsuccessful because of excessive pellet cracking. Wet binder additions of 1-, 2-, 3-, and 4-wt% Carbowax 6000® resulted in satisfactory pellets. In addition, 0.2-wt% Sterotex® was dry blended with the powder as a lubricant. Although various pretreatments for binder removal were investigated, the binder was found to be satisfactorily removed from the pellets during the normal sintering cycle.

Green pellets with densities of about 6.1 Mg/m^3 were pressed at moderate pressures of about 172 MPa (25,000 psi). Pellet densities of 95% TD were achieved when pellets were sintered at temperatures of 1650 to 1750°C for 4 to 8 h in a wet hydrogen atmosphere. The presence of water in the hydrogen aided in hydrocarbon removal.

Bettis researchers, who were working in support of the Large Seed Blanket Reactor (LSBR) Program, determined that ThO_2 powder made by direct denitration of thorium nitrate tetrahydrate could not be pressed and sintered to greater than 90% TD, even with a lengthy sintering cycle of 12 h at 1700°C (Johnson 1966) unless the powders were either wet ball milled for 24 h or fluid energy milled. Two to three wt% Carbowax® was used in the fabrication of these pellets. Pellets made by direct denitration appeared to be more sensitive to thermally induced cracking than those made with oxalate-derived powder.

ThO_2-UO_2 Experience

The major ThO_2-UO_2 fabrication campaigns produced pellet fuels for four reactors: the Borax IV reactor, the Elk River reactor, the Indian Point I reactor, and the LWBR.

Borax IV Reactor. The Borax IV reactor had the first large-scale loading of ThO_2-UO_2 fuel (Handwerk and Nolan 1959). The core contained 166,000 ThO_2-6.35 wt% UO_2 pellets made by Argonne National Laboratory (ANL). An additional 23,000 ThO_2 pellets were located in the blanket.

The fabrication process started with ThO_2 and U_3O_8 powders, which were mixed (not milled) in a ball mill with 2.5 wt% polyvinyl alcohol for 3 h. A small amount of water-containing aerosol was added to moisten the powder. The powder then was granulated through a 16-mesh screen. After drying, the granules were lubricated with 1 wt% of a 1:1 mixture of oleic acid in kerosene and pressed at 103 MPa (15,000 psi). Some of the organic materials were removed by pretreatment at 260°C before firing at 1700 to 1750°C for 2 h in air. Based on lattice parameter measurements, complete solid solution was judged to have formed during sintering.

Because of the lack of milling, the low forming pressure, and the short sintering time, sintered pellet densities determined by geometrical measurements were quite low, e.g., 83% TD. Water immersion densities of 98% TD indicated a high proportion of open porosity in the pellet microstructure.

Elk River Reactor. The ThO_2-4.3% UO_2 and ThO_2-5.2% UO_2 fuel pellets for the Elk River Reactor were fabricated by the Martin Company. Reactor startup was in 1962. The pellet specifications issued by the reactor manufacturer, Allis-Chalmers Manufacturing Company, permitted up to 0.4 wt% of sintering aid (TiO_2 or CaO) in the pellets (Allis-Chalmers Manufacturing Company, 1960). Minimum pellet density was specified to be 94% TD. Details of the actual pellet fabrication procedure and fuel characteristics were not published.

Indian Point I Reactor. In 1959-60 Babcock & Wilcox Company fabricated the ThO_2-UO_2 fuel core for the Indian Point I pressurized water reactor (Kerr et al. 1978). The stainless steel clad fuel rods were loaded with fuel pellets having nominal densities of 93% TD. Six compositions ranging from 0 to about

9 wt% UO_2 were fabricated from UO_2 and ThO_2 powders prepared by the Mallinkrodt Chemical Company and the Davison Chemical Company, respectively. The UO_2 was fully enriched in ^{235}U.

The batches, containing ThO_2, UO_2, and recycled fuel pellet scrap, were dry ball milled for 16 h, and then blended with 1 wt% polyvinyl alcohol binder and water in a planetary mixer. After thorough blending, semi-dry granules were formed by heating the blender while mixing. Drying of powder was completed in shallow trays under infrared heat lamps. Sterotex® die lubricant (0.5 wt%) was then blended with the powder in a twin-shell blender. Pellets were sintered in pusher furnaces in a cracked ammonia atmosphere at 1550 to 1650°C for approximately 6 h. A nominal sintered density of 93% TD was achieved.

The recycled scrap included in the powder batches consisted of both off-specification pellets from the fabrication campaign, and approximately 85% TD fuel pellets from the critical mass experiments used for the reactor core design. Reprocessed scrap pellets accounted for about 30% of the Indian Point I core A fuel loading. The sintered scrap reprocessing consisted of jaw crushing, followed by roll crushing, screening to a particle size less than 325 mesh, and then ball milling as part of the normal fabrication process. Scrap content and firing time and temperature were used in controlling final pellet density. Scrap recycle was also used to adjust ^{235}U content.

Light Water Breeder Reactor. During the 1960s, Bettis (Weinreich et al. 1977) developed a process for fabricating high-density, thoria-based fuel pellets for the LWBR, which achieved criticality in 1977. Ammonium diuranate-derived $^{233}UO_2$ powder, containing less than 10 ppm ^{232}U (Leitnaker et al. 1972) and oxalate-derived ThO_2 powder (Clayton 1976) were used to fabricate pellets with nominal densities of 97% TD. This exceptionally high pellet density was required to achieve a breeding ratio greater than one. The core comprises a seed-blanket-reflector arrangement of eight different ThO_2-UO_2 compositions

(as well as pure ThO_2) in four different pellet diameters. The maximum UO_2 content of the ThO_2-UO_2 pellets is less than 6 wt%. The core contains about 42,000 kg of thorium and 500 kg of uranium in 1.6 million ThO_2-UO_2 pellets and 1.3 million ThO_2 pellets.

A rather complex flowsheet was needed to fabricate the high-density Bettis ThO_2-UO_2 pellets. The ThO_2 and UO_2 powders were blended in a twin-shell blender and then activated and homogenized by double jet milling to give a powder specific surface area of more than 7.5 m^2/g. The milled powders were agglomerated during blending in a twin-shell blender (with intensifier bar) by an addition of 1.25 wt% Carbowax 6000® in oxylene solution. The agglomerated material was granulated through a 25-mesh screen and air dried in trays at 45°C. Sterotex® powder was added as a die lubricant (0.15 wt%) to the granules. Pellets were pressed in an automatic mechanical press to approximately 63% TD and were presintered in a CO_2 atmosphere for 4 h at 450°C, followed by a 3-h hold at 925°C. Sintering was performed in another furnace in a wet hydrogen-nitrogen atmosphere for a minimum of 12 h at 1790°C.

Several references describe the Bettis development of the fabrication process of pure ThO_2 as well as ThO_2-UO_2 pellets (Busby and Clayton 1976; Clayton 1976; Smid 1976). As would be anticipated, a number of powder processing steps, including calcining, milling, granulation, and binder additions, affect the quality of the sintered pellets.

The complex process needed to fabricate the high-density Bettis ThO_2-based pellets is not adaptable to remote fabrication. For example, the double jet milling required to achieve a sinterable powder is a very dusty operation and would be difficult to control and maintain in a remotely operated facility. The addition of binder to the powder and the debinding step are undesirable, and the high sintering temperatures would lead to furnace maintenance problems.

2.3.2 Laboratory-Scale Experience

Laboratory-scale experiments suggest that the processes used in major ThO_2 pellet fabrication campaigns can be simplified. Process steps that have potential for simplification are identified in the following review of

laboratory-scale fabrication studies relevant to ThO_2-based fuels. This discussion is divided into two parts: conventional pellet fabrication, and nonconventional pellet fabrication techniques, followed by a section on pellet fuel dissolution considerations.

Conventional Pellet Fabrication

The conventional pellet fabrication procedures that are relevant to ThO_2-based pellet fabrication are powder conversion, milling, blending, pellet pressing, and sintering.

Powder Conversion, Milling, and Blending Processes. Thoria powder derived from the oxalate process has been used in major ThO_2-based fuel production efforts and in most of the ThO_2 pellet fabrication studies. Even so, the literature includes only one report relating oxalate precipitation conditions to the fabrication and sintering behavior of the oxide (Kantan et al. 1958).

Thorium oxide powders have also been produced in the laboratory by the direct conversion of the nitrate (Harada et al. 1962; Pope and Radford 1974) and by the precipitation and decomposition of oxide precursors such as thorium benzoate, tannate, chloride, oxycarbonate, and carbonate (Harada et al. 1962; Moorthy et al. 1964). None of this latter work correlated precipitation parameters with the oxide fabrication and sintering characteristics.

The particles of oxalate-derived ThO_2 powder available in large quantities are typically flat, square platelets. In order to activate powder of this type and achieve sintered densities greater than 90% TD, these powders were jet milled at Bettis Atomic Power Laboratory (Weinreich et al. 1977) and high-energy wet milled at Atomic Energy of Canada Limited (AECL)(Jones et al. 1977). Both these milling processes are undesirable for a remotely operated fuel fabrication line.

By optimizing precipitation conditions, Lee and coworkers (1978) produced, on a laboratory scale, an oxalate-derived ThO_2 powder that sintered to greater than 95% TD without milling. Whether highly sinterable ThO_2 powders can be produced in large-scale production compaigns and whether more than 20 wt% UO_2 can be incorporated in this powder was not demonstrated.

Direct denitration of hydrated thorium nitrate produces a ThO_2 powder that is less sinterable than oxalate-derived powder. Powders produced by this method have had low surface areas and contained large, well-formed oxide crystallites. These powder characteristics may have resulted from the melting of the hydrated nitrate during decomposition of the nitrate. By decomposing anhydrous nitrate and thus preventing melting, it may be possible to produce a more highly sinterable powder.

Only limited work has been reported on the sintering behavior of coprecipitated ThO_2-UO_2 materials. Pope and Radford (1974) sintered ThO_2-66 wt% UO_2 coprecipitated powders and found that the sintering rate was slow: densities increased from 81 to 95% TD over 84 h at 1650°C. No attempt was made to improve the sinterability of this material by modifying precipitation or sintering conditions. Whether the slow sintering rate is inherent to coprecipitated ThO_2-UO_2 powders or whether it reflects the morphology of this particular precipitate was not determined.

Pellet Pressing and Sintering. The methods necessary to press acceptable pellets from ThO_2 powders can vary widely, depending on powder properties. Some powders require binders, lubricants, and high compacting pressures to achieve specified green density; these requirements are undesirable for a remotely operated process.

It may be possible to press ThO_2-based pellets without binders, but binders were needed in all the major fabrication campaigns. The most commonly used binder appears to have been Carbowax 6000® at additions of 1 to 4.5 wt%. The amount of binder used affects the compactibility of green powders and the porosity, density, and microstructure of sintered pellets (Burke 1969). Powder sources and fabrication processes that eliminate the need for binder additions are desirable.

The hard and abrasive nature of UO_2 and ThO_2 powders require that die wall lubrication be used during pellet pressing operations. Poor lubrication, poor die design, and rough die finish can cause stresses which are sufficient to crack the pellet. Die lubrication is usually achieved by adding a dry powder lubricant, normally one of the stearates, to the press feed. The blending

action not only mixes in the lubricant but can round off particles, which improves powder flow efficiency. Small lubricant additions of 0.2 to 0.3 wt% are usually sufficient; these amounts of lubricant are easily removed during early stages of sintering. Lubricant effects on pellet microstructure are minor, and any induced porosity is usually in the form of large, stable pores.

Compacting pressures as high as 965 MPa (140,000 psi) and as low as 172 MPa (25,000 psi) have been used to press variable powders to sintered densities greater than 90% TD (Beltram et al. 1965). Pressing problems are caused by variations in powder particle size, bulk density, and flow characteristics. These variations can result in nonuniform die fill and variable green and sintered densities. Hydraulic presses can be used to compensate for variable die fill caused by poorly flowing powders; however, such complex presses are not desirable in remotely operated facilities. Free-flowing powders that would fill the die cavity uniformly can be pressed in simple, single-acting mechanical presses to a constant density. Pellets pressed in a mechanical press with a properly designed, tapered die should sinter to right circular cylinders and thereby eliminate the need for centerless grinding. Development of such free-flowing powders would be highly advantageous for pellet fabrication in a remote operation because the grinding step and sludge recycle would be avoided.

Most ThO_2 sintering has been carried out in reducing atmospheres at about 1700°C for 4 to 8 h; however, sintering temperatures as low as 1550°C (Mohan and Moorthy 1971) and as high as 1790°C (Weinreich et al. 1977) have been reported as necessary to achieve required densities. Mohan and Moorthy (1971) looked at sintering times and temperatures for ThO_2-UO_2 compositions; temperatures greater than 1550°C were needed to get densities greater than 90% TD. Thoria has been sintered in both oxidizing and reducing atmospheres. Lynch (1965) showed that ThO_2-U_3O_8 mixtures can be sintered in air to form a solid solution of ThO_2-UO_2. A dilatometer study evaluating ThO_2-UO_2 mixture densification kinetics would help identify optimum sintering conditions, i.e., heating rates, temperature, and atmosphere.

Effect of Composition on Sintering of ThO_2-UO_2 Pellets. Although ThO_2 and UO_2 form a continuous series of solid solutions (Lambertson et al. 1953),

several investigators, including Handwerk, Abermathy, and Bach (1957) and Lynch (1965), found that pellet density decreased markedly with increasing UO_2 content with a minimum density occurring at a composition of about 50 wt% UO_2. Lee et al. (1978) found that pellets with densities greater than 95% TD could be achieved by a high-energy, wet milling process wherein a master mix of ThO_2-UO_2 was milled and blended with separately milled ThO_2. In an extensive investigation, Mohan and Moorthy (1971) found that pellets sintered at a temperature below 1400°C in H_2 had a minimum density at the middle of the composition range. However, at 1550°C, densities of 98% TD were reached in pellets containing 50 wt% UO_2. They also demonstrated that the minimum in the density-composition curve could be reduced by calcining the powders at 1200°C, but the final sintered density over the whole composition range was lowered.

The density decreases observed by various investigators varied considerably over the composition range because of different starting materials and variations in process steps such as mixing methods, compacting pressures, and sintering conditions. However, these studies clearly indicate that the densities of sintered ThO_2-UO_2 mixtures can be less than that of the single oxides. The mechanisms which lead to the reduced densities have not been identified. Berman (1972) observed the formation of large pores associated with 150-μm particles in a ThO_2 matrix. Although he did not measure diffusion coefficients for Th in UO_2 and U in ThO_2, he suggested that the large pores were due to the Kirkendall effect.

Based on PuO_2-UO_2 light water reactor (LWR) experience, complete solid solution formation may not be a prerequisite for ThO_2-UO_2 LWR pellet fuels. A uniform distribution of the fissile UO_2 phase will be required, but the presence of small, discrete UO_2 particles or UO_2-rich zones in the fuel will probably be acceptable. In the Bettis process, powders were co-jet milled in order to achieve required homogeneity and to increase powder activity (Weinreich et al. 1977). Control of process parameters may allow the production of powders that do not require high-energy milling to achieve required activity.

In addition to mechanical blending, powders may be coprecipitated to achieve homogeneity. However, the high degree of homogeneity achieved by coprecipitation may not be desirable or required.

Density and Microstructural Control In Fuels. The microstructure of pellet fuels is controlled to meet performance criteria such as densification behavior (Freshley et al. 1976) and gas release (Turnbull 1974). Although the densification and gas release behavior of ThO_2-based pellet fuels are not well known, control of fuel microstructures and densities will be required. The experience in controlling these parameters in UO_2 fuels is pertinent to ThO_2-based fuels.

The preparation of oxalate-derived ThO_2 powder today is similar to the early production of UO_2 powders in that intensive milling, high sintering temperatures, and long sintering times are often required to achieve pellet densities of 95% TD. As UO_2 powder production methods became more sophisticated, powder properties were improved to the extent that powders routinely sintered to higher densities. In order to reduce pellet densities to the required 93%- to 95%-TD range, lower sintering temperatures and/or times were used, resulting in fuel structures that could densify as much as 3 to 4% during irradiation. Pellet densification led to fuel column shortening, axial fuel gaps, and cladding collapse, which resulted in the imposition of operating constraints on several reactors.

Densification-resistant fuels can be achieved through control of pellet microstructure. Several approaches have been developed which result in the fuels containing relatively large pores in a high-density (98% TD) fuel matrix.

One approach to obtaining densification-resistant UO_2 fuels is to preslug powders at higher pressures than the final pelleting pressure, which results in microstructures containing large, open pores. Another approach is to add high-density green granules or granules of sintered UO_2; this approach can result in a microstructure with large fissure-like pores and a high degree of open porosity (Davis and Ferrell 1977). If UO_2 scrap pellets are oxidized to U_3O_8 and added to the press feed, the induced porosity can vary from clusters of pores to pores surrounding individual UO_2 granules. Fuel fabricators have also achieved stable densities by controlling the temperature used to produce the oxide powder during the calcining process.

Pore formers, materials which volatilize or burn out and leave pores behind, have been used successfully for porosity control in UO_2 and ThO_2-UO_2 systems (Hutchison and Johnson 1966; Williams et al. 1968). Ideally the pore former should be a hard, crystalline material that can be properly sized, is not affected by powder processing, does not enter into reactions with the fuel, and does not leave behind a carbonaceous residue.

Because large grain size increases diffusion distances for fission gas and vacancy migration, large grain sizes are specified in fuels to improve densification resistance and fission gas retention. Additives like CaO have been used to increase the grain size of oxides, including ThO_2 (Smid 1976). However, from the viewpoint of remotely operated fuel fabrication, the addition of a compound to enhance grain growth in ThO_2-based fuels is undesirable because of the additional process steps that would be required to fabricate the fuel.

Bettis investigators found that large, uniform grain size may not always be readily achieved in ThO_2-based fuels (Hutchison and Johnson 1966; Smid 1976). A picture-frame grain growth pattern has been noted with grains of 22 to 64 μm around the pellet periphery and grains of 11 μm or finer within the pellet. Observations of the coarser grain sizes surrounding surface cracks and holes drilled into pellets support the theory that a grain growth inhibitor which volatilizes during sintering may be present in ThO_2 fuels. Extensive grain growth work at Bettis showed that higher-than-normal powder calcining temperatures eliminated the tendency toward nonuniform grain growth in ThO_2 (Smid 1976). However, the powders formed at the higher calcination temperature were more difficult to process further. Higher-purity ThO_2 powders that did not exhibit this tendency were produced in the laboratory. The impurities or other factors that were the cause of the grain growth inhibition were not identified.

Nonconventional Pellet Fabrication

Extruded sol-gel fuels, pelletized sol-gel fuels, and impregnated fuels are examples of nonconventional pellet fabrication processes that have been considered by investigators as alternatives to pellet fuels produced by pressing of precipitated powders. These processes have potential for the fabrication of fuels in a remotely operated facility.

Extruded Sol-Gel Fuels. The feasibility of preparing ThO_2 and ThO_2-UO_2 fuels by extrusion and sintering of sol-gel clays was demonstrated by Fitts et al. (1968). The extrusion process requires the preparation of a ThO_2 or a ThO_2-UO_2 sol, which is concentrated by evaporation and filtered to form a clay. The clay is then extruded, cut to length, dried, and sintered. The results of the ORNL investigation showed that ThO_2 rods, which could be cut into typical pellet lengths if required, could be produced with stable densities between 70 and 98% TD by blending crushed, 325-mesh sintered ThO_2 with the clay before extrusion and then firing at 1150°C for 1 h in air. Subsequent resintering at temperatures up to 2000°C caused no significant changes in density or microstructure.

AECL is evaluating extrusion of sol-gel clays as part of a thorium recycle fuel program, and ThO_2-3 wt% UO_2 extruded rods have been sintered to 95% TD (Lane et al. 1978); however, high-density, crack-free rods are difficult to achieve.

Pelletized Sol-Gel Fuels. In addition to extruding fuels from sol-gel clays, fuels can be pelletized from sol-gel derived powders. A ThO_2 or ThO_2-UO_2 sol is prepared by one of the sol-gel processes, dried, and granulated into shard. The dried shard can be calcined, milled, and pressed into pellets. This approach offers the potential advantages of homogeneous mixtures, active powders, and low sintering temperatures. Crain and Hutchison (1966) were the first to report this method of pellet fabrication; they found that ThO_2-8 wt% UO_2 sol-gel powders could be pressed and sintered to 94% TD at 1350°C. However, the powders were difficult to compact: compacting pressures greater than 1 GPa (145,000 psi) were required, and the powders abraded die materials. Robbins and Stradley (1969) showed that high-density ThO_2-6.5 wt% pellets could be formed from sol-gel shard at the significantly lower compacting pressure of 414 MPa (60,000 psi). Pellets with sintered densities up to 95% TD could be readily fabricated by varying calcining temperature, moisture content, forming pressure, and sintering atmosphere. Burkhardt et al. (1969) used dried ThO_2 gel, which was calcined and milled to produce

pellets that sintered to 98% TD at 1700°C. They also added organic plasticizers to the milled shard and successfully extruded pellets. Although these studies are far from complete, they do demonstrate the feasibility of using sol-gel powders as a press feed material.

The potential also exists for fabricating pellet fuels using sol-gel spheres as the pellet press feed material. Combined efforts are currently underway at Oak Ridge National Laboratory (Tiegs 1978) and the Pacific Northwest Laboratory (Hart et al. 1979) to develop this approach for UO_2 and ThO_2 fuels. The advantages of using sol-gel spheres as a press feed material in remotely operated pellet fuel fabrication are: 1) limited dust generation during powder production and transport, 2) the free flowing characteristics of the spheres, which will ease material transport and improve die filling during pressing, and 3) the potential for reduced sintering temperature.

Impregnated Fuels. Another pellet fabrication technique being studied by (AECL) is an impregnation process in which fertile, low-density pellets prepared in a conventional fabrication plant are transferred to a shielded facility, where they are impregnated with a solution containing the fissile component (Lane et al. 1978). The pellets are subsequently rinsed, dried, sintered, and ground if necessary. This technique is not applicable to denatured fuel compositions because the amount of open porosity in the green ThO_2 pellets and the solubility of uranium in HNO_3 limits the concentration of the fissile component to less than 5 wt%.

Dissolution Considerations of ThO_2-UO_2 Fuels

In a complete fuel cycle, the irradiated fuel must be amenable to reprocessing. A number of wet and dry processing routes have been suggested, including the THOREX process, in which the spent fuel is dissolved in nitric acid, precipitated as a salt, and calcined to yield the oxide.

Additions of MgO, ZnO, or CaO to sintered ThO_2 sol-gel particles have been shown to improve the dissolution rates in nitric acid (Russell et al. 1967a, 1967b). In contrast, dissolution studies indicate that 1-wt% MgO additions to unirradiated ThO_2-UO_2 pellets do not result in enhanced dissolution rates (Pickett and Foule 1979). Additional work is required to determine

the need for dissolution aids in ThO_2-UO_2 pellet fuels. If dissolution aids are required in the fuel, these additions must be compatible with the fabrication method used to produce the fuel and must have no adverse effect on irradiation performance.

2.3.3 Summary and Evaluation of Pellet Fuel Fabrication

Results of large-scale pellet fabrication compaigns, as well as laboratory-scale experience, indicate that ThO_2-UO_2 fuels can be successfully manufactured using conventional pellet-forming techniques. However, in many cases, extensive powder milling, large binder additions, high pellet-forming pressures, and severe sintering conditions were required to achieve high-density pellets. Through improvements in powder quality or by use of materials like sol-gel-derived press feed, the potential exists for a pellet fuel fabrication process that can be employed in a remotely operated fabrication facility to produce ThO_2-based fuels containing greater than 20 wt% UO_2.

3.0 PROPERTIES OF ThO_2-BASED NUCLEAR FUELS

A thorough understanding of the thermo-physical properties of nuclear fuels is necessary to predict the behavior of fuels in a reactor. Petersen and Curtis (1970) have reviewed the fuel properties data compiled prior to 1970. More recently, Fink et al. (1977) and Kittel et al. (1977) reviewed the thermophysical properties of ThO_2 and ThO_2-UO_2. Petersen and Curtis tabulated the existing data but made no critical evaluations to determine the best data. Fink et al. and Kittel et al. identified the best data and descriptions for some properties, but they did not specify the reasons for their choices nor indicate what other data they considered.

This review of the properties of ThO_2-based fuels critically evaluates the data and attempts to identify by comparison the best data and descriptions for the properties considered.

To aid the reader, the fuel properties are discussed in three subsections: Thermophysical Properties, Chemical and Thermodynamic Properties, and Mechanical Properties. Properties are divided among these sections as shown here:

Thermophysical Properties	Chemical and Thermodynamic Properties	Mechanical Properties
• Thermal Expansion	• Crystal Structure and Lattice Parameter	• Elastic Moduli
• Thermal Conductivity	• Density	• Creep Behavior
• Diffusion	• Solid Solution Formation	• Fracture Strength
	• Stoichiometry	
	• Thermodynamic Properties	
	Heat Capacity	
	Vapor Pressure	
	Other Properties	

3.1 THERMOPHYSICAL PROPERTIES

These discussions cover thermal expansion, thermal conductivity, and diffusion. Each discussion identifies techniques for measuring the particular property and summarizes investigations relevant to ThO_2-based fuels.

3.1.1 Thermal Expansion

Accurate thermal expansion values for nuclear fuels are necessary so that fuel/cladding mechanical interactions can be minimized.

Techniques for Measuring Thermal Expansion

Thermal expansion can be measured by the change in length of a bulk specimen during heating using a dilatometer, telemicroscope, or interferometer. A detailed description of each of these procedures is given by Kingery (1959a). The thermal expansion is expressed as:

$$\% \text{ expansion} = \frac{\ell - \ell_0}{\ell_0} \times 100\% \qquad (1)$$

where ℓ_0 and ℓ are the specimen lengths at a reference temperature and a temperature T, respectively.

The thermal expansion can also be determined on the atomic scale by measuring the change in lattice parameter by x-ray diffraction. The thermal expansion determined by x-ray diffraction will be equal to the bulk measurements if the crystal structure of the material is isotropic. Since ThO_2 and UO_2 both crystallize in a cubic isotropic lattice, the bulk and x-ray measurements should be comparable.

The coefficient of thermal expansion can be defined in several ways. The average coefficient of thermal expansion ($\bar{\alpha}$) determined over the entire temperature range is expressed:

$$\bar{\alpha} = \frac{\ell - \ell_0}{\ell_0} \frac{1}{T - T_0} \qquad (2)$$

and the instantaneous coefficient of thermal expansion (α_i) determined at a specific temperature is expressed:

$$\alpha_i = \frac{1}{\ell_0} \frac{\delta \ell}{\delta T} \qquad (3)$$

Many times the method of calculating thermal expansion coefficients reported in the literature is not identified. Therefore, it is best to compare the reported percent linear expansion of samples, rather than the coefficient.

Impurities can affect the thermal expansion measurements, but generally only at temperatures approaching the melting point where the vacancy concentration, which is affected by impurities, increases rapidly as the melting point is approached. If sufficient amounts of impurities are present in the lattice, the bond strength, which is inversely proportional to thermal expansion, could be affected. However, the materials used in the studies reviewed here were at least 99.0% pure and the effect of impurities on thermal expansion should be negligible.

Porosity concentrations of 10% or less have little influence on thermal expansion. The effect of radiation on the thermal expansion of $(Th_{1-x}U_x)O_2$ has not been studied.

Thermal Expansion of ThO_2

The thermal expansion of ThO_2 has been investigated by a number of investigators under the conditions given in Table 2. The different thermal expansion determinations are in good agreement as shown in Figure 4 with increased scatter for temperatures above 1200°C. Since the scatter for all data was small, a regression analysis was used to fit the data to the equation:

$$\% \text{ expansion} = (-9.61 \times 10^{-6}) + (7.94 \times 10^{-4})T + (1.54 \times 10^{-7})T^2 - (2.29 \times 10^{-11})T^3 \quad (4)$$

where T is temperature (°C). One standard deviation for Equation 4 is 0.057.

Three studies were not included in this analysis although they were considered. Eisenstein (1946) did not report any data points, only the average thermal expansion coefficient. Valentich (1969) presented his data in graphical form, and individual data points could not be determined from his figures. The data of Lang and Knudsen (1956) was not included because 0.5 wt% CaO was

TABLE 2. Experimental Conditions and Results of ThO_2 Thermal Expansion Measurements

Reference	x in $(Th_{1-x}U_x)O_2$	Method	Sample Purity, %	Temp. Range, °C	Percent Expansion (T = °C)	Average Coefficient of Linear Thermal Expansion, 10^{-6}/°C
Geller and Yavorsky (1945)	0	dilatometer	NR[a]	200-1700	NR	10.21
Grain and Campbell (1976)	0	x-ray diffr.	99.9	25-1100	NR	9.1
Whittemore and Ault (1956)	0	telemicroscope	NR	25-500	NR	10.4
Brown and Chitty (1960)	0	x-ray diffr	99.5	0-1100	NR	9.07
Hirata et al. (1977)	0	x-ray diffr.	99.99	800-1800	$7.589 \times 10^{-6}T + 1.552 \times 10^{-9}T^2$	10.36
Wacthman et al. (1962)	0	interferometer	99.9	27-827	NR	9.28
Ohnysty and Rose (1964)	0	dilatometer	NR	25-2465	NR	10.89
Aronson et al. (1967)	0	x-ray diffr.	99.99	850-2100	NR	11.2
Hock and Momin (1969)	0	x-ray diffr.	99.9	850-2100	$-2.106 \times 10^{-2} + 8.383 \times 10^{-4}T + 9.995 \times 10^{-8}T^2$	10.62
Richardson (1935)	0	interferometer	99.0	100-600	NR	9.6
Kempter and Elliot (1959)	0	x-ray diffr.	99.9	26-1000	$8.1950 \times 10^{-6} + 1.121 \times 10^{-9}T$	9.32
	0.5	x-ray diffr.	99.8	26-1000	$8.8553 \times 10^{-6} + 1.329 \times 10^{-9}T$	10.18
Lang and Knudsen (1956)	0[b]	dilatometer	99.9	100-1400	NR	9.9
Springer et al (1967)	0	dilatometer	99.9	200-2000	$-6.33 \times 10^{-2} + 8.86 \times 10^{-4}T + 9.47 \times 10^{-8}T^2$	10.83
	0.1	dilatometer	99.9	200-2000	$-2.68 \times 10^{-2} + 9.50 \times 10^{-4}T + 6.72 \times 10^{-8}T^2$	10.94
	0.2	dilatometer	99.9	200-2000	$-2.90 \times 10^{-2} + 8.99 \times 10^{-4}T + 1.19 \times 10^{-2}T^2$	11.56

(a)NR = Not reported
(b)ThO_2-1/2 wt% CaO 99.9

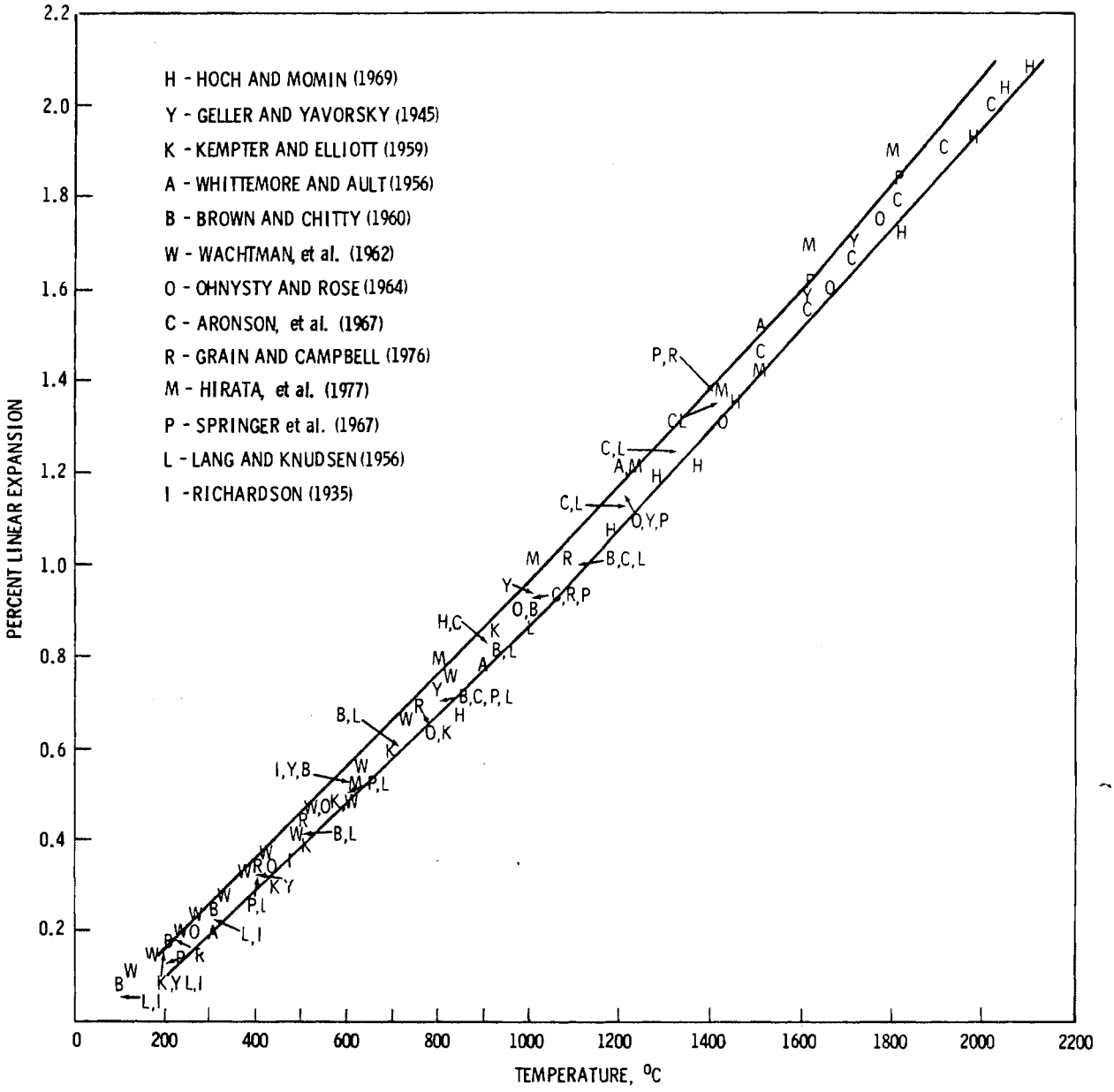

FIGURE 4. Percent Linear Expansion of ThO_2 as a Function of Temperature (from various studies)

added as a sintering aid. However, Equation 4 and the data of Lang and Knudsen as shown in Figure 5 are in good agreement, indicating that this CaO addition had little effect on thermal expansion.

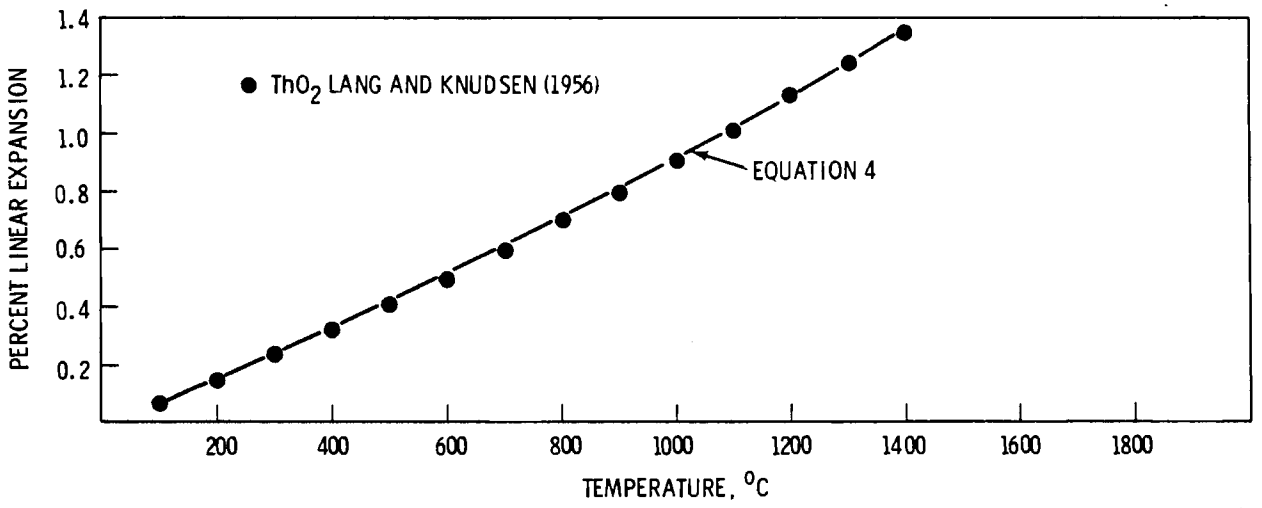

FIGURE 5. Comparison of Equation 4 for Thermal Expansion to the ThO_2 Thermal Expansion Data of Lang and Knudsen

Thermal Expansion of ThO_2-UO_2 Solid Solutions

Springer et al. (1967) measured the thermal expansion of pure ThO_2, ThO_2-10 wt% UO_2, and ThO_2-20 wt% UO_2 solid solutions. Figure 6 shows that the thermal expansion of pure ThO_2 is lower than that of pure UO_2 as reported by Touloukian et al. (1977). The data for the two ThO_2 and UO_2 solid solutions falls between the curves for ThO_2 and UO_2. Below 1000°C, there is little separation between the four sets of data, whereas above 1000°C the curves show increasing separation with increasing temperature. At 2000°C, the data for pure UO_2 is about 20% higher than that for pure ThO_2.

Kempter and Elliott (1959) measured the thermal expansions of pure ThO_2 and $(Th_{0.5}U_{0.5})O_2$ to 1000°C. As shown in Figure 7, the data for $(Th_{0.5}U_{0.5})O_2$ lies along the pure UO_2 curve of Touloukian et al. (1977), and their data for pure ThO_2 is not discernably different from the data of Springer et al. (1967) below 1000°C. Above 1000°C, the data of Springer et al. show that thermal expansion of ThO_2-UO_2 solid solutions increases with UO_2 content. However, this increase in expansion coefficient with UO_2 content is not described by the simple summing of the contribution of the pure components.

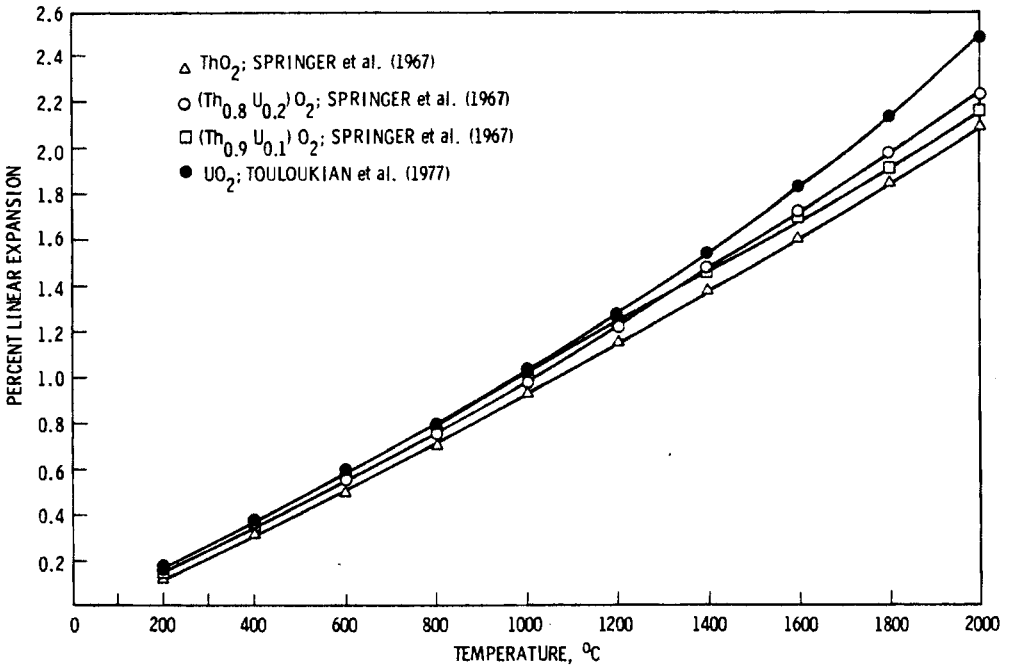

FIGURE 6. Percent Linear Expansion of $(Th_{1-x}U_x)O_2$ as a Function of Temperature

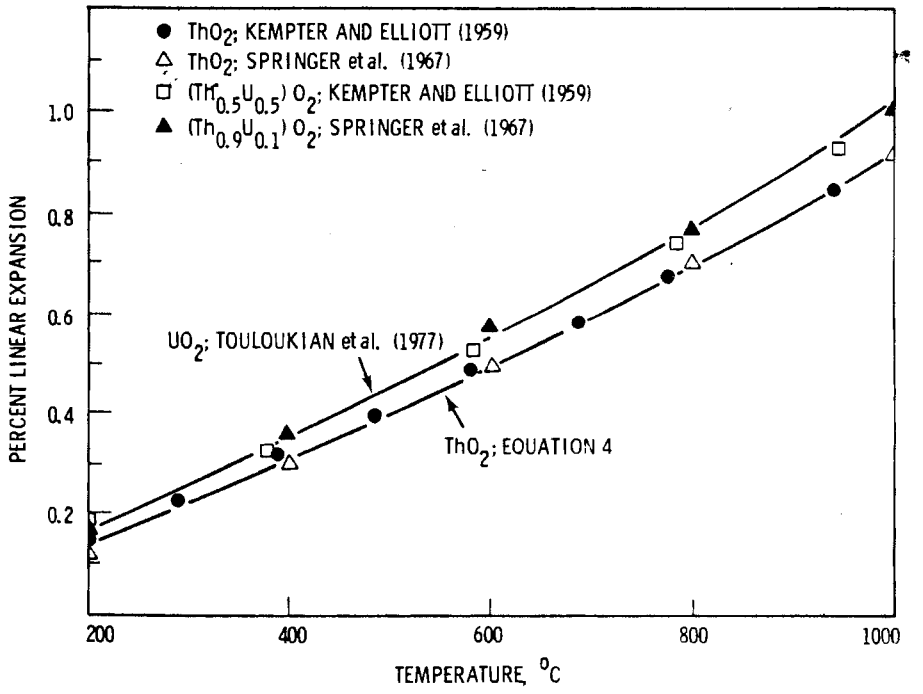

FIGURE 7. Comparison of the Thermal Expansion Data for the ThO_2, UO_2, and ThO_2-UO_2 Solid Solutions

Berman et al. (1972)[a] analyzed the data of Springer et al. (1967) and derived the equation:

$$L = 0.9983 + 5.13 \times 10^{-6}T + 2.5 \times 10^{-9}T^2 + (6.83 \times 10^{-3} + 2.5 \times 10^{-5}T)U \quad (5)$$

to express the relative expansion ($L = 1 + \Delta\ell/\ell_0$) as a function of temperature (T) in kelvins and the mole fraction UO_2 (U). Berman et al. (1972) used Equation 5 to describe the thermal conductivity of ThO_2-UO_2 solid solutions as a function of temperature and composition.

Equation 5 predicts thermal expansions that are higher than the actual data measured by Springer et al. (1967), Figures 8, 9, and 10. The difference between the actual and predicted values increases as temperature and UO_2 content increases. Although Equation 5 does not fit the data, there does appear to be sufficient data to derive an equation that accurately describes the thermal expansion of ThO_2-UO_2 as a function of temperature (200 to 2000°C) and composition (0 to 20 wt% UO_2).

Thermal Expansion - Summary and Evaluation

The thermal expansion of ThO_2 has been studied by numerous investigators and may be described by:

$$\% \text{ expansion} = -9.61 \times 10^{-6} + 7.94 \times 10^{-4}T + 1.54 \times 10^{-7}T^2 - 2.29 \times 10^{-11}T^3, \quad (4)$$

where T is temperature (°C).

(a) The coefficients of Equation 5 were obtained in a private communication from R. M. Berman and are not the same as those reported in Berman et al. (1972) because of an error in temperature conversion.

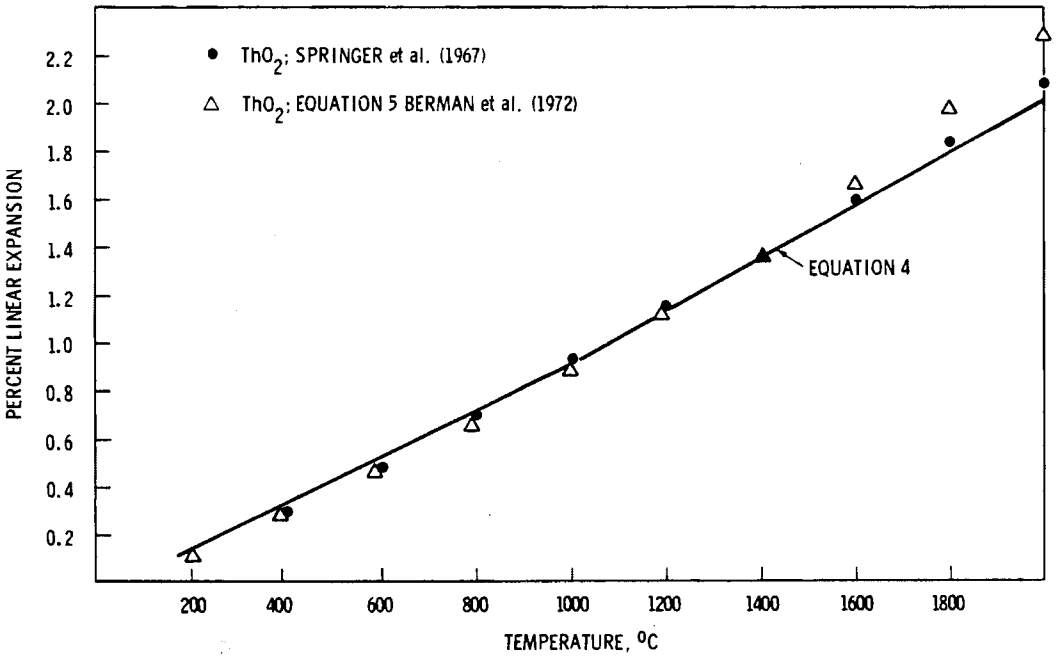

FIGURE 8. Thermal Expansion of ThO_2 (Data of Springer et al. and Equation 5 from Berman et al.)

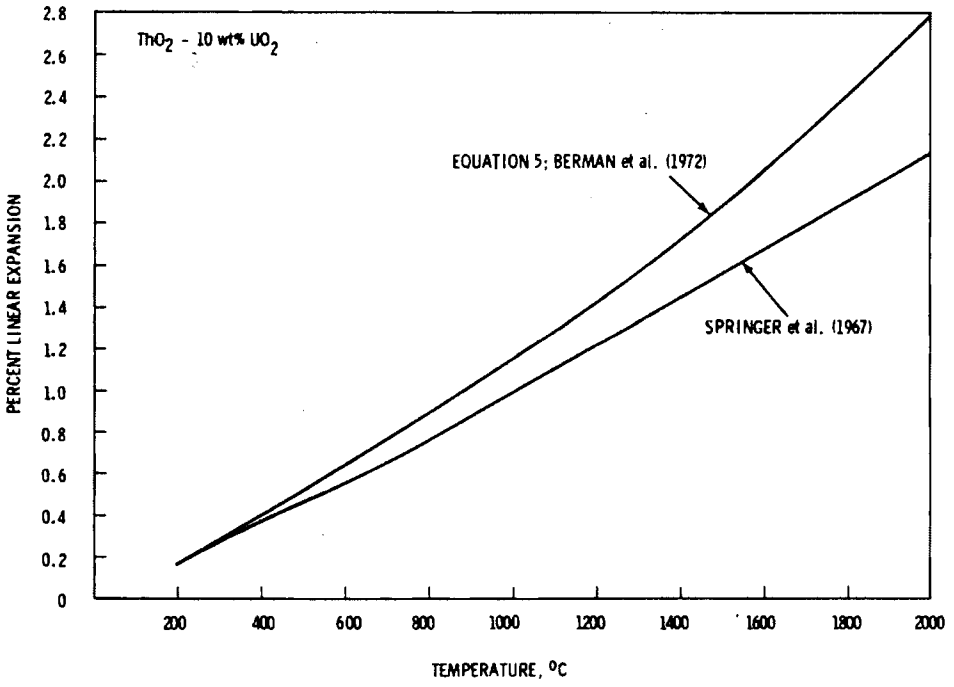

FIGURE 9. Thermal Expansion of ThO_2-10 wt% UO_2 (Data of Springer et al. and Equation 5 from Berman et al.)

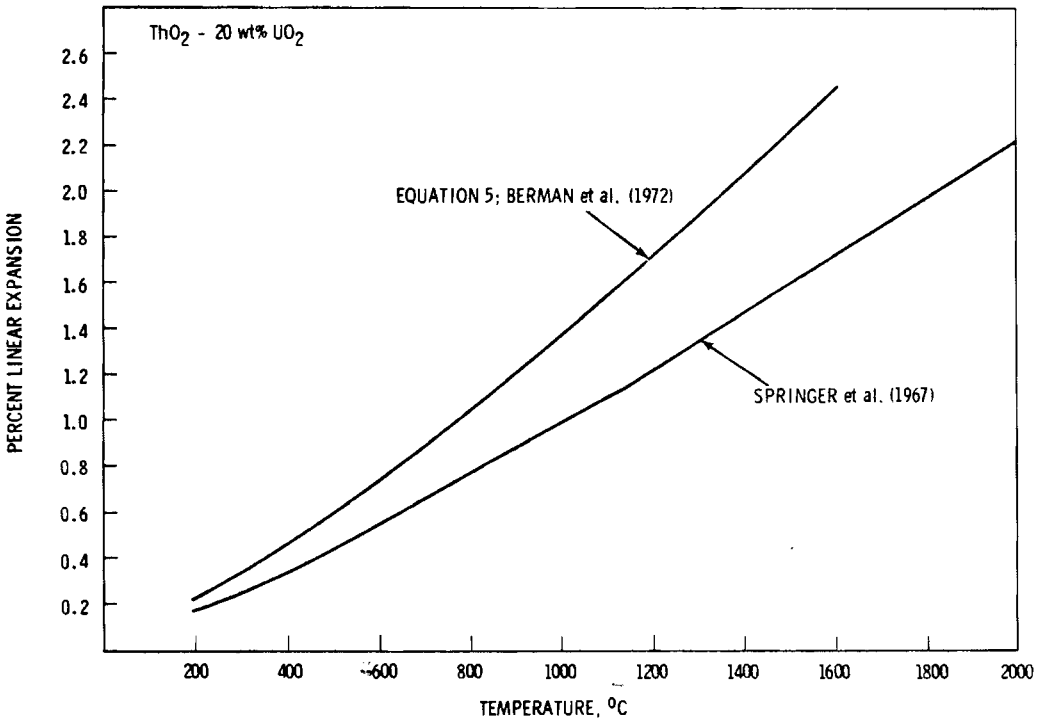

FIGURE 10. Thermal Expansion of ThO_2-20 wt% UO_2 (Data of Springer et al. and Equation 5 from Berman et al.)

The thermal expansion of ThO_2-UO_2 compositions has not been studied in as great detail as the thermal expansion of ThO_2. There is some evidence to show that below 1000°C the linear thermal expansion of compositions up to 50 wt% UO_2 are approximately equal to the expansions of pure ThO_2 and UO_2. Above 1000°C the thermal expansion is a function of the UO_2 content. Sufficient data is available in the literature to describe quantitatively the effect of UO_2 on thermal expansion for compositions containing up to 20 wt% UO_2.

3.1.2 Thermal Conductivity

Techniques for Measuring Thermal Conductivity

Two experimental techniques are used to measure the thermal conductivity of nuclear fuels. The conductivity of unirradiated and irradiated specimens has been based on thermal diffusivity measurement made by the flash laser method described by Parker et al. (1961). With this technique, the front face of a thin specimen, which is maintained in an isothermal environment, is

subjected to a short-duration laser pulse. The temperature rise of the back face of the specimen is recorded versus time and the thermal diffusivity (α) is calculated from:

$$\alpha = \frac{0.139\ell^2}{t_{\frac{1}{2}}} \tag{6}$$

where ℓ is the specimen thickness, and $t_{\frac{1}{2}}$ is the time required for the back face to reach one-half the maximum temperature increase following the thermal pulse. Thermal conductivity (λ) is calculated as the product of the thermal diffusivity, density (ρ), and heat capacity (C_p).

$$\lambda = \alpha C_p \rho \tag{7}$$

Thermal conductivity of in-pile fuels can be measured by the radial heat flow technique (Jacobs 1969). In this procedure the thermal conductivity is inferred from the heat input, determined by the fission and gamma heating processes, and the temperature gradients within the fuel, determined by thermocouples. This method can lead to large errors because the heat input cannot be measured directly and because of variations in crack patterns within the fuel.

Effects of Temperature on Thermal Conductivity

In most polycrystalline materials, the thermal conductivity decreases as temperature increases. Generally, the relationship of thermal conductivity to temperature (T) is described by

$$\lambda = \frac{1}{A + BT} \tag{8}$$

where A and B are empirically determined constants. The constant A describes the scattering of phonons by lattice impurities and imperfections, and B describes the phonon-phonon interaction. The effect of temperature by itself will not be discussed here because this data is typically examined in conjunction with the effects of composition and porosity on thermal conductivity.

Effects of Composition on Thermal Conductivity

The thermal conductivity of a solid solution is generally found to lie between the conductivities of the pure components. An estimate of the thermal conductivity of a solid solution may be obtained by summing the mole fraction contribution of each component (Kingery 1959b). Therefore, the thermal conductivity of a ThO_2-UO_2 mixture would be expected to fall between that of UO_2, as a lower bound, and that of ThO_2, as an upper bound. Because impurities and microstructure strongly influence conductivity, thermal conductivity must be determined experimentally when data with a high degree of precision is required for fuel performance modeling.

Springer et al. (1967) and Springer and Lagedrost (1968) calculated the thermal conductivity from the measured thermal diffusivity, density, and heat capacity of compositions containing 0 to 30 wt% UO_2 between 300 and 1900°C. These investigators found that the thermal conductivity lay between thermal conductivities of pure UO_2 and pure ThO_2. The experimental conditions for the studies reviewed here are given in Table 3. Springer et al. measured the lattice parameters of their specimens and found them to fall within 5% of Vegard's law, indicating the formation of solid solutions. Springer and Lagedrost did not determine the degree of solid solution formation. However, their specimens came from the same source and procedure as those of Springer et al. and were probably solid solutions.

Springer et al. describe the effect of UO_2 content on the thermal conductivity (W/cm-°C) of 100%-dense ThO_2-UO_2 solid solutions (λ_o) by:

$$\lambda_o = \left[0.79(1 + 0.09W) + 0.0185T\right]^{-1}(1 + 0.291W)(1 + 0.4W)^{-1} \quad (9)$$

where W is the weight percent UO_2 and T is the absolute temperature.

Berman et al. (1972) analyzed the data of Springer et al. and Springer and Lagedrost for the effect of composition on the thermal conductivity of $(Th_{1-x}U_x)O_2$. Berman et al. found the thermal conductivity of 100%-dense ThO_2-UO_2 solid solutions varied with composition and temperature as:

TABLE 3. Experimental Conditions for Thermal Conductivity Measurements for Unirradiated Fuels

Reference[a]	Thoria Fuel Composition, % UO_2	Firing Temperature, °C	Firing Time, h	Atmosphere	Percent Theoretical Density	Temperature Range, °C
Springer et al. (1967)	0 wt% 10 20	1725	12	H_2	75, 85, 95 75, 85, 95 75, 85, 95	300 to 1900
Springer and Lagedrost (1968)	3 to 30 wt%	1725	12	H_2	75 to 98	300 to 1900
Murabayashi (1970)	0 mole% 1 3 5 10	1700	5	H_2	NR[b]	20 to 800
Ferro et al. (1969)	1 mole% 4 10	1700	3	H_2	87 95 96	800 to 1400
Ferro et al. (1972)	6 mole% 10	1700	3	H_2	95 91	800 to 2200
Murabayashi et al. (1969)	0	1700	5	H_2	90 to 94	20

(a) All researchers used the flash laser method of measuring thermal conductivity.
(b) NR - not reported.

$$\lambda_o = \left[A_0 + A_1U + A_2U^2 + (B_0 + B_1U + B_2U^2)\right]T^{-1} \qquad (10)$$

where U is the mole fraction UO_2, T is the absolute temperature, and A_0, A_1, B_0, etc., vary with composition as given in Table 4.

TABLE 4. Values for the Constants A and B of Thermal Conductivity Equation 5

Fuel Composition Range, x in $(Th_{1-x}U_x)O_2$	Constants for $\lambda_o = \left[A_0 + A_1U + A_2U^2 + (B_0 + B_1U + B_2U^2)\right]T^{-1}$					
	A_0	A_1	A_2	B_0	B_1	B_2
0 to 0.1	0.9314	20.830	-281.018	0.01822	0.03414	0.1043
0.1 to 0.3	6.5219	-78,628	213.518	0.01158	0.14715	-0.3605
0.3 to 1.0	5.6964	-33.613	30.556	0.01310	0.07457	-0.0672

Figures 11a and 11b show that the thermal conductivities calculated with Equations 9 and 10[(a)] are within 5% of the actual data of Springer et al. (1967) over the entire range of compositions and temperatures studied and are within 10% of the actual thermal conductivity data of Springer and Lagedrost (1968), as indicated in Figures 12a and 12b. The difference between values predicted by Equations 9 and 10 is very small; however, because of the larger quantity of data used to derive it, Equation 10 is identified as the best estimate of the thermal conductivity of $(Th_{1-x}U_x)O_2$ up to 30 mole% UO_2. The lack of data above 30 mole% UO_2 precludes the use of either Equation 9 or 10 to describe the thermal conductivity of compositions containing greater than 30 mole% UO_2.

In deriving Equation 10, Berman et al. (1972) corrected the specimen density for thermal expansion using an equation that yields expansions that are 40 to 50% higher than measured values for compositions containing 10 to 20 mole% UO_2.[(b)] The use of this equation resulted in an error of only 3% in the calculated thermal conductivity for the ThO_2-20 wt% UO_2 composition at 1800°C.

(a) Appropriate corrections for specimen density were made using correction factors provided by Springer et al. for Equation 9 and Berman et al. for Equation 10.

(b) The preceding section discusses thermal expansion.

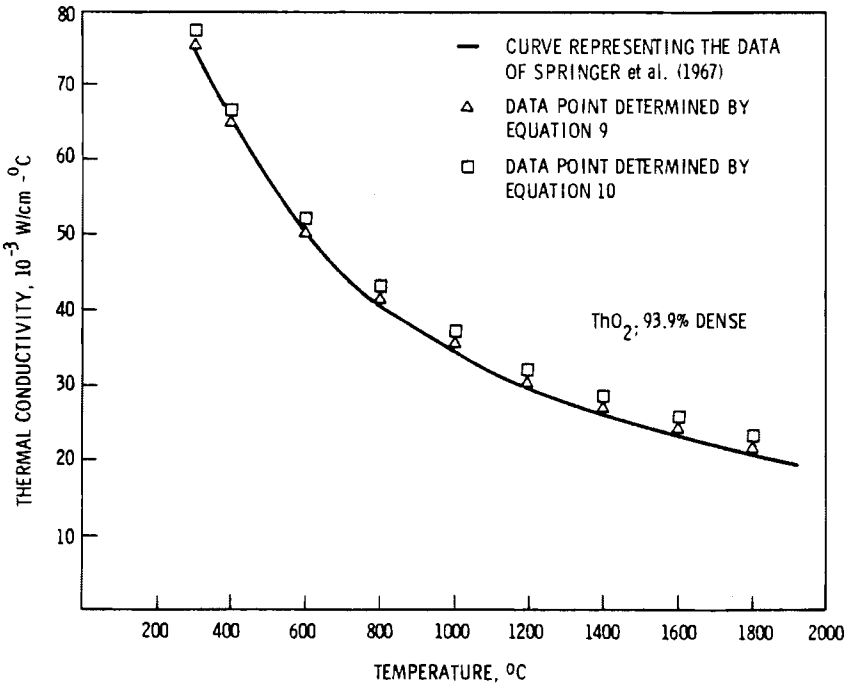

a. Thermal Conductivity of a 93.9%-TD Specimen of ThO_2

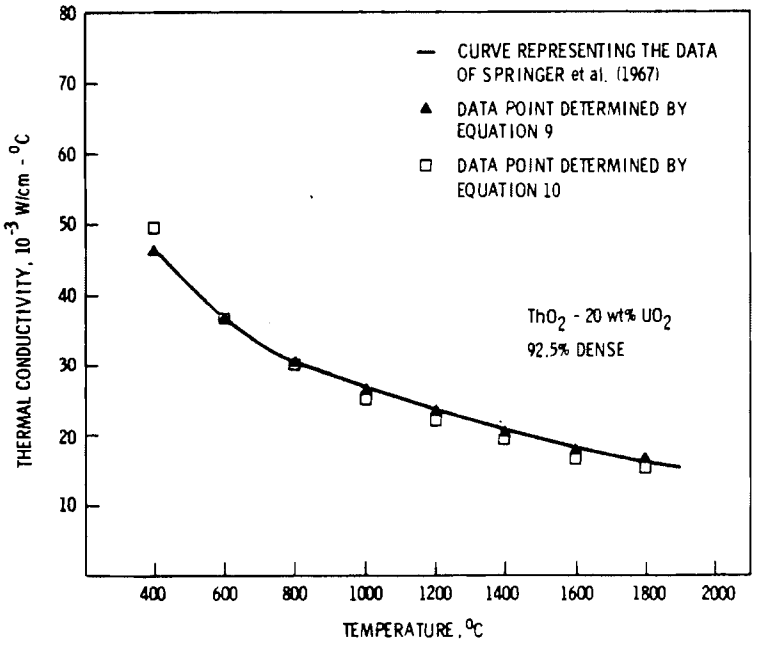

b. Thermal Conductivity of a 92.5%-TD Specimen of ThO_2-20 wt% UO_2

FIGURE 11. Comparison of Thermal Conductivity Equations 9 and 10 with the Data of Springer et al.

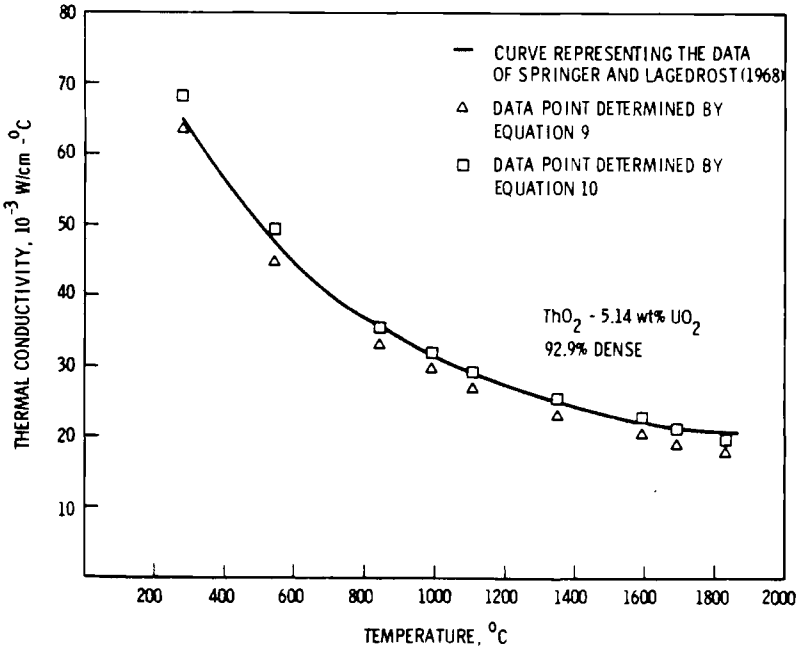

a. Thermal Conductivity of a 92.9%-TD Specimen of ThO_2-5.14 wt% UO_2

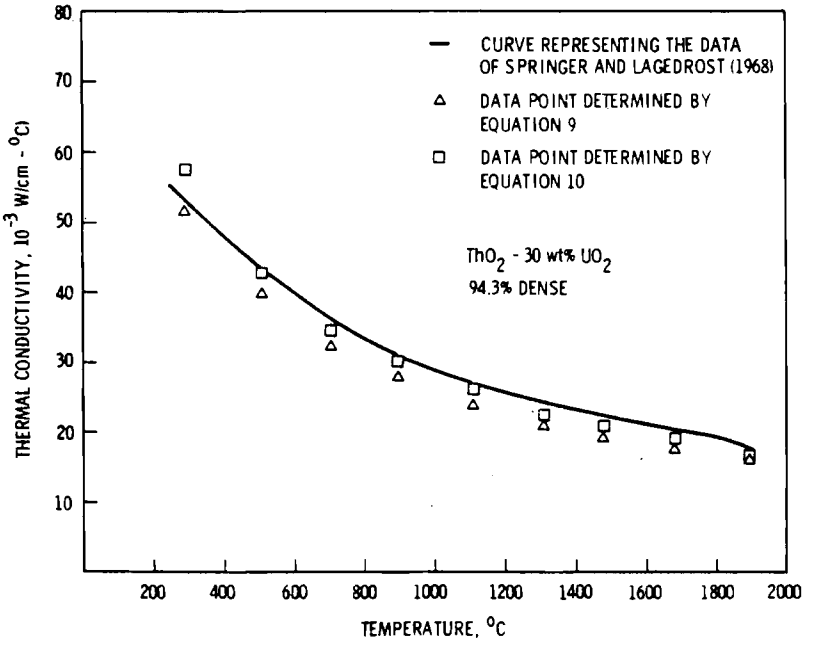

b. Thermal Conductivity of 94.3%-TD Specimen of ThO_2-30 wt% UO_2

FIGURE 12. Comparison of Thermal Conductivity Equations 9 and 10 with the Data of Springer and Lagedrost

Above 500°C, Springer and Lagedrost (1968) found the conductivity of the 30-wt%-UO_2 composition to be greater than the 20-wt%-UO_2 composition as shown in Figure 13. These curves in theory should be parallel, and the conductivity of the 30-wt%-UO_2 composition should be lower than the conductivity of the 20-wt%-UO_2 composition. Springer and Lagedrost could not offer an explanation for this behavior. Consistent with the experimental data of Spinger and Lagedrost, Equation 10 predicts that the conductivity of a 30-wt%-UO_2 composition will be greater than that of a 20-wt%-UO_2 composition above 500°C.

Equation 10 is based on thermal conductivity measurements made parallel to the pellet axis on pressed and sintered pellets. Springer and Lagedrost found that the conductivities were approximately equal for axially and radially measured specimens. However, Berman et al. (1972) found that Equation 10 could

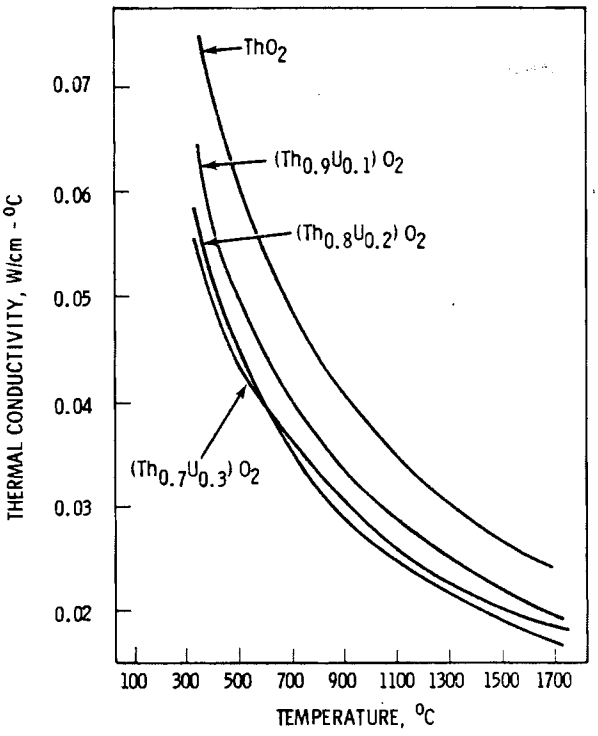

FIGURE 13. Thermal Conductivity of ThO_2-UO_2 Solid Solutions Calculated from Equation 10 as a Function of Temperature (corrected to 5% porosity by Equation 12)

not predict radial conductivities. Berman et al. did not attempt to explain this discrepancy in their analysis.

The thermal conductivity of ThO_2-UO_2 solid solutions as measured by Murabayashi (1970) is shown in Figure 14. The experimental conditions are given in Table 3. Murabayashi only presented his data in graphical form and did not do an analysis of the data in forms of Equation 8. Murabayashi confirmed the complete formation of the solid solution through lattice parameter measurements.

Murabayashi corrected his data to 95% TD. In Figure 15, the Murabayashi data are compared with the curve generated with Equation 10 corrected to 95% TD using Equation 12. The use of Equation 12 is discussed later in this report under the effects of porosity on thermal conductivity. The Murabayashi data fall 10 to 15% below the Equation 10 curve. The slopes of the two sets of data are approximately equal, indicating that the difference is caused by a change in the A term of Equation 10 which has been related to the impurity level of the specimen.

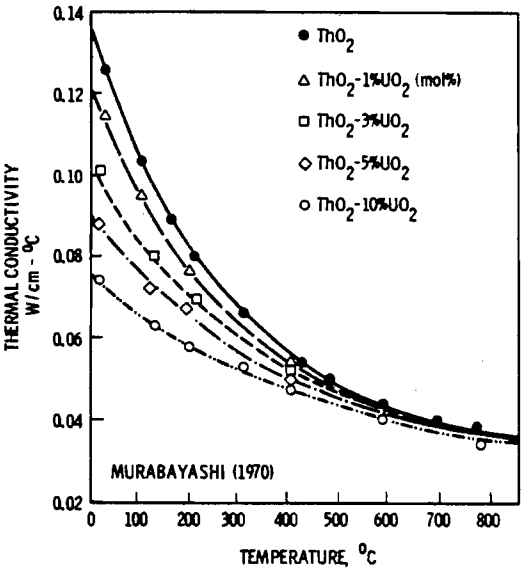

FIGURE 14. Thermal Conductivity of ThO_2-UO_2 Solid Solutions Determined by Murabayashi as a Function of Temperature (corrected to 5% porosity by Equations 14 and 15 where n was determined from the data)

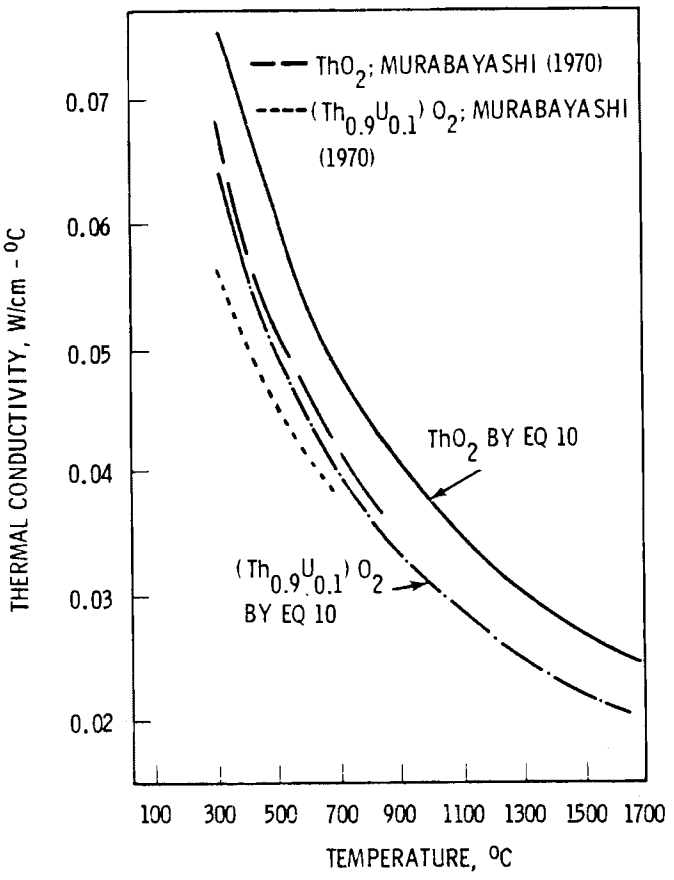

FIGURE 15. Comparison of the Data of Murabayashi and the Thermal Conductivity Calculated from Equation 10 for 95%-Dense Fuel Specimens

Ferro et al. (1969) measured the thermal conductivity of 1-, 4-, and 10-mole%-UO_2 compositions of ThO_2-UO_2. Ferro et al. (1969) did not determine the degree of solid solution formation. Two different 10-mole%-UO_2 specimens were measured and yielded thermal conductivities consistently differing by 15 to 20% across the temperature range from 800° to 1200°C; this may have been due to different impurity levels in the two specimens.

Figure 16 compares the data of Ferro et al. (1969) with the curves determined by Equation 14. The calculated and experimental curves are parallel for the 4 mole%-UO_2 compositions, but the data of Ferro et al. is approximately 10% less than Equation 10 would predict. The curves for 1- and 10-mole%-UO_2 compositions do not agree in either slope or intercept.

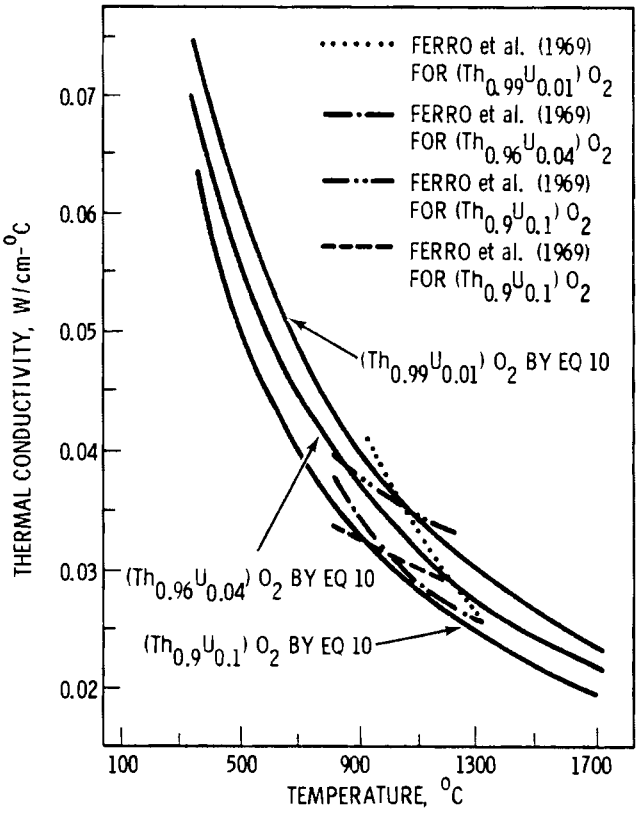

FIGURE 16. Comparison of the Data of Ferro et al. and the Thermal Conductivity Calculated from Equation 10 (corrected to 5% porosity by Equation 12)

Ferro et al. (1972) also measured the thermal diffusivity of ThO_2-6 mole% UO_2 and ThO_2-10 mole% UO_2, but did not calculate the thermal conductivity. For both compositions, the thermal diffusivity was at least 10% higher (and as much as 30% higher at temperatures >1200°C) than the Springer and Lagedrost (1968) data used by Berman et al. (1972). This would translate into an equal difference in thermal conductivity when calculated from equal heat capacity and density data.

The data of Springer et al. (1967) and Springer and Lagerost (1968) appear to be the most extensive and should be sufficient to describe the thermal conductivity of $(Th_{1-x}U_x)O_2$ as a function of temperature from 300 to 1900°C and compositions ThO_2 to ThO_2-30wt%-UO_2. At present, Equation 10, derived from the data of Springer et al. and Springer and Lagedrost, gives the thermal conductivity within 10% for compositions containing 0 to 30 wt% UO_2 between 300 to 1900°C.

Effect of Porosity on Thermal Conductivity

The thermal conductivity of a porous material (λ_p) is generally found to be a fraction of the conductivity of a 100% dense material (λ_o). There are two major theories used to relate the effect of porosity on thermal conductivity. These are the modified Loeb equation (Loeb 1954)

$$\frac{\lambda_p}{\lambda_o} = 1 - \alpha p \tag{11}$$

and the Maxwell-Eucken equation (Belle et al. 1967).

$$\frac{\lambda_p}{\lambda_o} = \frac{1 - p}{1 + \beta p} \tag{12}$$

where p is the pore fraction and α and β are porosity correction factors that depend on the pore shape, size, and distribution.

Springer et al. (1967) used the Maxwell-Eucken equation to describe the effect of porosity on their data. The porosity correction factor (β) was found to vary as a function of composition:

$$\beta = \frac{1 + 0.092W}{0.67 + 0.282W} \tag{13}$$

where W is the composition in terms of wt% UO_2. The thermal conductivities calculated using Equations 9, 12 and 13 are within 5% of the measured data shown in Figures 11a and 11b. Springer and Lagedrost (1968) found that their data was in good agreement with β determined by Equation 13.

Marino (1970; 1971) attempted to estimate the porosity correction factor β of Equation 12 by using the Fricke (1924) analysis for the thermal conductivity of a material containing a random distribution of isolated ellipsoids, i.e., pores. The porosity correction factor β was described as a function of the conductivity of the pores, the axial ratio of the pores, and temperature.

Assuming a constant pore gas composition, Marino (1970; 1971) analyzed the ThO_2-10 wt% UO_2 data of Springer et al. (1967) at three different porosities. The axial ratio of the pores was varied to seek the best fit for β that would give consistent λ_o values, i.e., all λ_o calculated for each measured λ_p at a constant temperature would be within 9% (experimental error of the data) of each other. A unique solution for β could not be found for the data; instead, a wide range of β values as shown in Figure 17 gave satisfactory results.

Marino (1970; 1971) measured the axial ratio of the pores from the photomicrographs of a 93% dense ThO_2-10 mole% UO_2 specimen and found a unique solution for the porosity correction factor. As a function of temperature, β ranged from 0.47 at 300°C to 0.31 at 1600°C. The axial ratio, and therefore β, could not be determined for densities less than 90% TD because of interconnecting pores.

Berman et al. (1972) applied the method outlined by Marino to the data from Springer et al. (1967) and Springer and Lagedrost (1968). This analysis yielded unique porosity correction factors (β) ranging from 1.25 at 400°C to 1.10 at 2200°C.

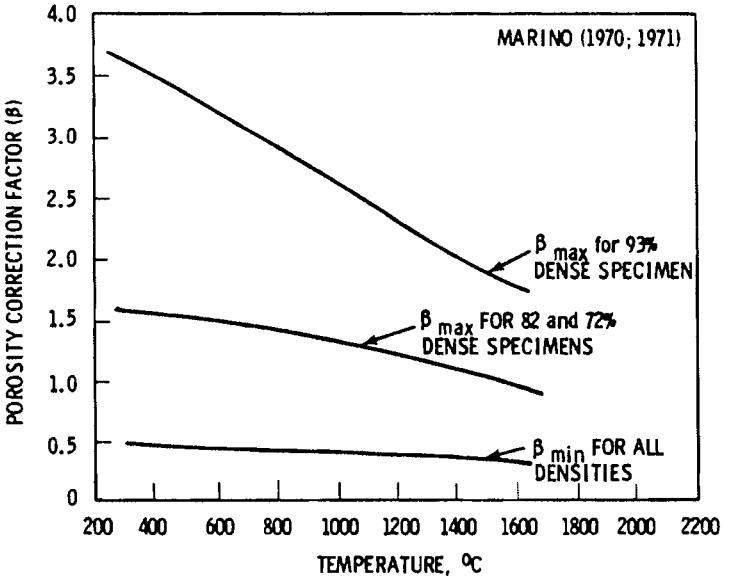

FIGURE 17. Porosity Correction Factor (β) Range for 93%-, 82%-, and 72%-Dense ThO_2-10 wt% UO_2 Versus Temperature

Murabayashi et al. (1969) found that their data for the thermal conductivity of ThO_2 best fit a modified Maxwell equation of the form

$$\frac{\lambda_p}{\lambda_o} = \frac{(2 - 3p_f)(1 - p)}{2 + p} \tag{14}$$

where p is the pore fraction and

$$p_f = 1 - (1 - p)^n \tag{15}$$

where n is an empirical constant equal to 2.4 for this data. A more detailed analysis of this paper is not warranted because: 1) these experiments were carried out at a composition (pure thoria) and temperature (20°C) that have little value for nuclear fuel applications, and 2) the small test sample (11 data points) and a narrow porosity range (<5%) may have biased the results.

Although the porosity correction factors for Equation 12 determined by Springer et al. (1967) (1.5, 0.55, and 0.45 for 0-, 10-, and 20-wt% UO_2, respectively), Marino (1970, 1971) (0.3 to 0.5), and Berman et al. (1972) (1.1 to 1.25) differ markedly, these values represent a difference of only 3 to 4% in λ_p's calculated from λ_o for porosities of less than 10%. Differences in thermal conductivity of 3 to 4% are considered small; however, because of the larger quantity of data analyzed, the effect of porosity is probably best described by Berman et al. (1972), but only for the data analyzed.

Effect of Radiation on Thermal Conductivity

In general, the thermal conductivity is expected to decrease as a material is irradiated. This decrease is attributed to radiation damage to the lattice, and pellet cracking. The thermal conductivity measurements of irradiated and unirradiated materials can be approximately equal when the lattice damage is annealed during irradiation at high temperatures or thermal cycling as would occur during out-of-pile thermal conductivity measurements.

Jacobs (1970) compared the unirradiated and in-pile-irradiated thermal conductivities of ThO_2-10 wt% UO_2 in Figure 18 under the conditions shown

in Table 5. The data were fitted to Equation 8 and the thermal conductivity of the unirradiated specimen (λ_{un}) varied with temperature, T(^{o}C), as shown in Equation 16:

$$\lambda_{un} = (8.4703 + 0.02551T)^{-1} \qquad (16)$$

TABLE 5. Experimental Conditions for Thermal Conductivity Measurements for Irradiated Fuels

Reference	Fuel Composition, mole% UO_2	Burnup, 10^{18} fission/cm^3	Average Irradiation Temperature, ^{o}C	Measurement Method	Conductivity Temperature Range, ^{o}C
Jacobs (1970)	10	0.26	600	in-pile, radial heat flow method	300 to 900
Matolich and Storhok (1970)	3	2.3	900	out-of-pile flash laser method	300 to 1200
	7	2.3	725		300 to 1200
	10	27.4	1260		300 to 1100
	15	400.0	NR(a)		300 to 1200

(a) Not reported

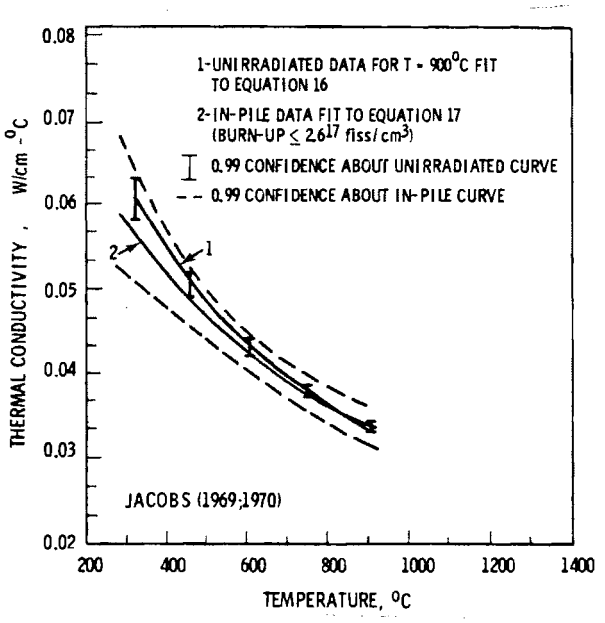

FIGURE 18. In-Pile-Irradiated and Unirradiated Thermal Conductivity of ThO_2-10 wt% UO_2

The thermal conductivity of the irradiated specimen (λ_{irr}) varied with temperature, T(^{o}C), as shown in Equation 17:

$$\lambda_{irr} = (10.5181 + 0.02003T)^{-1} \qquad (17)$$

Jacobs concluded that there is no statistical difference at the 0.99 confidence level between the thermal conductivity of unirradiated ThO_2-10 wt% UO_2 and ThO_2-10 wt% UO_2 irradiated to 0.26 x 10^{18} fissions/cm^3.

Matolich and Storhok (1970) measured the thermal conductivities of three irradiated ThO_2-UO_2 compositions by the flash laser technique. These measurements were made out-of-pile under the conditions given in Table 5. No significant difference between the unirradiated and irradiated measurements was observed for the ThO_2-3 wt% UO_2 compositions. Matolich and Storhok concluded that this was due to the high irradiation temperature, where the lattice damage was annealed.

In contrast, the post-irradiation conductivity of ThO_2-15 wt% UO_2 was lower than the unirradiated conductivity. Even after thermal cycling between 300 and 1200^{o}C, the λ_{irr} was still approximately 55% below λ_{un}. The lack of an annealing effect was attributed to the high burnup (400 x 10^{18} fissions/cm^3).

The thermal conductivity of irradiated ThO_2-10 wt% UO_2 was higher than that of the unirradiated material. Matolich and Storhok (1970) attributed this anomalous result to the presence of large columnar grains, which are believed to increase the thermal conductivity of the material. Annealing during measurement had no effect on the thermal conductivity, but this was expected because of the high irradiation temperature. These results indicate that the effect of irradiation on thermal conductivity is not well understood and requires further evaluation.

Berman et al. (1972) attempted to fit the data of Jacobs (1969, 1970) and Matolich and Storhok to

$$\lambda_{irr}^{-1} = \lambda_{un}^{-1} + \frac{C + DF}{T} \qquad (18)$$

where T is the temperature (K), F is the burnup x 10^{-20} in fissions per cubic centimeter, and C and D are empirically determined constants. The analysis was complicated by variations in fission product content and in pore gas content within the sample. Berman et al. could only suggest using 17.3 and 5.92 as estimates for the constants C and D, respectively.

Effects of Stoichiometry on Thermal Conductivity

In general, as the deviation from stoichiometry increases, the thermal conductivity of polycrystalline materials decreases. This decrease is attributed to a decrease in the lattice periodicity which reduces the phonon mean free path.

Kingery (1959b) measured the thermal conductivity of stoichiometric and non-stoichiometric composition containing 26 mole% UO_2. The non-stoichiometric composition was prepared by heating sintered specimens in air at 500°C for an unspecified period of time. The stoichiometry of this sample was not evaluated. Kingery found the thermal conductivity of the stoichiometric compositions was higher then the nonstoichiometric compositions. The difference between the two data sets was at least 10% and varies with temperature. From these data, thermal conductivity as a function of stoichiometry cannot be determined.

No other data describing the effect of stoichiometry on the thermal conductivity of ThO_2-UO_2 compositions has been reported.

Thermal Conductivity - Summary and Evaluation

At present, the equations

$$\lambda_o = \left[A_0 + A_1U + A_2U^2 + (B_0 + B_1U + B_2U^2)\right] T^{-1} \qquad \text{(same as 10)}$$

and

$$\lambda_p = \lambda_o \frac{1-p}{1+\beta p} \qquad \text{(same as 12)}$$

most accurately describe the effect of absolute temperature (T), composition (U), and pore fraction (p) on the thermal conductivity of ThO_2-UO_2 solid solutions.

The values for the constants A_0, B_0, etc., are listed in Table 4, and an average porosity correction factor (β) was found to lie between 1.25 at 400°C and 1.10 at 2200°C. These equations describe the thermal conductivity of solid solutions up to 30 wt% UO_2, but are only within 10% of the experimentally determined data. Sufficient data are not available to describe the effect of UO_2 above 30 wt%.

Although there are not enough data to determine the effect of radiation on conductivity, there is some evidence to suggest that at high irradiation temperatures the radiation damage is annealed, and the thermal conductivities of irradiated and unirradiated materials are approximately equal. The effect of radiation on thermal conductivity should be studied in greater detail.

The effect of stoichiometry on thermal conductivity has not been adequately described for ThO_2-UO_2 compositions.

Thermal conductivity is affected by such material characteristics as porosity (including pore fraction, shape, and distribution) and impurity level. These variables are generally determined by the fabrication procedure and are unique to a given specimen. Therefore, once a standard fabrication procedure is adopted, a limited study of the thermal conductivity of ThO_2-UO_2 compositions containing up to 30 wt% UO_2 should be made to determine if the data vary from the equations derived from the literature data. Additional data will have to be generated if the thermal conductivity of compositions containing more than 30 wt% UO_2 are of interest.

3.1.3 Diffusion

From the viewpoint of fuel swelling, densification and thermal migration of cation and anion species, diffusion properties of fuel components are important to fuel performance. In this section, the diffusion of Th, U, and O in $(Th_{1-x}U_x)O_2$ will be discussed.

There are two major diffusion paths in polycrystalline materials. Diffusion taking place through the individual grains is defined as lattice diffusion, while faster, short-circuit diffusion will occur along grain boundaries and dislocations. Diffusion through single crystals is usually equated with lattice

diffusion unless a substructure is present. When a reported diffusion coefficient includes the contributions of more than one path, it is called the apparent diffusion coefficient. An attempt is made in this review to indicate when more than one process may have contributed to the reported diffusion coefficient.

Measured diffusion rates are dependent on material properties such as defect concentration, impurities (not only the amount but the physical properties of each, such as ionic radius and valency), grain size, grain boundary size, and dislocation concentration. Calculated diffusion coefficients may be accurate only for the specimen on which it is measured, making it difficult to compare the results of various investigators. In this section the "best data" will not be identified; instead, the data will be displayed graphically.

Techniques For Measuring Diffusion

Diffusion is measured by determining the concentration of the diffusing species as a function of time, temperature, and diffusion distance. For ThO_2 and UO_2, cation diffusion is measured by depositing a radioactive tracer isotope of the cation on the surface of the bulk specimen. The specimen is annealed and the concentration of the diffusion species is measured by sectioning, alpha-ray spectrometry, or surface activity decrease. These techniques are described by Kingery (1959a) and Alcock et al. (1966).

The diffusion of oxygen is generally measured by the gas-solid isotopic exchange method, whereby the rate of exchange of an oxygen isotope with the solid is used to determine the oxygen diffusion coefficient.

Diffusion of Thorium in ThO_2

Poteat and Morgan (1968) measured the diffusion coefficient of ^{230}Th in single and polycrystalline ThO_2 by alpha-ray spectrometry. Table 6 gives the experimental conditions for diffusion measurements made by Poteat and Morgan and other researchers.

Poteat and Morgan report that, because of the grain boundary contribution, the diffusion coefficient in the polycrystalline specimens is slightly greater than in the single crystals. Figure 19 shows the Poteat and Morgan data. The

TABLE 6. Experimental Conditions for the Diffusion of Various Atoms in $(Th_{1-x}U_x)O_{2+y}$

Reference	Diffusing Atom	Host Lattice	Method	Type of Diffusion Measured
Poteat and Morgan (1968)	Th	ThO_2 (a)	^{230}Th tracer, α-ray spectrometry	apparent
Poteat and Morgan (1968)	Th	ThO_2 (b)	^{230}Th tracer, α-ray spectrometry	apparent
Hawkins and Alcock (1968)	Th	ThO_2 (b)	^{230}Th tracer, α-ray spectrometry	apparent
King (1971)	Th	ThO_2 (a)	^{228}Th tracer, sectioning	lattice
King (1971)	Th	ThO_2 (a)	^{228}Th tracer, sectioning	dislocation via subgrains
Furuya (1968)	U	ThO_2 (b)	^{237}U tracer, α-ray spectrometry	lattice
Furuya (1968)	U	ThO_2 (b)	^{237}U tracer, α-ray spectrometry	grain boundary
Furuya (1968)	U	$(Th_{0.5}U_{0.5})O_2$ (b)	^{237}U tracer, α-ray spectrometry	lattice
Furuya (1968)	U	$(Th_{0.5}U_{0.5})O_2$ (b)	^{237}U tracer, α-ray spectrometry	grain boundary
Matzke (1967)	U	ThO_2 (b)	^{233}U α-ray spectrometry	apparent
Edwards et al. (1963)	O	ThO_2 (b)	^{18}O, gas-solid exchange	lattice
Ando et al. (1976)	O	ThO_2 (a)	^{18}O, gas-solid exchange	lattice
Lee and Alcock (1971)	Th and U	$(Th_{0.25}U_{0.75})O_{2+y}$ (b)	^{230}Th and ^{233}U tracers, α-ray spectrometry	apparent
Lee and Alcock (1971)	Th and U	$(Th_{0.5}U_{0.5})O_{2+y}$ (b)	^{230}Th and ^{233}U tracers, α-ray spectrometry	apparent

(a) Single crystal
(b) Polycrystalline

TABLE 6. (contd)

Reference	Temperature Range °C	Atmosphere	Diffusion Coefficient (D_o),[a] cm /s	Activation Energy (Q) kcal/mol
Poteat and Morgan (1968)	1300 to 2300	air (<1800°C) argon (>1800°C)	2.0×10^{-7}	74.0
Poteat and Morgan (1968)	1300 to 2200	air (<1800°C) argon (>1800°C)	2.6×10^{-7}	69.0
Hawkins and Alcock (1968)	1600 to 2100	air (10^{-20} to $10^{-0.7}$ atm PO_2)	1.25×10^{-7}	58.8
King (1971)	1850 to 2050	NR[b]	0.35	149.5
King (1971)	1850 to 2050	NR	8×10^{-14}[c]	37.3
Furuya (1968)	1800 to 2000	NR	1.1×10^{-4}	76.4
Furuya (1968)	1800 to 2000	NR	2.35×10^{-9}[c]	47.9
Furuya (1968)	1800 to 2300	NR	7.59×10^{-4}	85.9
Furuya (1968)	1800 to 2300	NR	1.04×10^{-7}[c]	64.2
Matzke (1967)	1400 to 1550	H_2	$D = 2 \times 10^{-14}$ (1400°C) $D = 2 \times 10^{-15}$ (1550°C)	NR
Edwards et al. (1963)	850 to 1550	NR	4.4	65.8
Ando et al. (1976)	845 to 1646	NR	1×10^{-6} (1100°C) 5.73×10^{-2} (1100°C)	17.6 49.9
Lee and Alcock (1971)	1400	CO/CO_2	NR	NR
Lee and Alcock (1971)	1400	CO/CO_2	NR	NR

(a) $D = D_o \cdot e^{-Q/RT}$
(b) NR = not reported
(c) For grain boundary diffusion the grain boundary width (in cm) is included in the diffusion coefficient and the units become cm^3/s.

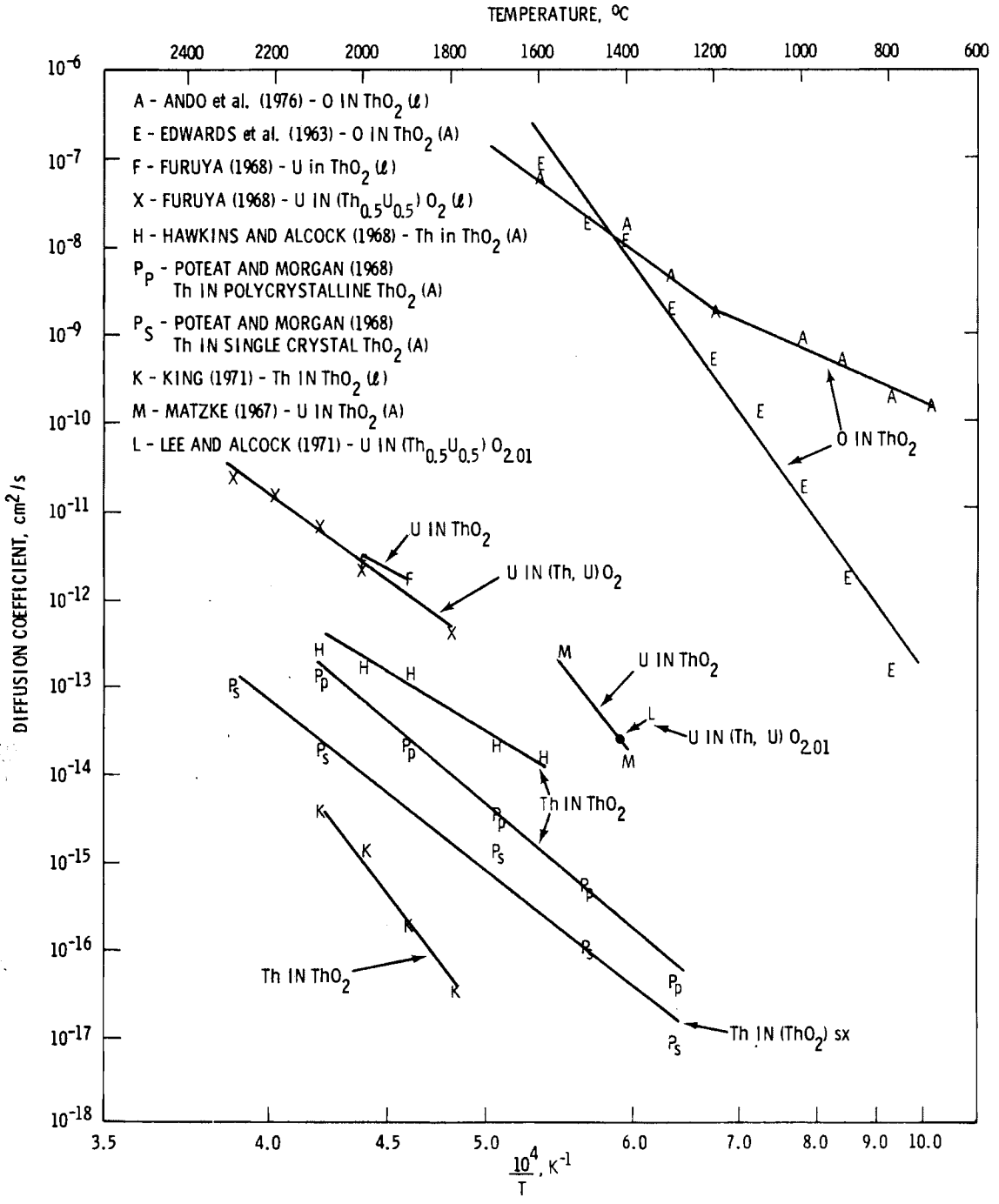

FIGURE 19. Diffusion Coefficient as a Function of Temperature (A - Apparent Diffusion Coefficient, ℓ - Lattice Diffusion Coefficient, sx- single crystal)

microstructure of the single crystals was not examined to determine if a substructure had developed that could have affected the diffusion rate. They also observed that at constant temperature, as the diffusion distance increased, the diffusion coefficient increased for both polycrystalline and single-crystal specimens. Although Poteat and Morgan did not attempt to explain this behavior, it may be concluded that they observed lattice diffusion near the surface and some type of short circuit diffusion as the diffusion distance increased. Therefore their diffusion coefficients should be considered to be apparent rather than lattice values.

Hawkins and Alcock (1968) measured the diffusion of ^{230}Th in polycrystalline thoria by alpha-ray spectrometry. Their data is within one order of magnitude of the data of Poteat and Morgan shown in Figure 19. Hawkins and Alcock also found that thorium diffusion is independent of oxygen pressure, indicating that ThO_2 does not deviate from stoichiometry. Hawkins and Alcock felt that they measured lattice diffusion coefficients. They reasoned that the grain boundary contribution was a very small portion of the total diffusion due to the large grain size (100 μm) of the specimens. However, they did not attempt to quantify the grain boundary contribution; therefore, these data are interpreted as apparent diffusion coefficients.

King (1971) found the lattice diffusion of thorium in single crystal ThO_2 to be one to two orders of magnitude below the data of Poteat and Morgan (1968) and Hawkins and Alcock (1968). King attributes this difference to the sectioning technique he used and the failure of Poteat and Morgan and Hawkins and Alcock to sufficiently analyze their data for the contributions of grain boundary and dislocation diffusion. Most sectioning techniques are only accurate to 0.5 μm; however, King states that using his technique he is able to obtain sections of 0.04 μm (400 Å), enabling him to differentiate between lattice diffusion at small diffusion distance (x) and short circuit diffusion through the dislocation substructure as x increases. King considers his data to represent lattice diffusion.

The wide range of diffusion coefficients reported for thorium in ThO_2 (Figure 19) occurs because of the different physical characteristics of each specimen studied, various measuring techniques, and the varying contributions of lattice, surface, and grain boundary diffusion.

Diffusion of Uranium in ThO_2

Furuya (1968) measured the diffusion of ^{237}U by alpha-ray spectrometry in polycrystalline ThO_2. His results were one to four orders of magnitude greater than the diffusion of thorium in thoria as shown in Figure 19. Furuya observed that the concentration versus diffusion distance (x) exhibits a tail at large x which, Furuya reasoned, was caused by grain boundary diffusion. By extrapolating the tail of the curve to smaller x, the grain boundary portion of the apparent diffusion coefficient could be subtracted to give the lattice diffusion coefficient. Furuya found that, depending on the grain boundary size, the grain boundary diffusion of uranium was one to two orders of magnitude greater than lattice diffusion.

Matzke (1967) measured the apparent diffusion of ^{233}U in polycrystalline ThO_2 as a part of a study of Xe gas migration. At 1600°C Matzke's data intersect the extrapolated data of Furuya (Figure 19); however, the two data sets have different slopes.

At present, reported diffusion coefficients for cations in ThO_2 cover a wide range of values. Additional experimental work is required for a more accurate definition of the diffusion coefficient of Th and U in ThO_2.

Diffusion of Oxygen in ThO_2

Edwards et al. (1963) measured the apparent diffusion of ^{18}O by the gas-solid exchange method in polycrystalline thoria under the experimental conditions given in Table 6. Their results (Figure 19) reveal that the diffusion coefficient of oxygen is six to eight orders of magnitude greater than the diffusion of thorium. Edwards et al. made no attempt to separate lattice and grain boundary diffusion. They believe the diffusion of oxygen is controlled by intrinsic defects with a large concentration of anion defects resulting in the greater oxygen diffusion rate relative to cation diffusion.

Ando et al. (1976) measured the lattice diffusion of oxygen by the gas exchange method in single-crystal ThO_2 and observed that oxygen diffusion was not affected by either annealing the specimen at 1550°C before the diffusion experiment or by the specimen size. Ando et al. found a change in slope (activation energy) between 1100°C and 1200° as shown in Figure 19.

Below 1100°C, they concluded that the diffusion is controlled by extrinsic defects and above 1100°C by intrinsic defects, especially Frenkel-type defects.

Above 1100°C the data of Edwards et al. (1963) and Ando et al. (1976) are in good agreement (Figure 19). However, below 1100°C the difference in the data increases as temperature decreases. This difference could be due to different impurity levels of the diffusion specimens, whereby the impurities would affect the extrinsic defect concentration, which Ando et al. believe controls diffusion below 1100°C.

Based on these data, the diffusion coefficient of oxygen in ThO_2 was judged to be six or more orders of magnitude greater than the diffusion coefficients of either thorium or uranium.

Diffusion of Uranium in ThO_2-UO_2 Solid Solutions

The lattice diffusion coefficient of uranium in polycrystalline $(Th_{0.5}U_{0.5})O_2$ measured by Furuya (1968) is shown in Figure 19. As described previously, Furuya separated grain boundary diffusion from lattice diffusion. The lattice diffusion coefficients Furuya reported for uranium in $(Th_{0.5}U_{0.5})O_2$ are approximately equal to the ones he measured for uranium in ThO_2; however, to conclude that the diffusion coefficients of uranium in all ThO_2-UO_2 solid solutions are equal would be premature. Furuya found that the grain boundary diffusion was one to two orders of magnitude greater than the lattice diffusion, depending on the grain boundary size.

Lee and Alcock (1971) measured the diffusion of uranium and thorium in ThO_2-UO_2 solid solutions at 1400°C as a function of ThO_2 content (50 and 25 mole% ThO_2) and stoichiometrics of 2.01 to 2.19. The experimental details are given in Table 6. They found the diffusion coefficients of thorium and uranium in the solid solution specimens to be approximately equal. Although there is considerable scatter in their data shown in Figure 20, they determined that the diffusion coefficient (D) of thorium or uranium in $(Th_{1-x}U_x)O_{2+y}$ can be described by

$$\log D = \frac{2}{5} \log \frac{y}{x-y} + C(T) \qquad (19)$$

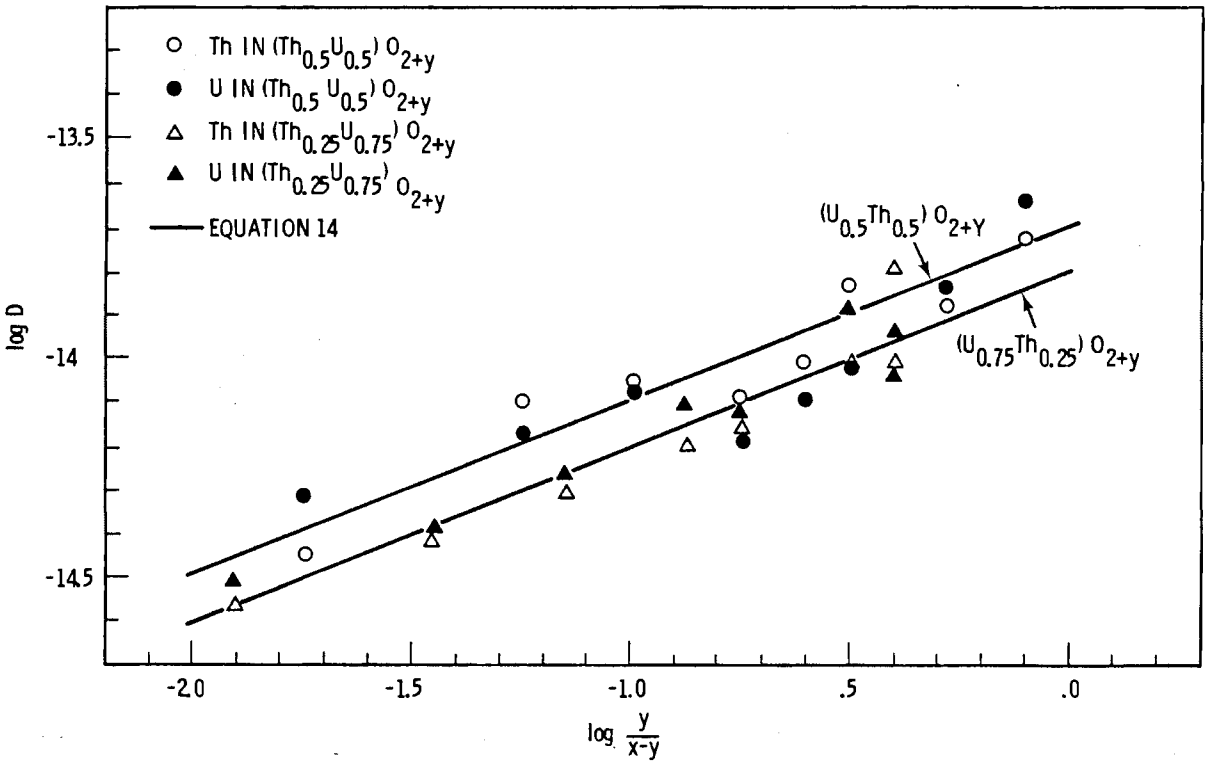

FIGURE 20. Diffusion Coefficient of Th and U as a Function of Composition and Stoichiometry at 1400°C for $(Th_{1-x}U_x)O_{2+y}$

where C(T) is a constant for a given temperature and y is the deviation from stoichiometry. Although Lee and Alcock did not give the C(T) values for the two compositions tested, the value of C(T) estimated from Figure 20 is approximately -13.8 for $(Th_{0.25}U_{0.75})O_{2+y}$ and -13.7 for $(Th_{0.5}U_{0.5})O_{2+y}$.

Lee and Alcock (1971) attributed the observed increase in D as y increased and x decreased (shown in Figure 20) to the formation of a U^{5+}-O_i-U^{5+} defect complex. The increase in interstitial oxygen (O_i) concentration leads to increased cation vacancies and cation diffusion coefficients.

For near-stoichiometric compositions (y = 0.01), Equation 19 predicts a diffusion coefficient for $(Th_{0.5}U_{0.5})O_{2.01}$ that is within an order of magnitude of the data of Furuya extrapolated to 1400°C. No other data are available to check the accuracy of Equation 19.

It should be kept in mind that Equation 19 was determined at one temperature from only two solid solution compositions $(Th_{0.25}U_{0.75})O_{2+y}$ and $(Th_{0.5}U_{0.5})O_{2+y}$ and may not accurately describe the entire range of solid solutions.

Equation 19 is also limited mathematically and should only be used within the experimental limits ($x \geq 0.5$, $0.01 < y < 0.19$) for which it was determined. For stoichiometric compositions, the diffusion coefficient cannot be determined by Equation 19.

Diffusion of Oxygen and Thorium in ThO_2-UO_2 Solid Solutions

No studies have been made concerning the diffusion of oxygen in ThO_2-UO_2 solid solutions. Other than Lee and Alcock (1971), discussed in the section on uranium diffusion in solid solutions, no researchers have studied thorium diffusion in solid solutions of ThO_2-UO_2.

Diffusion - Summary and Evaluation

The self-diffusion of oxygen is six to seven orders of magnitude greater than the diffusion of thorium or uranium in ThO_2. Therefore, diffusionally controlled processes such as sintering in ThO_2-based systems will be rate limited by the diffusion of the cation.

Data concerning the diffusion properties of thoria-urania solid solutions are very limited. Limited evidence exists to show that the rates of diffusion of uranium and thorium in solid solutions are approximately equal. The diffusion of oxygen in ThO_2-UO_2 solid solutions has not been studied. A large body of data is available to describe cation diffusion in ThO_2, but as with many oxide systems, these data exhibit a large amount of scatter. Cation diffusion of ThO_2-UO_2 should be studied in greater detail. This would be helpful in understanding the sintering and fission gas release properties of ThO_2-UO_2 solid solutions.

3.2 CHEMICAL AND THERMODYNAMIC PROPERTIES

This report section reviews studies of the lattice parameter, density, solid solution formation, and stoichiometry of ThO_2-based fuels. This section also discusses various thermodynamic properties, including heat capacity and vapor pressure.

3.2.1 Crystal Structure and Lattice Parameter

It is well documented that both ThO_2 and stoichiometric UO_2 crystallize in the cubic fluorite crystal structure. The unit cell consists of a face-centered cubic array of thorium (or uranium) ions with oxygen occupying one-half of the available tetrahedral sites. There are four molecules of ThO_2 (or UO_2) per unit cell.

Kempter and Elliott (1959), Mauer and Bolz (1955), and Brown and Chitty (1960) all found the ThO_2 lattice parameter at 25°C to be 5.5971 Å. Cohen and Berman (1966) and Swanson and Tatge (1953) report values of 5.5975 Å and 5.5997 Å, respectively. A lattice parameter of 5.5971 Å appears to be the best value for ThO_2.

Christensen (1963) found that as the UO_2 content increased, the lattice parameter decreased and closely approximated Vegard's law up to 95 wt% UO_2 (Figure 21). Christensen observed anomalous behavior in the lattice parameter above 95 wt% UO_2.

Cohen and Berman (1966) measured the lattice parameter over the entire range of ThO_2-UO_2 solid solutions after quenching specimens from 1200°C to room temperature. They found the lattice parameter (a_o) for $(Th_{1-x}U_x)O_{2+y}$ to vary with UO_2 content (x) and deviation from stoichiometry (y) as

$$a_o = 5.5975 - 0.127x - 0.09y - 0.1xy \qquad (20)$$

for compositions containing less than 50 mol% UO_2 and

$$a_o = 5.5975 - 0.127x - 0.140y \qquad (21)$$

for compositions containing between 50 mol% and 95 mol% UO_2. These equations fit Cohen's and Berman's data to 0.2% for single-phase cubic solid solutions. For stoichiometric compositions, the equations derived by Cohen and Berman are in good agreement with the data of Christensen. Christensen only presented his data graphically; therefore, a statistical comparison of his work with Cohen's and Berman's was not made. Above 95 mol% UO_2, Cohen and Berman observed anomalous behavior similar to Christensen (1963).

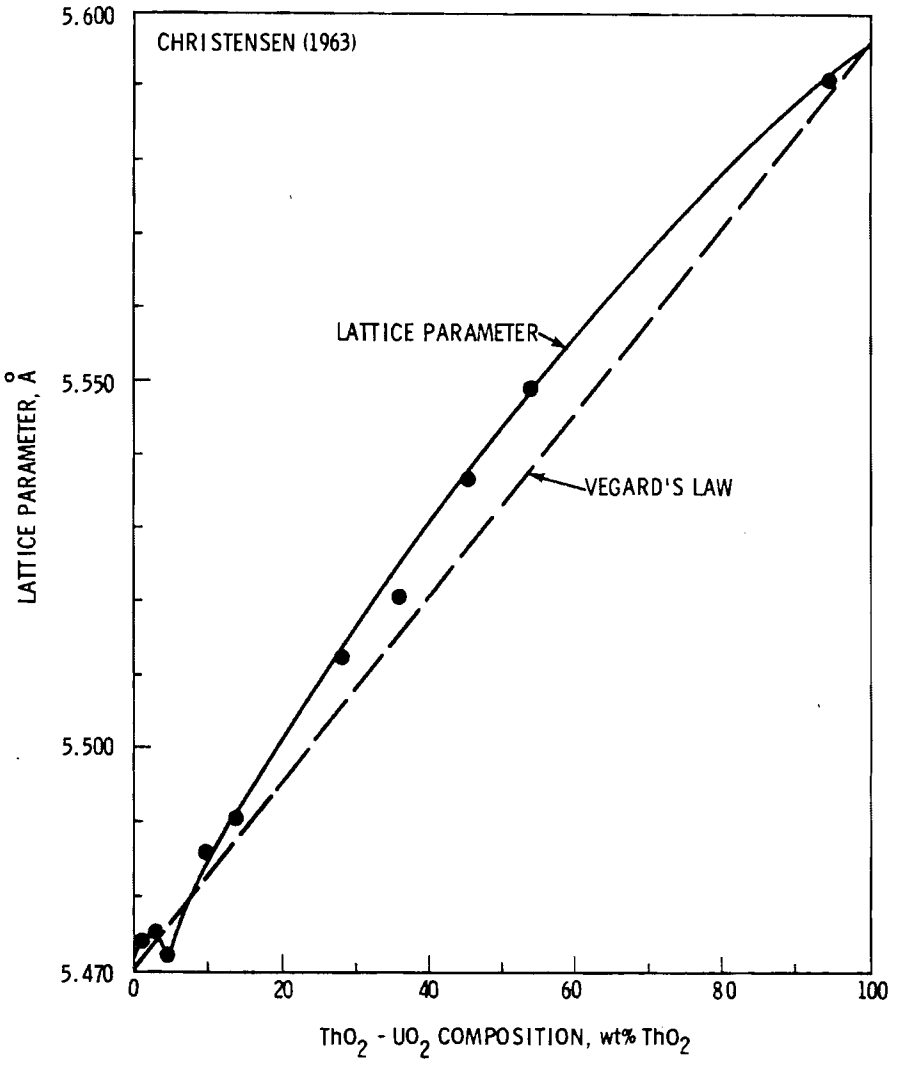

FIGURE 21. Lattice Parameter as a Function of UO_2 Content at 25°C

3.2.2 Density

The theoretical density (ρ_0) of a material may be calculated from a knowledge of its crystal structure, composition, and lattice parameters using the equation:

$$\rho_0 = \frac{N(\Sigma F_i M_i)}{VA} \qquad (22)$$

where N is the number of atoms per unit cell, F_i is the atom fraction of each constituent, M_i is the atomic weight of each constituent, A is Avogardo's number (6.02×10^{23}), and V is the volume of the unit cell in cm^3. For cubic structures $V = a^3$ where a is the lattice parameter. Based on a lattice parameter of 5.5971 Å, the theoretical density of ThO_2 calculated by Equation 22 is 10.002 g/cm^3.

The variation of density with temperature of a solid can be determined by:

$$\rho_T = \frac{\rho_0}{(1 + \Delta\ell/\ell_0)^3} \qquad (23)$$

where ρ_0 and ρ_T are the densities at a reference temperature and some temperature, T, respectively, and $\Delta\ell/\ell_0$ is the linear thermal expansion. For ThO_2, $\Delta\ell/\ell_0$ can be determined by Equation 4.

Cohen and Berman (1966) measured the lattice parameter of $(Th_{1-x}U_x)O_2$ at 25°C and calculated the theoretical density as a function of UO_2 content using Equation 22; Figure 22 shows their data. The anomalous lattice parameters at compositions above 95 wt% UO_2 were not considered in these calculations.

The effect of temperature on the density of ThO_2-UO_2 solid solutions cannot be determined until the effect of composition on thermal expansion data is reanalyzed. When this analysis is complete, Equation 23 can be used to determine the density as a function of composition and temperature.

3.2.3 Solid Solution Formation

Thoria and urania meet all of the criteria to form complete series of solid solutions:

- identical crystal structure
- cation radii within 10% of being equal
- equal valence.

A number of investigators have shown that ThO_2 and UO_2 form solid solutions of the substitutional type where uranium is substituted for thorium.

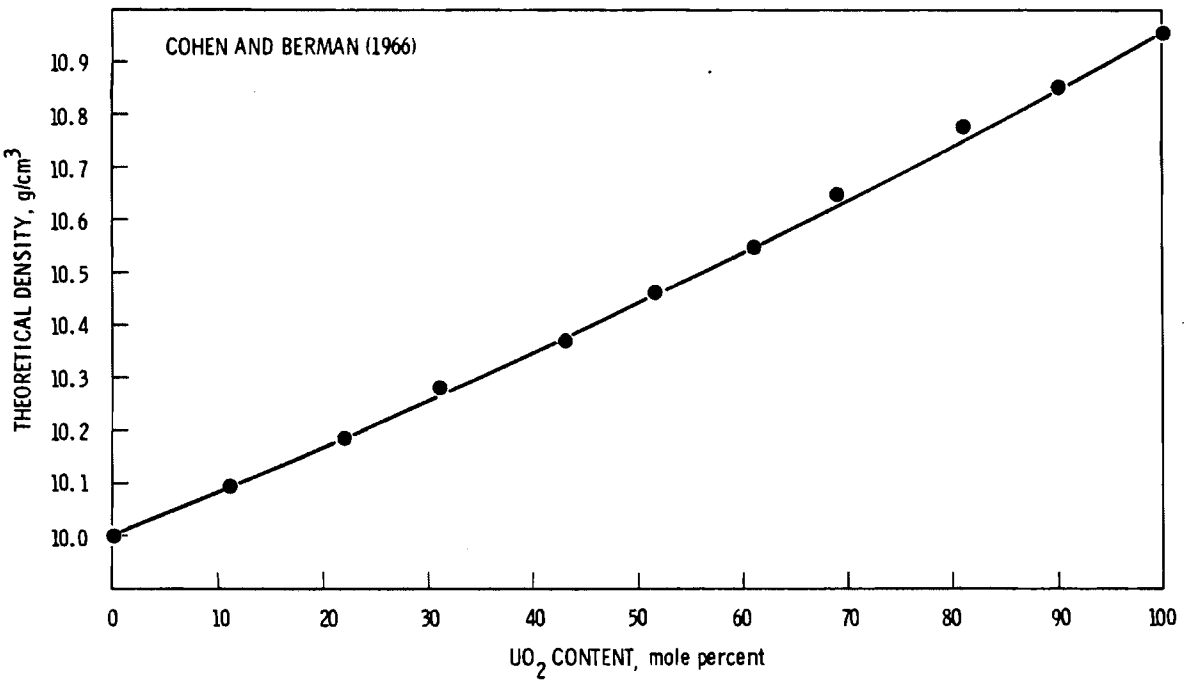

FIGURE 22. Theoretical Density of ThO_2-UO_2 Compositions as a Function of UO_2 Content at 25°C

With an exception of anomalous behavior at compositions containing more than 95 wt% UO_2, Christensen (1963) and Cohen and Berman (1966) found that ThO_2 and UO_2 form a complete series of solid solutions. Although this anomalous behavior has not been explained, Cohen and Berman maintain that it is due to the formation of U_4O_9.

Anderson et al. (1954) studied the x-ray diffraction patterns of a wide range of compositions as a function of temperature. Table 7 lists the preparation and experimental conditions for this solid solution study as well as the other studies discussed earlier. Anderson et al. found that the fluorite structure was the stable phase for all compositions below 200°C regardless of the experimental conditions. Above 200°C, stoichiometric compositions were stable in the fluorite structure; however, with compositions above 50 mol% UO_2, oxidizing conditions resulted in other crystalline phases. These conditions produced nonstoichiometric compositions and will be discussed in the section on stoichiometry.

TABLE 7. Preparation and Experimental Conditions for Solid Solution Formation Studies

Reference	Composition, mole % UO_2	Sintering Conditions			Oxidation Conditions			Comments
		Temp, °C	Time, h	Atmosphere	Temp, °C	Time, h	Atmosphere	
Cohen and Berman (1966)	0 to 100	1750	48 to 100	H_2	500 to 1320	0.5 to 72	Steam and air	Homogenized in argon at 1200°C for 72 to 240 h
Anderson et al. (1954)	1 to 100	1700 to 2100	NR[a]	vacuum	100 to 900	NR	0.07 to 120 atm of oxygen	
Lynch (1965)	2.5 10.0 30.0 50.0 70.0 90.0	1200 to 1650	18	H_2	0 to 1200	48	Air	Sintered samples were crushed, reduced in H_2 atmosphere to the stoichiometric composition, and then oxidized.

(a)NR = Not reported

3.2.4 Stoichiometry of ThO_2 and $(Th_{1-x}U_x)O_{2+y}$

In contrast to UO_2, thoria does not deviate measurably from the stoichiometric composition of ThO_2. Hawkins and Alcock (1968) measured the cation diffusion in ThO_2 and found it to be independent of oxygen pressure. From this they concluded that ThO_2 does not deviate from stoichiometry.

Cohen and Berman (1966) determined thermogravimetrically that the solubility of oxygen in ThO_2 at 1200°C is zero; i.e., $y = 0$. The lack of oxygen solubility was attributed to the inability of the thorium ions to change from a 4+ to a higher valency in order to balance the charge of the excess oxygen.

Lynch (1965) measured by weight change the deviation from stoichiometry in air as a function of the oxidation temperature (0 to 1200°C) for various stoichiometric compositions of $(Th_{1-x}U_x)O_2$; Table 7 lists the experimental conditions. In general Lynch found that the deviation from stoichiometry (y) increased as the UO_2 content (x) increased, approaching a maximum at 400°C as shown in Figure 23. The oxygen solubility decreased as the oxidation temperature increased above 400°C. No explanation was offered for this decrease in solubility. Lynch's data indicate that the maximum oxygen solubility increases as the sintering temperature decreases. The samples sintered at 1650°C may have had less free UO_2 than those sintered at 1200°C. The amount of free UO_2 could have affected the oxygen solubility.

Cohen and Berman (1966) showed that when compositions containing less than 50 mol% UO_2 are heated in air to 1200°C (see Table 7 for the experimental conditions) the oxygen solubility is limited by the UO_2 content as shown in Figure 24.

Cohen and Berman observed that when compositions containing greater than 50 mol% UO_2 were heated in air to 1200°C the maximum O/M ratio without structural change is 2.25. When this limit is exceeded, an orthorhombic phase, identified as U_3O_8, accommodates the excess oxygen. Gilpatrick and Secoy (1966) did not observe an orthorhombic phase at 1200°C until the UO_2 content reached 60 mole%. The difference in observations has not been explained.

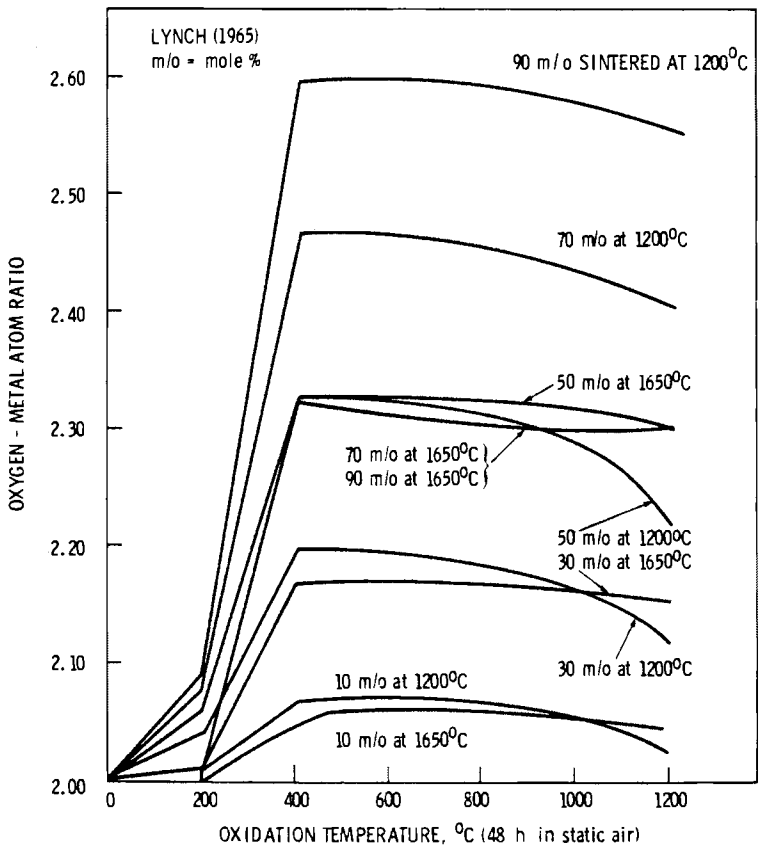

FIGURE 23. Oxidation Characteristics of Stoichiometric ThO_2-UO_2 Solid Solutions Sintered in H_2 for 18 h at 1200°C and 1650°C

Cohen and Berman (1966) found a second cubic phase when compositions containing more than 60 mol% UO_2 with O/M ratio between 2.18 and 2.25 were heated below 1200°C for 200 plus hours. They identified this phase as U_4O_9; it was not found in equilibrium with the orthorhombic phase and sometimes disappeared after additional annealing. They concluded that this was a metastable phase for which the stable phase was U_3O_8.

Cohen and Berman concluded that the oxygen enters the lattice interstitially. The number of available interstitial sites is limited by the UO_2 content, reaching a maximum number of sites at 50 mol% UO_2. Above the oxygen solubility limit in compositions containing greater than 50 mol% UO_2, orthorhombic U_3O_8 accommodates the excess oxygen, while compositions below 50 mol% UO_2 remain a single cubic phase in equilibrium with the atmosphere.

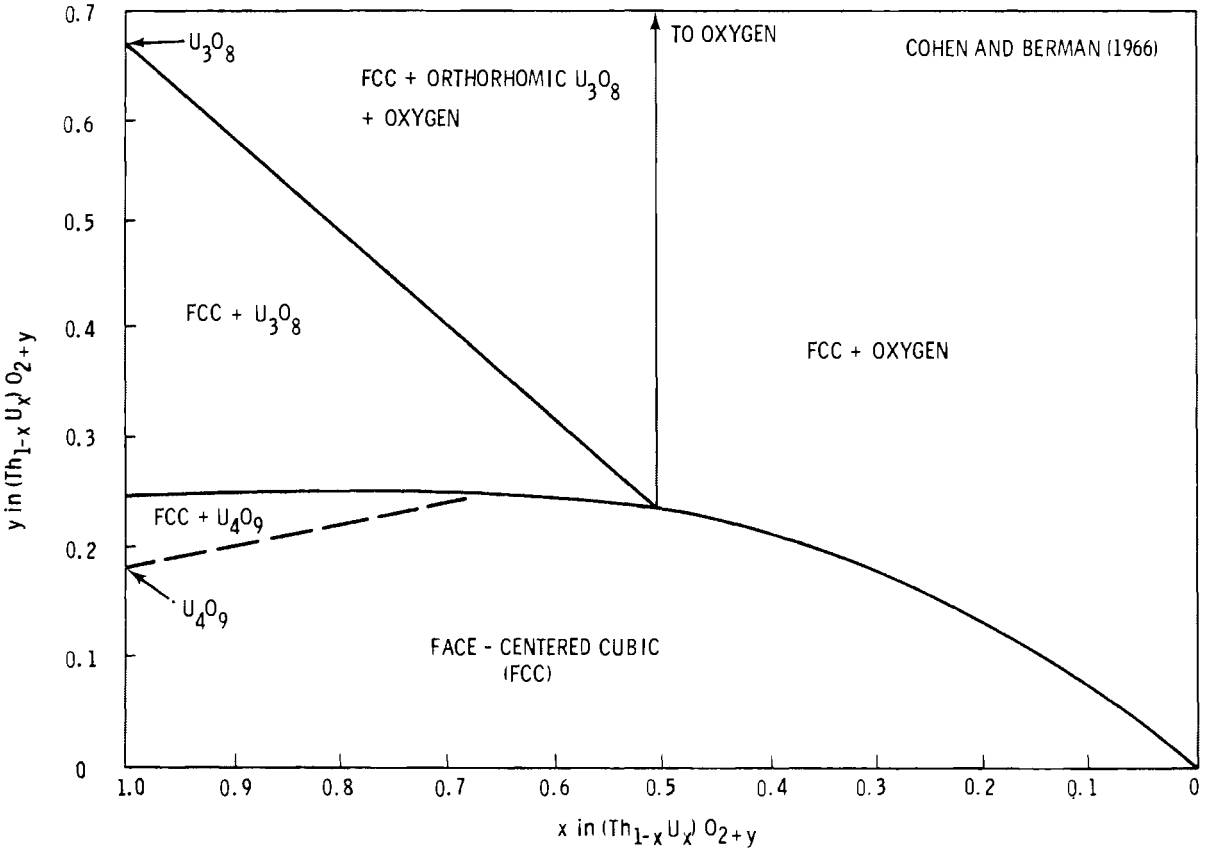

FIGURE 24. Tentative Phase Diagram of the ThO_2-UO_2 System at 1200°C

Anderson et al. (1954) agree that the oxygen solubility is dependent on the geometry of the structure and the number of interstitial sites available for oxygen occupation. However, the oxygen solubility of compositions containing greater than 50 mol% UO_2 without a phase change was found to lie between y = 0.32 and 0.34 when oxidized in air at 400°C. The difference in oxygen solubility limits found by Anderson et al. and Cohen and Berman (1966) is probably due to different preparation and experimental conditions. Above 600°C, Anderson et al. found the fluorite structure replaced by a new single-phase structure when the oxygen solubility was exceeded in compositions containing greater than 70 mol% UO_2. Anderson et al. believed this phase to be orthorhombic, but they could not completely identify it.

3.2.5 Melting Temperature

The melting temperature of ThO_2 is 3300°C ± 100°C as noted by Benz (1969) and Lambertson et al. (1953).

The melting temperature of ThO_2-UO_2 solid solutions has been studied by Christensen (1963). He found that the melting point increases as the UO_2 content decreases as shown in Figure 25.

3.2.6 Heat Capacity

Several thermodynamic functions, such as entropy and free energy, can be calculated from the heat capacity (Cp); it is also used to calculate the thermal conductivity of a material.

The heat capacity is determined from enthalpy data. A material at some high temperature is dropped into a calorimeter maintained at a low temperature (0 to 35°C). The heat absorbed by the calorimeter is equal to the difference in the enthalpy of the material between the high and low temperatures. The heat capacity is the first derivative of the enthalpy with respect to temperature.

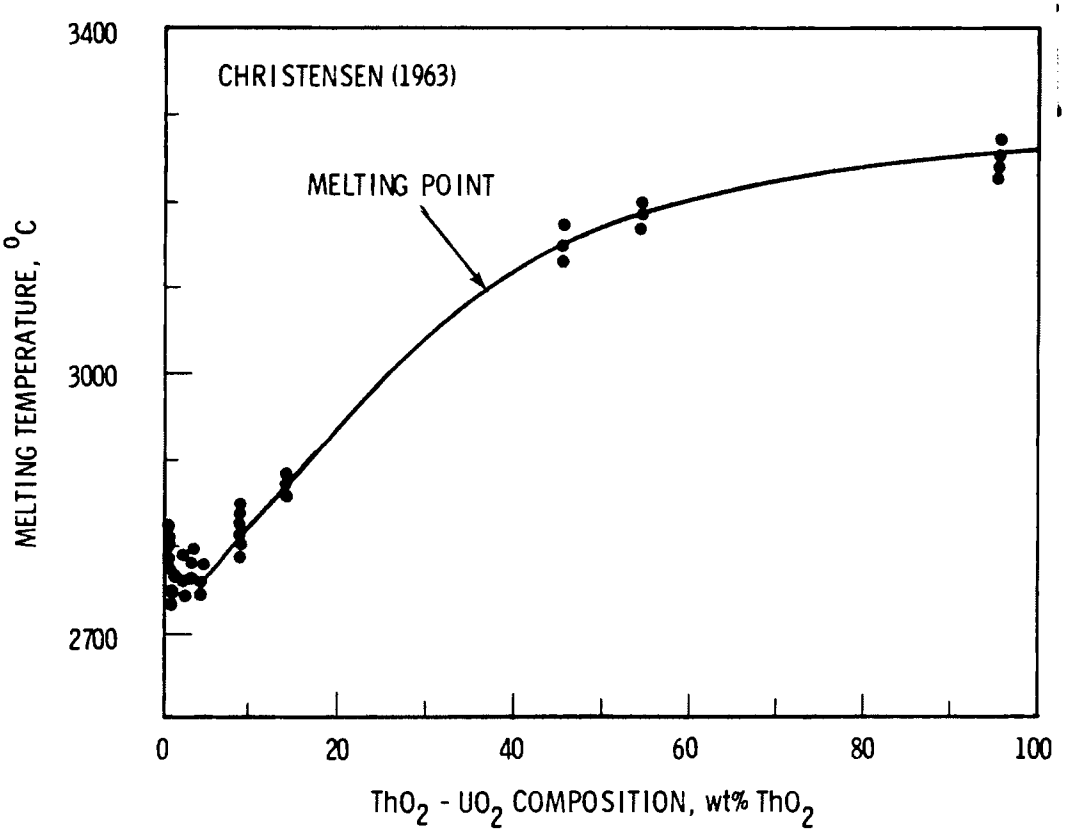

FIGURE 25. Melting Point for ThO_2-UO_2 Solid Solutions as a Function of ThO_2 Content

Godfrey et al. (1966) analyzed the ThO_2 heat capacity data of Southard (1941), Victor and Douglas (1961), and Hock and Johnston (1961). Southard determined data for the temperature range from 150 to 900 K; Hock and Johnston's data covered the range from 1183 to 2480 K; Victor and Douglas measured heat capacity from 123 to 927°C. The heat capacity in all of these studies was determined by the calorimeter method. Godfrey et al. found that

$$Cp = 6.27 \times 10^{-2} + 8.46 \times 10^{-6}T - 8.31 \times 10^{2}T^{-2} \qquad (24)$$

can best describe the heat capacity data for ThO_2 where T is the absolute temperature and Cp has the units calories per gram degree celsius Equation 24 gives a good approximation (within 2 to 3%) of the data as shown in Figure 26.

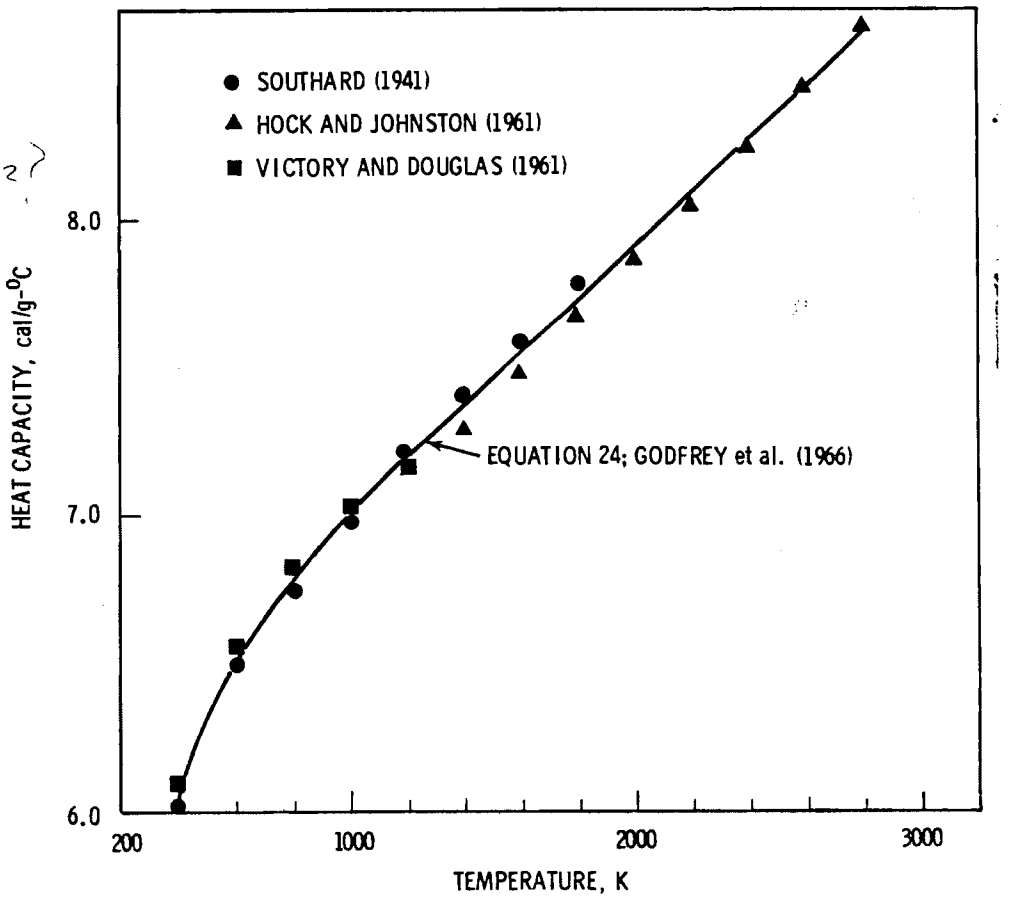

FIGURE 26. Comparison of the ThO_2 Heat Capacity Data of Several Researchers with the Heat Capacity Equation 24

Springer et al. (1967) measured the enthalpy of sintered solid solutions containing 0, 10, and 20 wt% UO_2 between 0 and 2060°C by the calorimeter method. The heat capacity determined from the enthalpy data can be expressed as a function of temperature T (K) by:

$$Cp = A + BT + CT^{-2} \qquad (25)$$

where A, B, and C are constants (given in Table 8) for the three compositions tested, and Cp has the units calories per gram-degree celsius. The ThO_2 heat capacity curves determined from the data of Springer et al. (1967) and from Equation 24 of Godfrey et al. (1966) are in good agreement as shown in Figure 27. The maximum difference between the curves is 3% at 2000°C. Therefore, either equation will suffice to describe the heat capacity of ThO_2.

TABLE 8. Heat Capacity Equation Constants (Springer et al. 1967)

wt% UO_2	Constants for $C_p = A + BT + CT^{-2}$		
	A	B	C
0	6.027×10^{-2}	9.124×10^{-6}	-416.9
10	6.319×10^{-2}	6.490×10^{-6}	-628.4
20	6.465×10^{-2}	6.266×10^{-6}	-767.7

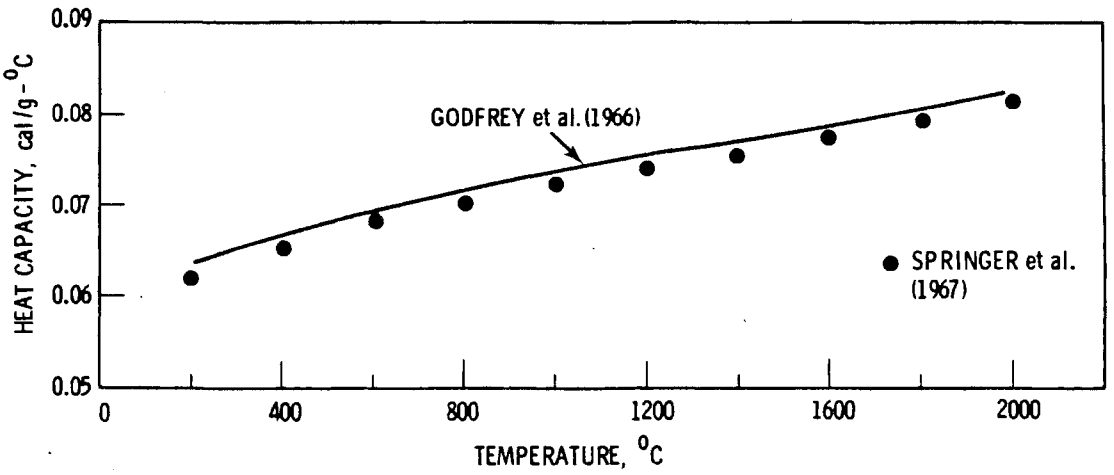

FIGURE 27. Comparison of ThO_2 Heat Capacity Data of Springer et al. with the Heat Capacity Equation 24

Below 800°C, the heat capacity curves of Springer et al. (1967) for solid solution compositions lie between the ThO_2 and UO_2 curves as shown in Figure 28. Above 900 and 1200°C, however, the heat capacity curves for solid solutions of 10 and 20 wt% UO_2, respectively, fall below the ThO_2 curve. No explanation was given by Springer et al. for this behavior.

Generally, the Neumann-Kopp rule applies to solid solutions, where the heat capacity of the solid solution is equal to the mole fraction sum of the individual compounds making up the solid solution. The heat capacity in Figure 28 is not simply related to composition, and summing the mole fraction contributions would not yield the measured values.

The heat capacity over the entire range of ThO_2-UO_2 solid solutions should be investigated to confirm the results of Springer et al. and to extend the data for compositions containing greater than 20 wt% UO_2.

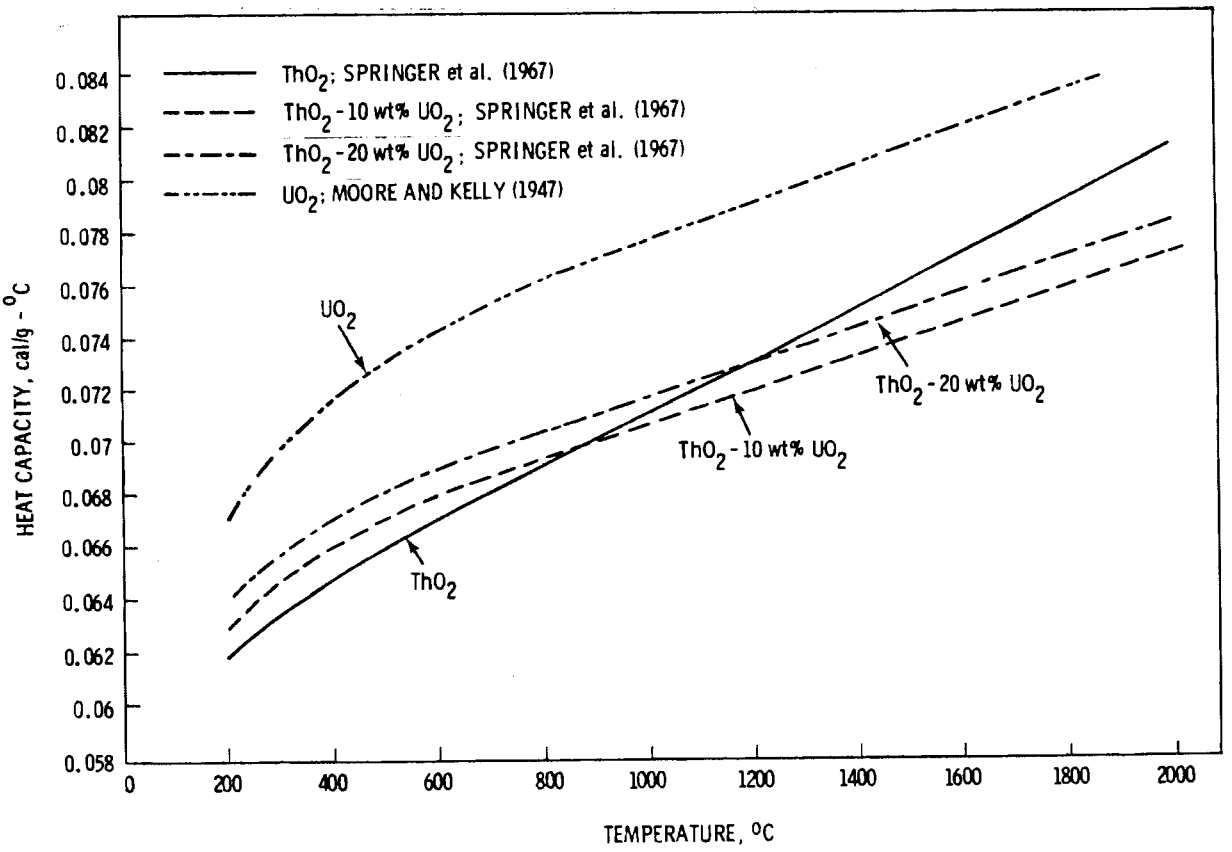

FIGURE 28. The Effect of UO_2 on the Heat Capacity of ThO_2

Berman et al. (1972) analyzed the 0-and 10-wt%-UO_2 data of Springer et al. (1967) to derive an equation for the heat capacity of ThO_2-UO_2 solid solutions as a function of temperature T (K) and composition U (mole fraction UO_2) in terms of calories per gram-degree celsius:

$$Cp = (6.034 + 2.984U)10^{-2} + (9.134 - 26.91U)10^{-6}T - (4.174 - 21.6U)10^{2}T^{-2} \quad (26)$$

Equation 26 is within 1% of the ThO_2 and ThO_2-10 wt% UO_2 data of Springer et al. (1967) as shown in Figures 29 and 30. Below 800°C, Equation 26 is in excellent agreement with the ThO_2-20 wt% UO_2 data of Springer et al.; however, the difference between Equation 26 and the data increases above 800°C, reaching a maximum of 5% at 2000°C as shown in Figure 31. For compositions of more than 20 wt% UO_2, the slope of the heat capacity curve decreases above 800°C, approaching zero at 35 wt% UO_2. Above 35 wt% UO_2, the slope of the heat capacity curve above 1000°C calculated with Equation 26 is negative. Between 0 and 10 wt% UO_2, Equation 26 fits the data well; however, additional work is needed to confirm the results

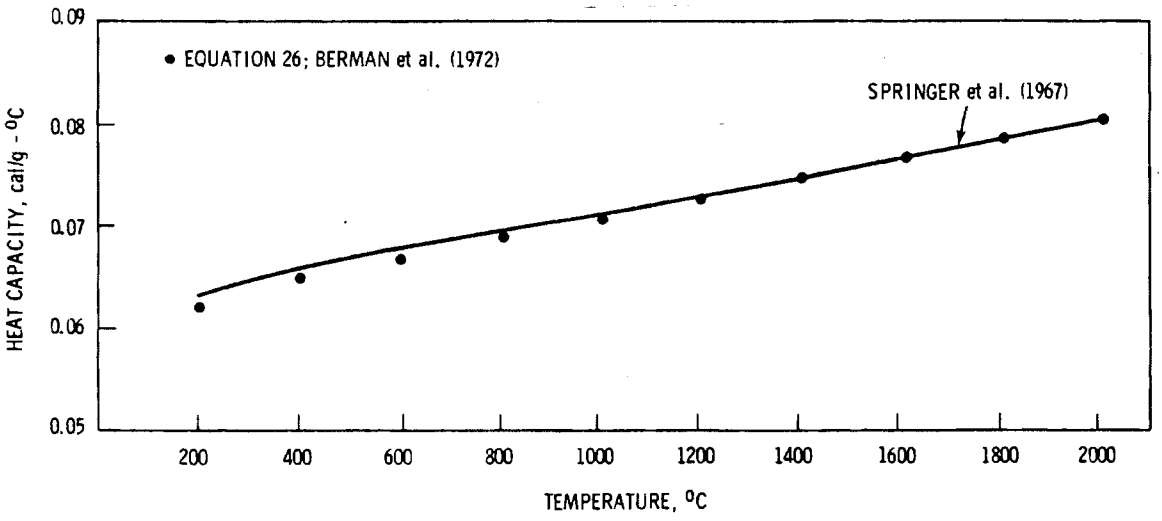

FIGURE 29. Comparison of the ThO_2 Heat Capacity Data of Springer et al. with Points Determined from the Heat Capacity Equation 26

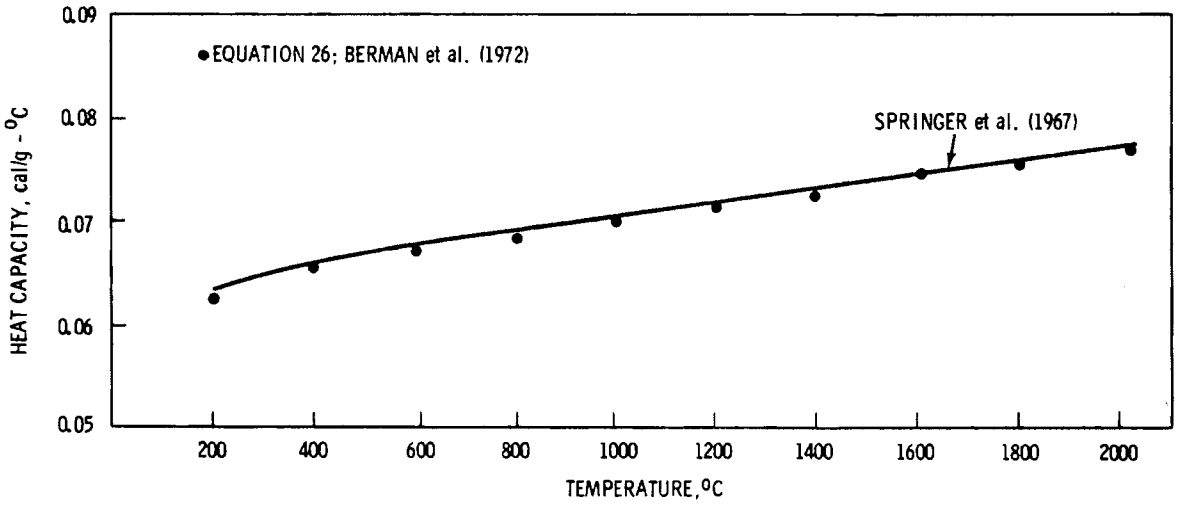

FIGURE 30. Comparison of the Heat Capacity Data of Springer et al. with Points Determined from the Heat Capacity Equation 26 for ThO_2-10 wt% UO_2

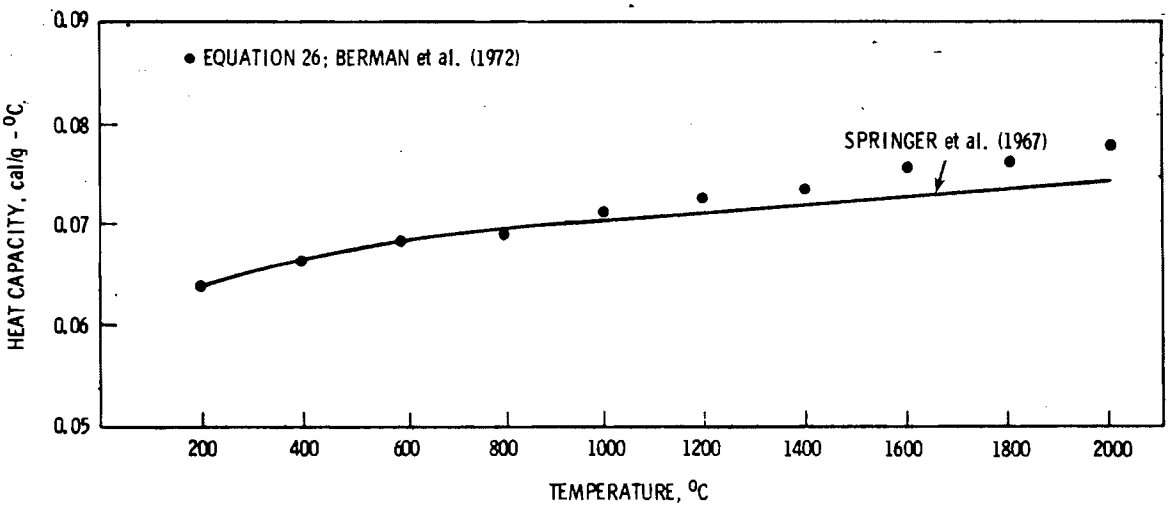

FIGURE 31. Comparison of the Heat Capacity Data of Springer et al. with Points Determined from the Heat Capacity Equation 26 for ThO_2-20 wt% UO_2

of Springer et al. (1967) and to extend the data base to compositions containing more than 20 wt% UO_2.

3.2.7 Vapor Pressure of $(Th_{1-x}U_x)O_2$

The vapor pressure reported in all of the studies reviewed was determined from the rate of evaporation or weight loss. Two methods employed to determine the vapor pressure of a specimen in vacuum are the Langmuir and Knudsen effusion techniques. In each, the vapor pressure (P) is calculated from the rate of evaporation by:

$$P = 2.256 \times 10^{-2} \, W/(At)(T/M)^{\frac{1}{2}} \qquad (27)$$

where M is the molecular weight of the vapor, W is the weight loss of the specimen in grams, A is the area in square centimeters, t is the time in seconds, and T is the absolute temperature.

The Langmuir method involves the sublimation of molecules from a free surface, whereas the Knudsen effusion method measures the amount of vapor escaping through a small hole of known area. The minimum pressure detectable by the Langmuir method is 10^{-10} atm, while the Knudsen method is most accurate in the range of 10^{-7} to 10^{-5} atm (Kingery 1959a).

The number of subliming molecules must equal the number of molecules condensing on the solid if the equilibrium vapor pressure is to be determined. The use of a properly designed closed container for Knudsen measurement can insure equilibrium conditions; however, using the Langmuir method, a portion of the vapor molecules that strike the solid may not condense, resulting in calculated pressures that are less than equilibrium pressures. To account for this, Equation 27 is divided by an accommodation coefficient (α), i.e., the fraction of gaseous molecules that strike the solid, but do not condense. The accommodation coefficient is determined from the ratio of the pressures determined by the Langmuir method to the Knudsen method.

In a third technique, the transpirational method, an inert gas is passed over the specimen, removing the vapor at a rate dependent on the rate of vaporization and the flow rate of inert gas. The volume fraction of the vapor

contained in the inert gas is measured and the partial pressure (P) of the vapor determined from:

$$P = \frac{Vs}{Vs + Vg} \tag{28}$$

where Vs is the volume of transported substance and Vg is the volume of transporting gas. The transpirational method is only accurate at pressures greater than 10^{-3} atm.

A more detailed description of each of these methods is contained in Kubaschewski et al. (1967), Kingery (1959a), and Margrave (1969).

The experimental conditions and results of relevant vapor pressure studies are given in Table 9. Alexander et al. (1967), Shapiro (1952), and Wolff and Alcock (1962) all assumed the vapor species above ThO_2 was composed of $ThO_2(g)$. After comparing the x-ray diffraction patterns of condensed vapor, Hock and Johnston (1954) concluded that 2 to 10% of the vapor was ThO(g) and the remainder $ThO_2(g)$; however, the dissociation of ThO_2 to $ThO_{(g)}$ was not taken into account when they derived the vapor pressure equation in Table 9.

Shapiro (1952) and Wolff and Alcock (1962) both assumed the accommodation coefficient equaled one. The good agreement of the vapor pressure data obtained by the Langmuir method (Shapiro 1952 and Wolff and Alcock 1962) and Knudsen method (Ackermann et al. 1963) as shown in Figure 32 indicate that the accommodation coefficient was indeed one. The ThO_2 vapor pressure data of Shapiro (1952), Wolff and Alcock (1962), and Ackermann et al. (1963) are all in good agreement as shown in Figure 32. Therefore, the individual data points of these three studies were combined into a single regression analysis. The vapor pressure of ThO_2 between 2000 and 3000 K is best described by:

$$\log P_{ThO_2} = 8.19 - 3.5919 \times 10^4/T \tag{29}$$

where T is the absolute temperature and P is the vapor pressure in atmospheres. The fit of Equation 29 to the data is good as shown in Figure 33. Equation 29 has a standard deviation of 0.101.

TABLE 9. Vapor Pressure Studies

Reference	Vapor	Temperature Range, K	Method of Measurement	Equation Relating Vapor Pressure as a Function of Absolute Temperature	Pressure Units
Ackermann et al. (1963)	ThO_2 and ThO	2000 to 3000	Knudsen effusion	$\log P_{ThO_2} = 7.64 - 3.44 \times 10^4/T$ $\log P_{ThO} = 8.70 - 3.79 \times 10^4/T$	atm
Aitken et al. (1966)	UO_3 over $(Th_{0.94}U_{0.06})O_{2.03}$	1500 to 1900	transpiration	$\log P_{UO_3} = 8.32 - 3.3198 \times 10^4/T$	atm
	UO_3 over $(Th_{0.8}U_{0.2})O_{2.1}$	1500 to 1900	transpiration	$\log P_{UO_3} = 11.43 - 3.7313 \times 10^4/T$	atm
	UO_3 over $(Th_{0.75}U_{0.25})O_{2.13}$	1500 to 1900	transpiration	$\log P_{UO_3} = 13.02 - 3.9808 \times 10^4/T$	atm
	UO_3 over $(Th_{0.5}U_{0.5})O_{2.24}$	1500 to 1900	transpiration	$\log P_{UO_3} = 15.20 - 4.2568 \times 10^4/T$	atm
Alexander et al. (1967)	ThO_2	2000 to 3000	transpiration	$\log P_{ThO_2} = 7.13 - 3.4041 \times 10^4/T$	atm
	UO_2 over ThO_2-8 wt% UO_2	2000 to 3000	transpiration	$\log P_{UO_2} = 7.29 - 3.2863 \times 10^4/T$	atm
	UO_2 over ThO_2-20 wt% UO_2	2000 to 3000	transpiration	$\log P_{UO_2} = 7.79 - 3.2468 \times 10^4/T$	atm
	UO_2	2000 to 3000	transpiration	$\log P_{UO_2} = 7.54 - 2.9389 \times 10^4/T$	atm
Shapiro (1952)	ThO_2	2050 to 2250	Langmuir method (assumed accommodation coefficient = 1)	$\log P_{ThO_2} = 11.53 - 3.71 \times 10^4/T$	mmHg
Wolff and Alcock (1962)	ThO_2	2100 to 2500	Langmuir method (assumed accommodation coefficient = 1)	$\log P_{ThO_2} = 9.07 - 3.7988 \times 10^4/T$	atm
Hock and Johnston (1961)	ThO_2	2400 to 2700	Knudsen effusion	$\log P_{ThO_2} = 12.145 - 7.82 \times 10^{-4}T - 3.7695T^{-1}$	atm

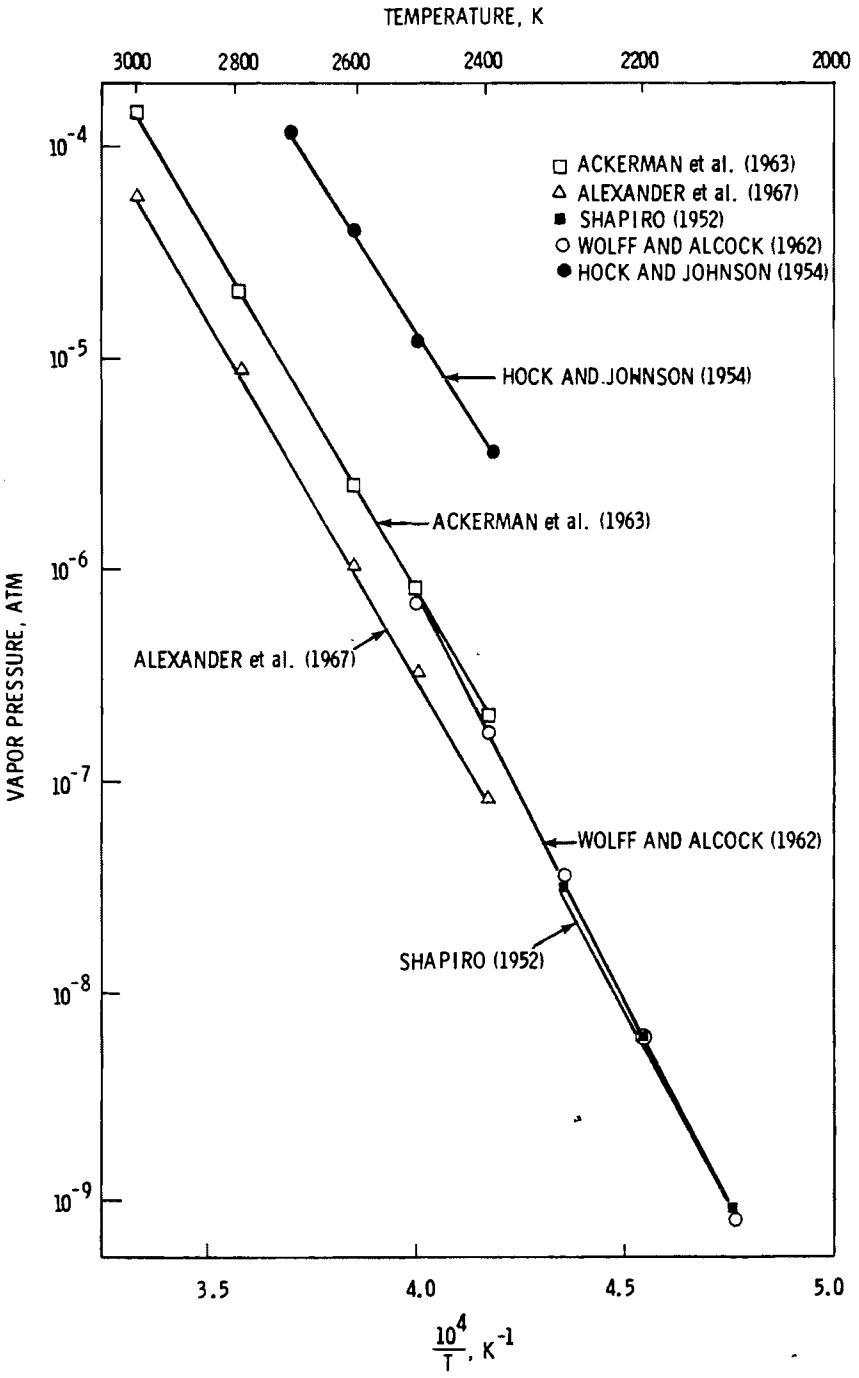

FIGURE 32. Vapor Pressure Curves for ThO_2 as a Function of Temperature

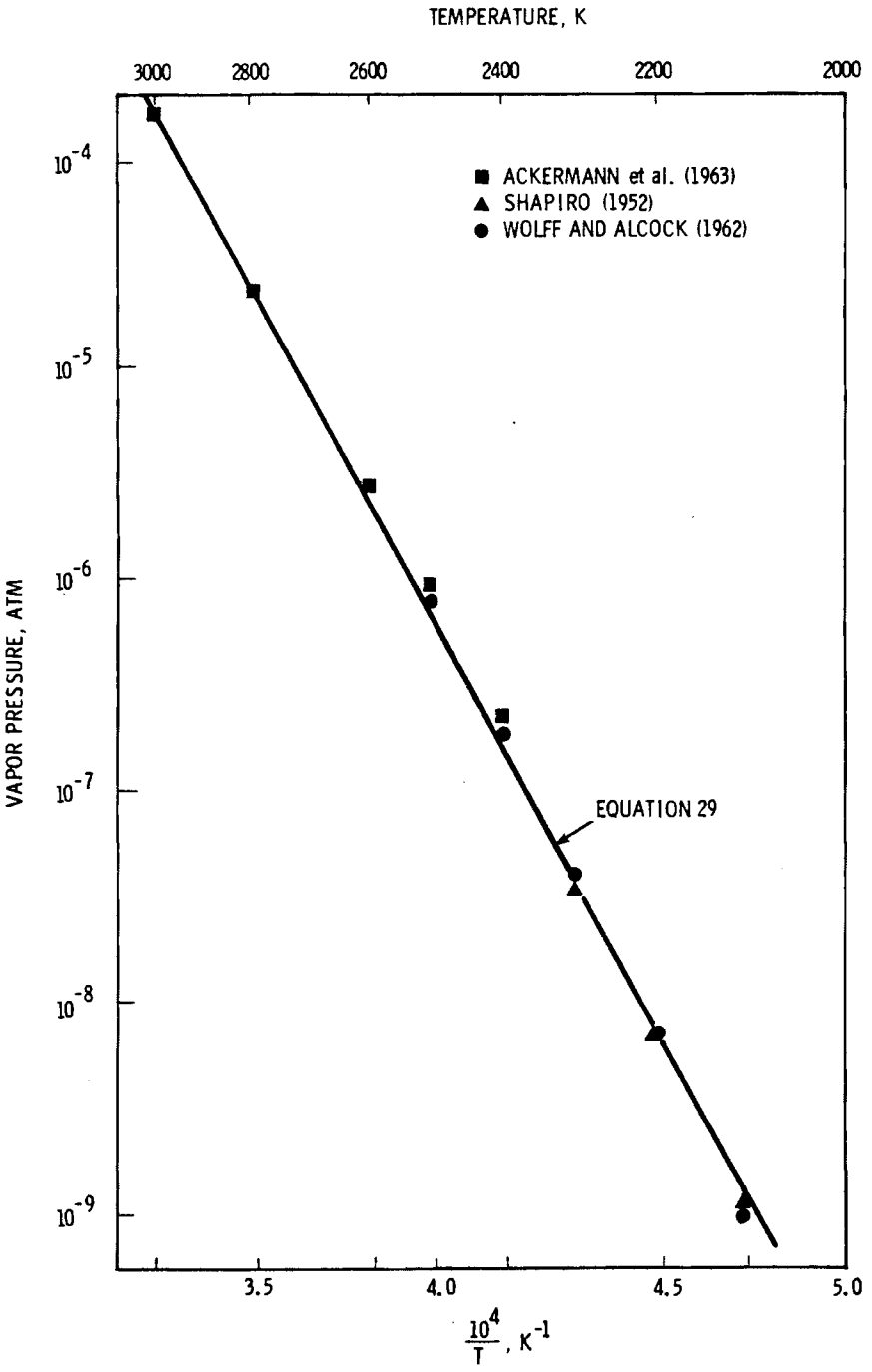

FIGURE 33. Comparison of Various Vapor Pressure Data with the Curve Predicted by Equation 29 for ThO_2

Alexander et al. (1967) and Hock and Johnston (1954) found vapor pressure curves that are respectively one-half and one order of magnitude different from what most others (Ackermann et al. 1963; Shapiro 1952; Wolff and Alcock 1962) have observed. The different vapor pressures observed by Hock and Johnston cannot be explained. The low vapor pressures measured by Alexander et al. (1967) could have been caused by using the transpirational method which is inaccurate below 10^{-3}atm.

Alexander et al. (1967) determined the UO_2 vapor pressure of 8- and 20-wt%-UO_2 solid solutions. The vapor pressure is shown as a function of temperature in Figure 34. Assuming the experimental error of Alexander et al. is systematic for UO_2, ThO_2-UO_2, and ThO_2, the important conclusion to be drawn from Figure 34 is that the vapor pressure of UO_2 will be higher than the vapor pressure of ThO_2 above ThO_2-UO_2 solid solutions containing 8 wt% or more UO_2, leading to the preferential loss of UO_2 from solid solutions at elevated temperatures.

Aitken et al. (1966) measured the volatilization of uranium oxide from various ThO_2-UO_2 compositions. The results are summarized in Table 9 and Figure 35. Aitken et al. believe that the major vaporizing species was UO_3, although experimental evidence was not given to support this assumption.

Although there are experimental differences, the vapor pressure curves of Aitken et al. and Alexander et al. are within an order of magnitude when the ThO_2-20 wt% UO_2 data of Aitken et al. is extrapolated into the temperature range of Alexander et al. and vice versa as shown in Figure 36. This indicates that the vapor species could have been of the same composition in each study.

3.2.8 Other Thermodynamic Properties of Interest

Godfrey et al. (1966) have tabulated various thermodynamic data for ThO_2 between 298 and 3000 K from several studies (Southard 1941; Victor and Douglas 1961; and Hock and Johnston 1961) as shown in Table 10. Peterson and Curtis (1970) completed the low-temperature (10 to 300 K) region of Table 10 using the heat capacity data of Osborne and Westrum (1953).

Peterson and Curtis (1970) determined the heat and free energy of formation for ThO_2 (Table 11) from the data in Table 10 and other studies (Huber et al. 1952; Hultgren et al. 1963; and Stull and Sinke 1956).

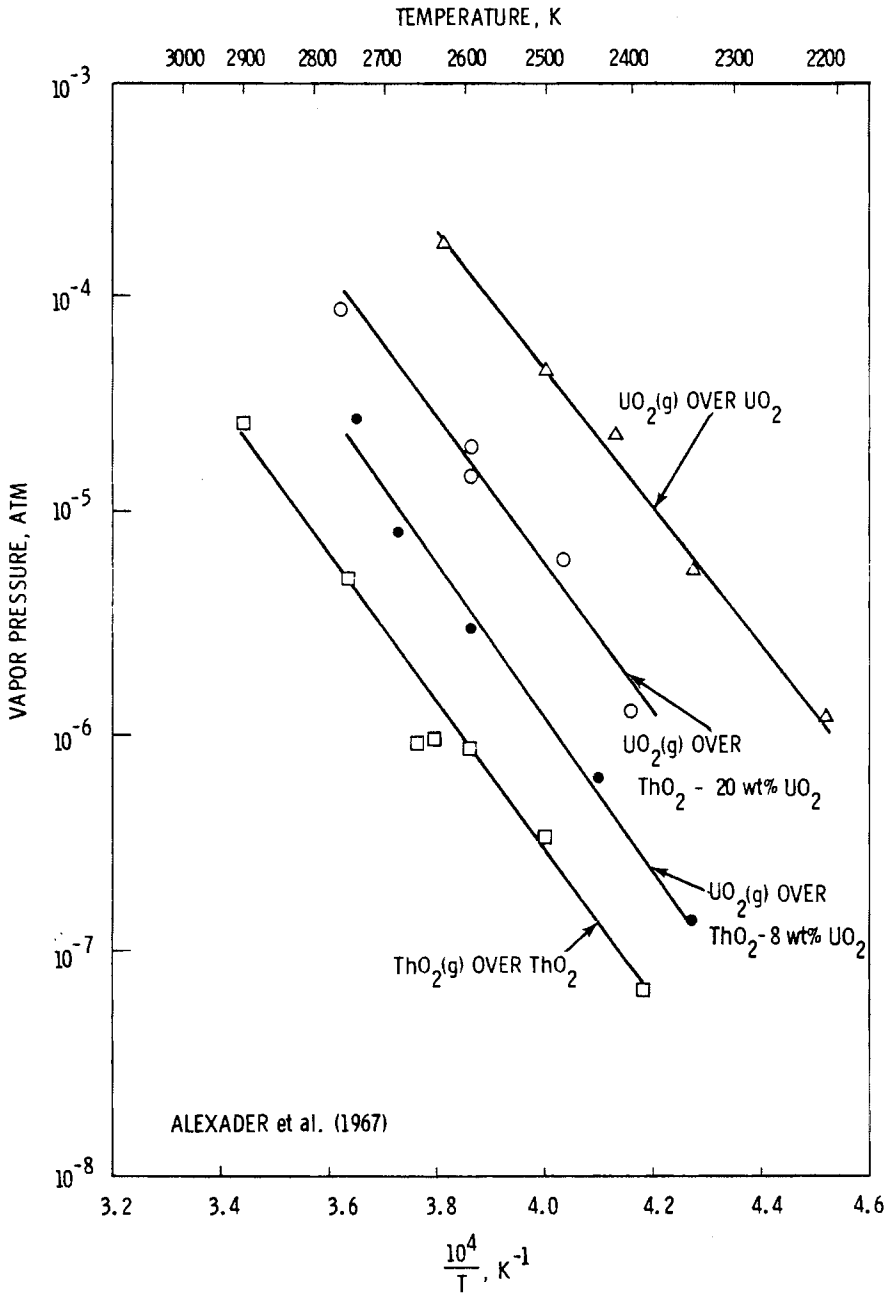

FIGURE 34. Experimentally Measured Vapor Pressure Data over Various ThO_2-UO_2 Compositions

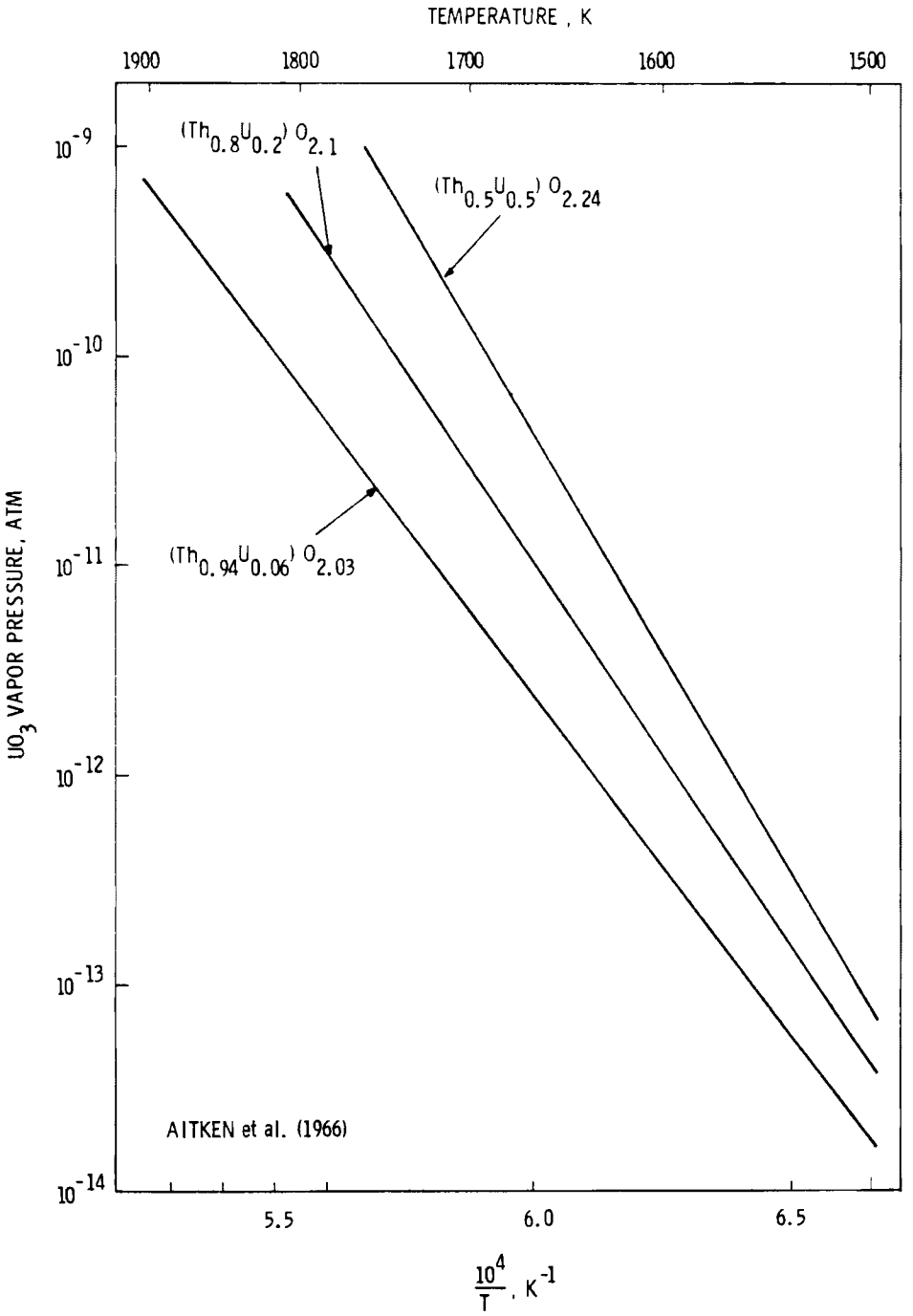

FIGURE 35. UO_3 Vapor Pressure Above $(Th_{1-x}U_x)O_{2+y}$

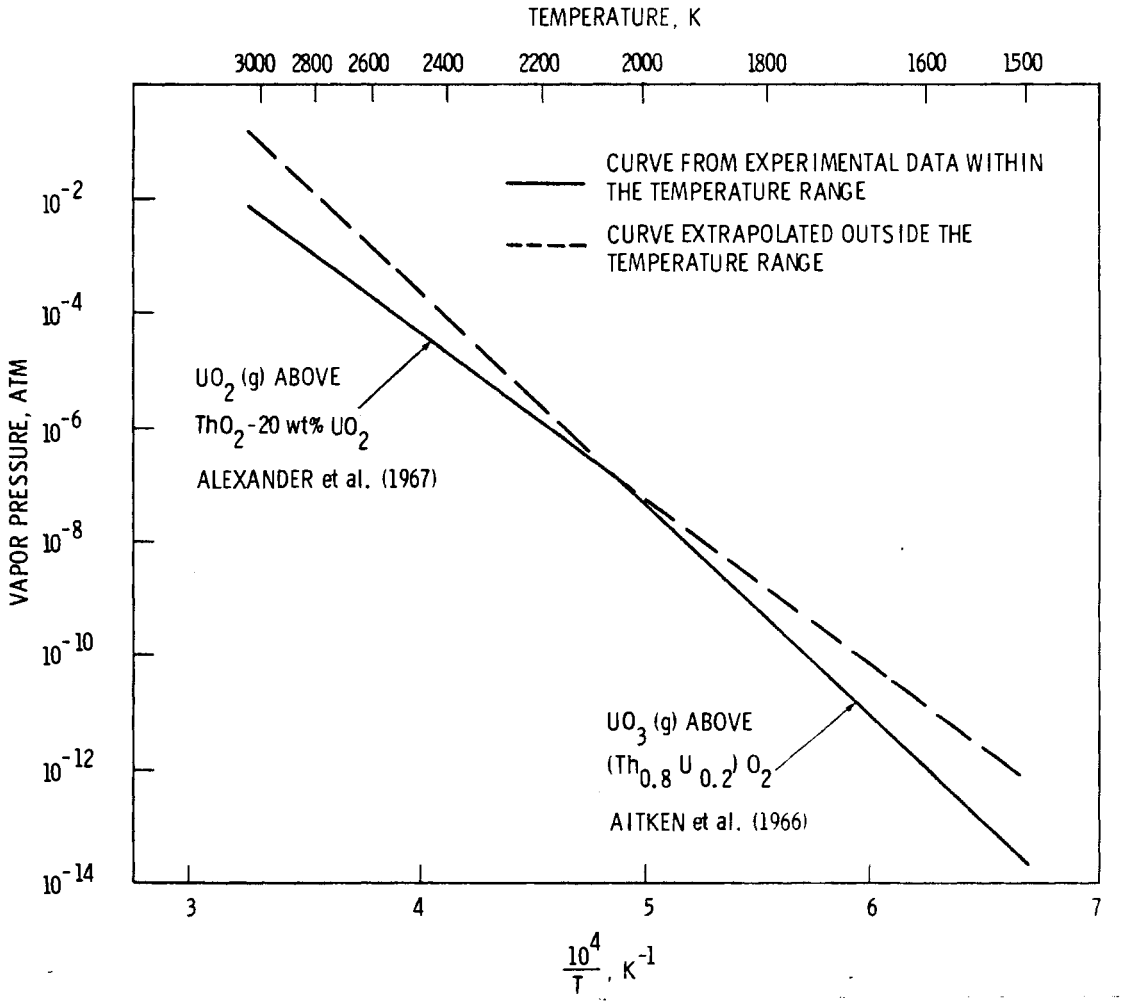

FIGURE 36. Comparison of the Vapor Pressure Data of Alexander et al. and Aitken et al.

Kubaschewski et al. (1967) describe the free energy of formation of ThO_2 by:

$$\Delta G_f = -293,400 - 1.61T \log T + 47.7T \quad (30)$$

where T is the absolute temperature and ΔG_f has the units calories per mole (cal/mol). The data used to determine Equation 30 was not referenced by Kubaschewski et al.

TABLE 10. Thermodynamic Functions of ThO_2

Temperature, ^oK	Heat Capacity (C_p), cal/mol-K	Enthalpy (H^o-H^o), cal/mol	Entropy (S^o), cal/mol-K	$-(G^o-H^o)/T$, cal/mol-K
10	0.032	0.08	0.011	0.003
50	2.430	38.60	1.068	0.296
100	6.246	257.3	3.948	1.375
150	9.546	655.1	7.129	2.762
200	11.97	1196.5	10.227	4.244
250	13.64	1839.1	13.088	5.732
298	14.76	2524.4	15.593	7.126
300	14.79	2551	15.68	7.18
400	16.08	4103	20.14	9.88
500	16.80	5750	23.81	12.31
600	17.29	7456	26.92	14.49
700	17.68	9205	29.61	16.46
800	18.01	10990	32.00	18.26
900	18.30	12806	34.13	19.91
1000	18.58	14650	36.08	21.43
1100	18.84	16521	37.86	22.85
1200	19.09	18417	39.51	24.17
1300	19.34	20338	41.05	25.40
1400	19.58	22284	42.49	26.58
1500	19.81	24254	43.85	27.68
1600	20.05	26247	45.13	28.73
1700	20.28	28264	46.36	29.74
1800	20.51	30304	47.52	30.69
1900	20.74	32366	48.64	31.60
2000	20.97	34452	49.71	32.48
2100	21.20	36561	50.74	33.33
2200	21.43	38693	51.73	34.14
2300	21.66	40847	52.69	34.92
2400	21.88	43024	53.61	35.69
2500	22.11	45224	54.51	36.42
2600	22.34	47446	55.38	37.13
2700	22.56	49691	56.23	37.83
2800	22.79	51958	57.05	38.50
2900	23.01	54248	57.86	39.19
3000	23.24	56560	58.64	39.79

Sources: Godfrey et al. 1966; Peterson and Curtis 1970

TABLE 11. Heat and Free Energy of Formation of ThO_2

Temperature, ^oK	Heat of Formation $(-\Delta H_f)$, kcal/mol	Free Energy of Formation $(-\Delta G_f)$, kcal/mol
298.15	293.2	279.4
400	293.0	274.7
500	292.8	270.2
600	292.6	265.7
700	292.4	261.2
800	292.2	256.8
900	292.0	252.4
1000	291.8	248.0
1100	291.7	243.6
1200	291.6	239.0
1300	291.4	234.9
1400	291.3	230.6
1500	291.2	226.0
1600	291.1	221.9
1700	291.7	217.5
1800	291.6	213.2
1900	291.6	208.8
2000	296.0	204.3
2500	295.4	181.5
3000	294.2	158.8

Source: Peterson and Curtis 1970

Ackermann et al., (1963) using the data from a number of studies, (Southard 1941; Hock and Johnston 1961; Osborne and Westrum 1953; Huber et al. 1952; Stull and Sinke 1956) describe the free energy of formation (cal/mol) of ThO_2 by:

$$\Delta G_f = -296{,}000 + 46.38T \qquad (31)$$

where T, the absolute temperature, is limited to between 2000 and 3000 K. Above 2000 K, Equation 31 is within 1 kcal/mol of Peterson and Curtis (1970) and between 5 to 8 kcal/mol more positive than Kubaschewski et al. (1967) as shown in Figure 37. Extrapolating below 2000 K, the agreement of Equation 31 with Peterson and Curtis and Kubaschewski et al. is within 5 kcal/mol. Since the data used to determine Equation 30 were not given, Equation 31 should be used to calculate the free energy of formation of ThO_2.

Aitken et al. (1966), assuming the solid solution behavior of ThO_2-UO_2 was ideal, describe the free energy of formation of $(Th_{1-x}U_x)\ O_2$ as a function of composition by:

$$\Delta G_f(x) = (1 - x)\ \Delta G_f(ThO_2) + x\ \Delta G_f(UO_2) + RT\ x\ln\ [x + (1 - x)\ln(1 - x)] \quad (32)$$

where x is the mole fraction UO_2, R is the gas constant, T is temperature (K), and $\Delta G_f(ThO_2)$ and $\Delta G_f(UO_2)$ are the free energy of formation of ThO_2 and UO_2, respectively. Equation 32 is the sum of the heat of mixing and the free energy contributions of the pure components. Experimental data are not available to compare with the free energies predicted by Equation 32.

Aronson and Clayton (1960) measured the electromotive force (emf) in an electrochemical cell containing $(Th_{1-x}U_x)O_{2+y}$ with x from 0.29 to 1.0 and y from 0.02 to 0.16. The partial molar free energies, enthalpies, and entropies of the solution of oxygen in solid solutions of ThO_2-UO_2 were calculated from the emf measurements.[(a)] Aronson and Clayton found that the partial molar entropy became more negative as the oxygen or thorium content increased (Table 12). Between 71 and 100 mol% UO_2, the partial molar free energies are approximately equal for equal values of y. Below 70 mol% UO_2 (at constant y) the partial molar free energy became less negative as the UO_2 content decreased. At compositions containing less than 70 mol% UO_2, the free energy became less negative as the oxygen content increased.

(a) The partial molar properties are the changes in properties that occur when a mole of oxygen gas is transferred to the solid.

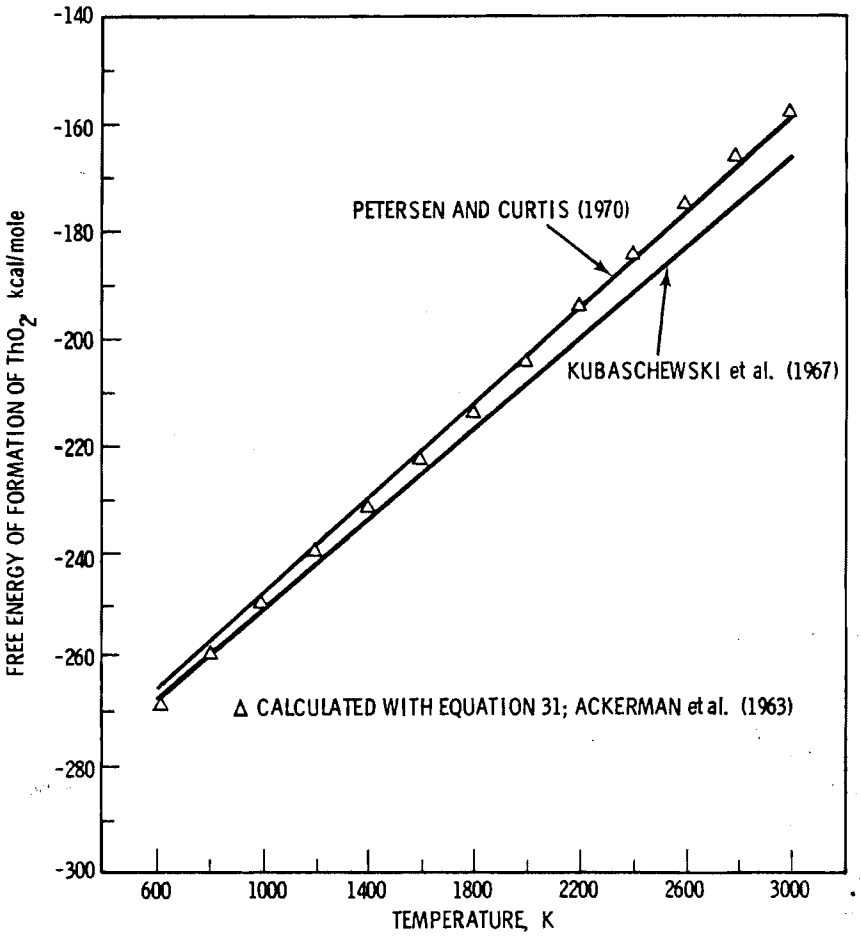

FIGURE 37. Free Energy of Formation of ThO_2

In a review paper, Roberts et al. (1958) reported the partial molar heat of solution of oxygen in ThO_2-UO_2 compositions.(a) In support of the findings of Aronson and Clayton, Roberts et al. showed a decreasing heat of solution with increasing UO_2 content (Table 13). No data were given on the stoichiometry, free energy, or entropy of the compositions tested.

(a) The data, reviewed by Roberts et al. (1958), was not referenced and could not be checked for accuracy.

TABLE 12. Partial Molar Free Energies, Entropies, and Enthalpies of Solution of Oxygen in $(Th_{1-x}U_x)O_{2+y}$

Mole Fraction Composition of $(Th_{1-x}U_x)O_{2+y}$		Partial Molar Free Energy($-G_{O_2}$), kcal/mol at 1250 K	Partial Molar Entropy($-S_{O_2}$), eu/mol	Partial Molar Enthalpy of Solution ($-H_{O_2}$), kcal/mol
x[(a)]	y			
1	0.013	54.2	6.3	62
1	0.018	53.2	6.4	61
1	0.044	51.2	12.8	67
1	0.044	51.1	6.8	60
1	0.051	50.3	12.2	66
1	0.075	49.5	13.6	66
1	0.078	49.4	12.7	65
1	0.087	47.3	16.7	67
1	0.112	45.8	18.3	69
1	0.128	44.0	22.5	72
1	0.142	42.1	25.3	74
1	0.143	42.0	24.3	72
1	0.160	39.8	27.1	74
1	0.164	40.1	27.0	74
1	0.181	37.6	28.0	73
1	0.184	37.7	27.6	72
1	0.198	35.1	27.9	70
1	0.203	35.2	29.4	72
0.90	0.042	51.8	8	62
0.90	0.042	52.4	13	69
0.90	0.076	48.7	17	70
0.90	0.081	48.4	17	70
0.90	0.123	44.7	23	73
0.90	0.126	44.7	21	71
0.90	0.157	40.7	29	77
0.71	0.046	50.9	14	68
0.71	0.049	50.9	14	68
0.71	0.084	47.2	21	74
0.71	0.092	46.9	28	82
0.71	0.121	44.0	34	85
0.71	0.133	42.9	29	80
0.71	0.152	40.3	34	83
0.71	0.154	40.2	35	84
0.52	0.044	47.5	20	72
0.52	0.045	46.8	22	74
0.52	0.079	43.4	22	72
0.52	0.087	44.4	31	83
0.52	0.119	39.8	35	84
0.52	0.122	39.5	34	82
0.52	0.152	35.7	40	85
0.52	0.152	35.2	35	78
0.29	0.019	45.4	22	72
0.29	0.027	43.2	19	67
0.29	0.046	37.3	24	67
0.29	0.053	36.2	26	69
0.29	0.053	36.8	30	74
0.29	0.069	33.5	30	71
0.29	0.073	33.1	34	76

(a)The data for x values of 1 are taken from the work of S. Aronson and J. Belle. (1958)

TABLE 13. Effect of Fuel Composition on Oxygen Pressure and the Partial Molar Heat of Solution of Oxygen

UO_2 Content in $(Th_{1-x}U_x)O_2$, x	Partial Molar Heat of Solution of Oxygen, kcal/mol	O_2 Pressure at 850°C, cm
1.0	69	--
0.25	60 to 70	--
0.0597	44	0.013
0.033	39	0.1
0.018	33	0.5
0.012	25	1.6
0.0076	17.5	2.0
0.0053	14.5	3.0

Source: Roberts et al. 1958

3.2.9 Chemical and Thermodynamic Properties - Summary and Evaluation

Both ThO_2 and UO_2 crystallize in the fluorite crystal structure and are capable of forming a complete series of solid solutions up to 95 mol% UO_2. As the UO_2 content increases the lattice parameter decreases, closely following Vegard's law. Compositions containing greater than 95 mol% UO_2 depart from ideal solid solution behavior, possibly due to the formation of U_4O_9.

The theoretical density of thoria at room temperature (ρ_o) is 10.002 g/cm^3 and increases as the UO_2 content increases. Although the effect of composition and temperature on the density of ThO_2-UO_2 solid solutions has not been described, data are available to do so.

Pure ThO_2 does not deviate measurably from stoichiometry. The deviation from stoichiometry of ThO_2-UO_2 solid solutions is a function of the UO_2 concentration, sintering conditions, and oxidation conditions (time, temperature, and atmosphere). In general, compositions containing less than 50 mol% UO_2 can be oxidized to some maximum value, dependent on the UO_2 content. Above this maximum value, the solid solutions are in equilibrium

with the atmosphere. Compositions containing greater than 50 mol% UO_2 oxidize to a maximum value independent of the UO_2 concentration. Above the maximum, a two-phase region of cubic and orthorhombic structures exists. Below the solubility limit all compositions are single cubic phase.

The heat capacity (Cp) for ThO_2 is described by:

$$Cp = 7.14 \times 10^{-2} + 9.62 \times 10^{-6}T - 9.46 \times 10^{2}T^{-2} \quad \text{(same as Eq. 24)}$$

where T is the absolute temperature, and Cp has the units calories per gram degree celsius.

For ThO_2-UO_2 solid solutions containing between 0 and 10 wt% UO_2, the heat capacity may best be described by:

$$Cp = (6.034 + 2.984U)10^{-2} + (9.134 - 26.91U)10^{-6}T + (4.174 + 21.6U)10^{2}T^{-2} \quad \text{(same as Eq. 26)}$$

where U is the mole fraction UO_2 and Cp has the units calories per gram-degree celsius. Above 10 wt% UO_2, Equation 26 is unreliable and should not be used. Equation 25 can be used to describe the heat capacity of a 20-wt%-UO_2 composition. Additional data are needed before heat capacity can be described over the entire range of ThO_2-UO_2 compositions.

The vapor pressure of ThO_2 above pure ThO_2 can be determined from:

$$\log P_{ThO_2} = 8.19 - 3.5919 \times 10^{4}/T \quad \text{(same as Eq. 29)}$$

where T is the absolute temperature and P is the vapor pressure in atmospheres. A similar equation to describe the ThO_2 vapor pressure above ThO_2-UO_2 solid solutions does not exist. The UO_2 vapor pressure above ThO_2-UO_2 solid solutions increases with the UO_2 content.

The free energy of formation of ThO_2 in calories per mole may be expressed by:

$$\Delta G_f(ThO_2) = 296{,}000 + 46.38T \qquad \text{(same as Eq. 31)}$$

where T is the absolute temperature. A number of useful thermodynamic properties of ThO_2 are tabulated in Table 10.

The thermodynamic functions of ThO_2-UO_2 have not been tabulated. When the relationship between heat capacity and composition is better understood, these functions can be derived.

3.3 MECHANICAL PROPERTIES OF ThO_2

This discussion of ThO_2 mechanical properties includes sections on elastic moduli, creep behavior, and fracture strength.

3.3.1 Elastic Moduli

Comprehensive studies by Spinner et al. (1962, 1963) provide a solid data base for the elastic properties of polycrystalline ThO_2 as measured by the dynamic resonance technique. Wolfe and Kaufman (1967) have carefully analyzed the elastic properties data in the literature. Most of this discussion is based on their analysis. No information on the elastic moduli of ThO_2-UO_2 mixed oxides is available.

Elastic Constants

Macedo et al. (1964) measured the elastic constants of single-crystal ThO_2 at 250°C and found the following:

$$C_{11} = 367 \text{ MPa},$$
$$C_{12} = 106 \text{ MPa},$$
$$C_{44} = 79.7 \text{ MPa}.$$

The elastic moduli of theoretically dense polycrystalline materials can be derived from the single-crystal elastic constants with the Voigt-Reuss-Hill

(Voigt 1910; Reuss 1929; Hill 1952) approximation and the general relationships of elementary elasticity theory. Table 14 compares the moduli calculated from the data of Macedo with those measured on porous ThO_2 and extrapolated to theoretical density by Spinner et al. (1962) and by Wolfe and Kaufman (1967). The results in Table 14 form an accurate set of data for the elastic constants of fully dense, polycrystalline ThO_2. Wolfe and Kaufman suggest that their data and the data of Macedo et al. are best because of the agreement. However, the differences could be due to unknown pore shape, distribution, and orientation, so unless the material is fully characterized, a 3% uncertainty can be expected between various data sets.

Effect of Porosity on Elastic Moduli

The elastic properties of ceramics are sensitive to pore concentration, size, shape and distribution. Spinner et al. (1962) established porosity-dynamic moduli relationships for polycrystalline ThO_2, and their Young's modulus data are plotted in Figure 38 along with other relevant data. Wolfe and Kaufman (1967) analyzed these data and proposed a linear relationship between Young's modulus and porosity:

$$E = 249.1\ (1 - 2.21p) \qquad (33)$$

where E is Young's modulus in MPa and p is the volume fraction of porosity.

TABLE 14. Room Temperature Elastic Moduli for Fully Dense Polycrystalline ThO_2

Young's Modulus (E), MPa	Shear Modulus (G), MPa	Bulk Modulus (K), MPa	Poisson's Ratio	Reference
249.1	97.2	193.0	0.284	Calculated by Macedo et al. (1964)
261.0	100.6	215.3	0.297	Extrapolated by Spinner et al. (1962)
249.1	96.9	192.8	0.285	Extrapolated by Wolfe and Kaufman (1967)

Spinner et al. (1962) found that their data could be divided into two distinct groups; they suggested that the pore shape of the samples having the low modulus (closed circles in Figure 38) deviated to a greater degree from perfect spheres than the pores in the other samples. The low-modulus data set was ignored in deriving Equation 33. However, no ceramographic evidence was offered, so none of the data can be ignored, and the use of Equation 33 beyound 10% porosity is not justified. Material with greater porosity requires detailed structural characterization. Similar data have been generated for the shear modulus (Spinner et al. 1962), and the following equation (Wolfe and Kaufman 1967) should be accurate to 10% porosity:

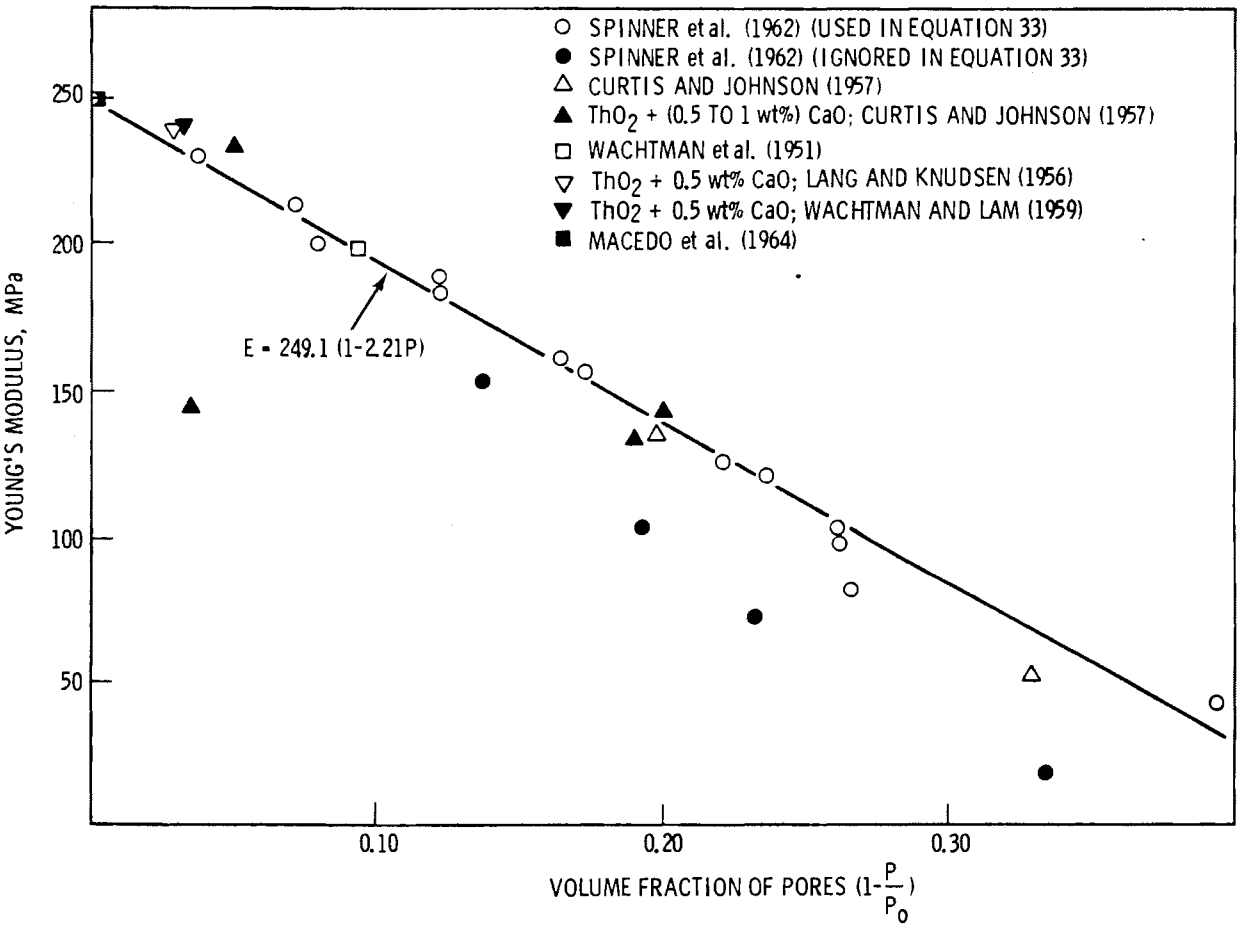

FIGURE 38. Relationships Between Porosity and Young's Modulus for ThO_2

$$G = 96.9(1 - 2.12p) \quad (34)$$

where G is the shear modulus in MPa.

Effect of Temperature on Elastic Moduli

Several investigators have studied the effect of temperature on the elastic moduli of polycrystalline ThO_2 (Spinner et al. 1963; Lang and Knudsen 1956; Wachtman and Lam 1959) and their results are fairly consistent. Differences can be attributed to minor deviations in technique and sample characteristics. A compilation of data is plotted in Figure 39. The relative modulus decreases linearly with temperature up to 1000°C. At higher temperatures the modulus drops off more rapidly with temperature. Spinner et al. (1963) fitted their data to the type of temperature dependence relationship suggested by Wachtman et al. (1961) in the following equation:

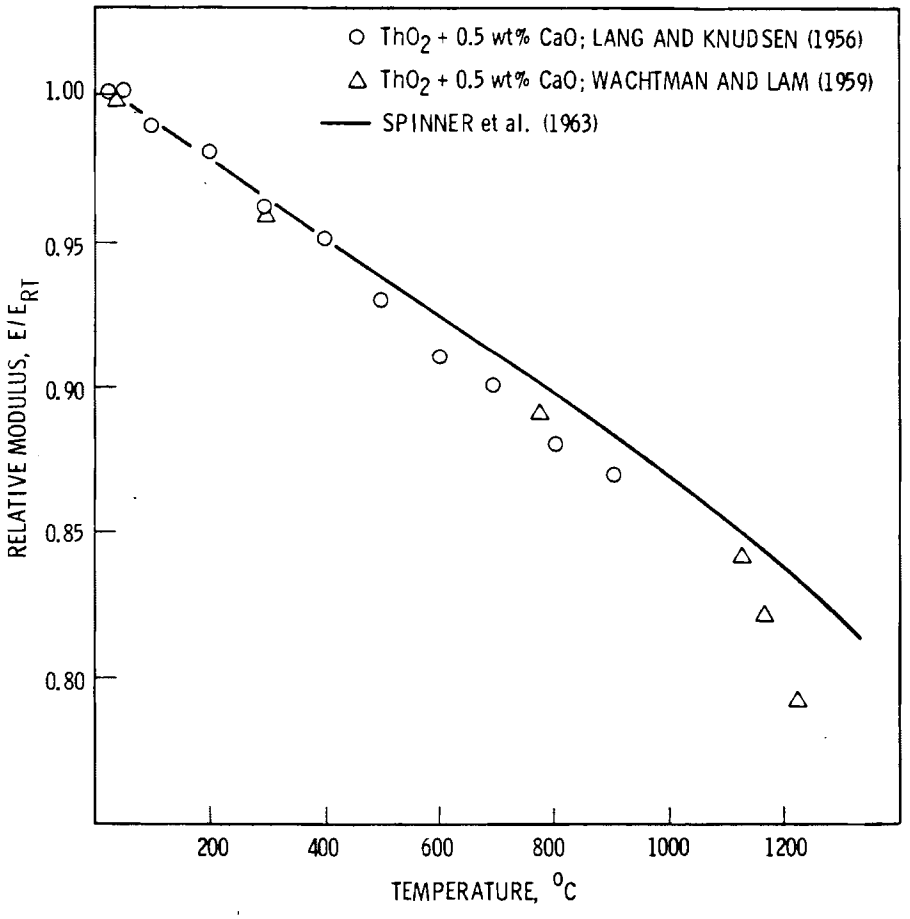

FIGURE 39. Relationship Between Temperature and Relative Modulus

$$E/E_{RT} = 1.023 - 1.405 \times 10^{-4} T \exp(-181/T) \quad (35)$$

where E_{RT} is Young's modulus at room temperature and T is the absolute temperature. At temperatures greater than 800°C the relative modulus drops off faster than Equation 35 predicts. Equation 35 can also be used to predict the effect of temperature on the relative shear modulus (G/G_{RT}), which means that Poisson's ratio is independent of temperature.

Wachtman and Lam (1959) attribute the deviation from linearity to viscous slip at grain boundaries. This suggests that any additives that form a glassy phase at grain boundaries will reduce the high-temperature mechanical properties of ThO_2.

A single study by Marlowe and Kaznoff (1969) indicated that elastic moduli for UO_2 are about 12% lower than elastic moduli for ThO_2, less sensitive to porosity, and similar in temperature dependence.

3.3.2 Creep Behavior

The creep properties of ThO_2 have been reviewed (Wolfe and Kaufman 1967; Petersen and Curtis 1970; Kittel et al. 1977; Seltzer et al. 1971) more times than they have been measured (Morgan and Hall 1966; Poteat and Yust 1966; Wolfe 1970). Empirical expressions relating the creep rate of polycrystalline materials to the parameters that influence creep can be estimated over restricted ranges using the classical creep equation:

$$\dot{\varepsilon}_s = A\sigma^n \exp - \left[\frac{Q_c}{R\bar{T}}\right] \quad (36)$$

where

$\dot{\varepsilon}_s$ is the steady state creep rate,
Q_c is the activation energy for creep,
R is the gas constant,
T is the absolute temperature,
σ is the stress,
n is the stress exponent, and
A is a material-dependent parameter.

The parameter A is a function of composition, grain size, porosity and impurities. Seltzer et al. (1971) reviewed some of these dependencies for UO_2, and a considerable amount of UO_2 creep data has been generated since then. Olsen (1975) has proposed a steady state creep equation which takes into account all of the available UO_2 data; no such generalized relationship exists for ThO_2 or ThO_2-UO_2 creep.

Morgan and Hall (1966) showed that ThO_2 creep rate in compression is initially enhanced by small additions of CaO, but after several hundred hours the creep rate approaches that for pure ThO_2. Table 15 summarizes the available creep data for ThO_2, which allows estimation of some of the parameters in Equation 36.

The stress dependence of creep rate is plotted in Figure 40. The stress-dependent exponent is 1 for fine-grained ThO_2 at low stresses, indicating diffusion-controlled creep. At higher stresses the stress exponent increases, suggesting a change in mechanism. The coarse-grained material has a stress exponent of about 4, indicating dislocation creep. Arrhenius plots for the

TABLE 15. Creep Properties of ThO_2 and ThO_2-10 wt% UO_2

Material	Grain Size, μm	Volume of Pores, %	Stress Exponent (n)	Activation Energy (Q_c), kJ/mol	Reference
ThO_2	10	2.5	1-1.6	469	Poteat and Yust (1966)
ThO_2	15	1.5	1	--	Wolfe (1970)
ThO_2	220	1.5	4	682	Wolfe (1970)
ThO -10 wt% UO_2	30	3.0	1	--	Wolfe (1970)
ThO -10 wt% UO_2	120	3.0	4	502	Wolfe (1970)

ThO_2 creep data are shown in Figure 41, and the activation energy in the low stress region varies from about 470 kJ/mol for the fine-grained material to 680 kJ/mol for coarse-grained material. Wolfe (1970) carried out some creep tests on ThO_2-10 wt% UO_2 samples, and the stress exponents, grain size dependency, and activation energies are similar to pure ThO_2. Unfortunately, there are not sufficient data on similar grain size samples to indicate the

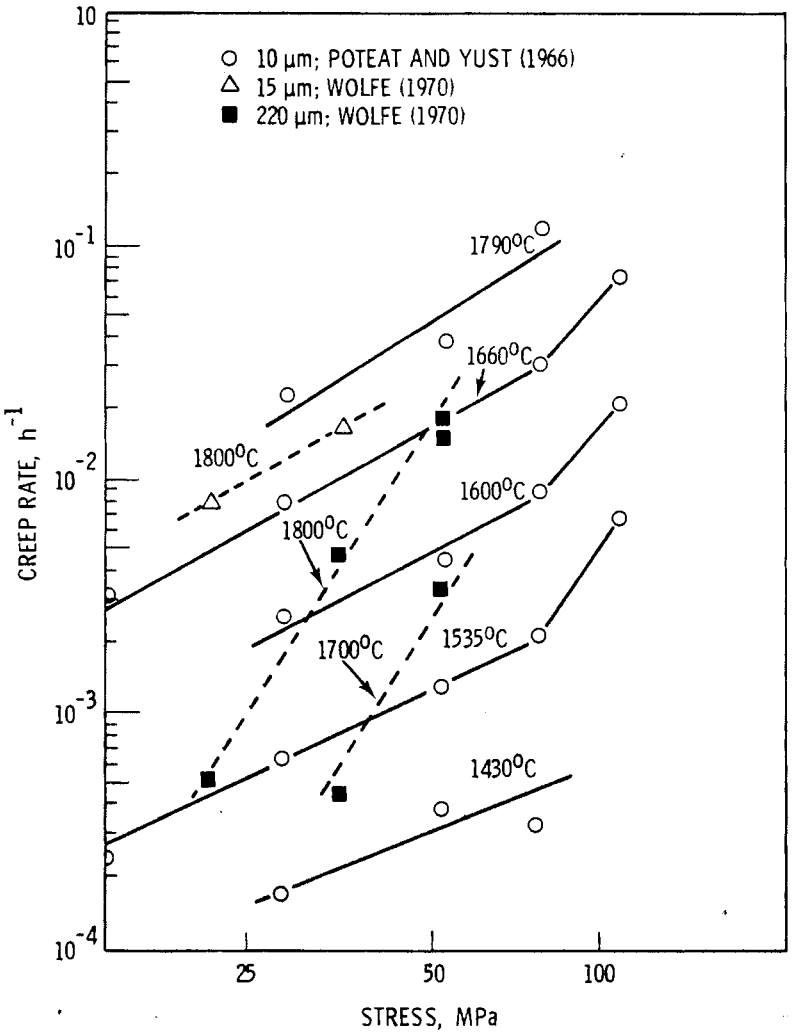

FIGURE 40. Steady-State Creep Rate for ThO_2 in Compression as a Function of Applied Stress[2]

effect of UO_2 on concentration creep rates. Kittel et al. (1977) compared ThO_2 and UO_2 creep behavior and show that, in general, stress dependencies, activation energies, and creep rates are similar. However, much more information is needed before a reliable creep equation can be estimate for ThO_2.

Creep rates of UO_2 are significantly enhanced during irradiation, and the temperature dependency can be totally masked by fission-induced creep at temperatures below 850°C. The creep behavior of ThO_2 will also be strongly influenced by irradiation, but no data have been generated.

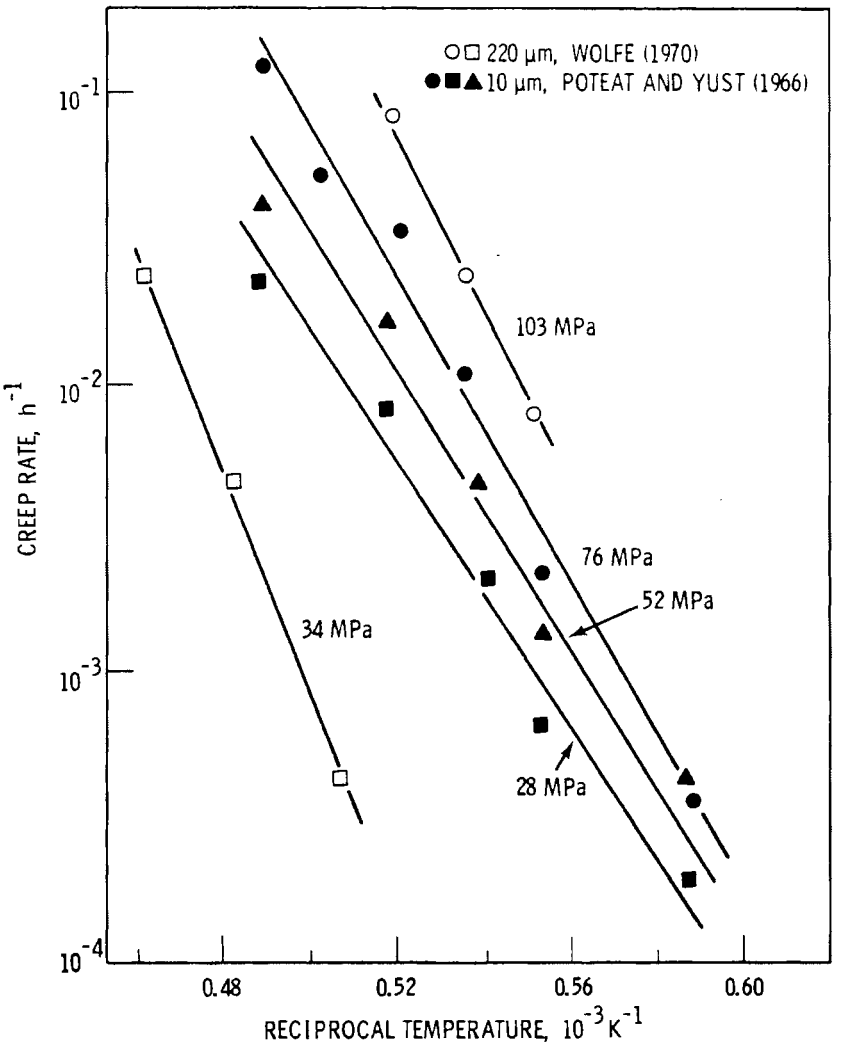

FIGURE 41. Steady-State Creep Rate for ThO_2 in Compression as a Function of Temperature

3.3.3 Fracture Strength

The fracture strength of polycrystalline ceramics is very sensitive to microstructural features. Knudsen (1959) attempted to relate the effect of porosity and grain size on the flexural strength of porous polycrystalline ceramics and used ThO_2 as a model material. Knudsen fitted his results to an equation of the form

$$S = kG^{-a}e^{-bp} \qquad (37)$$

where

S is fracture strength, MPa
G is grain size, μm
p is the pore volume fraction, and
k, a, and b are empirical constants.

Although there seems to be some controversy about interpretation of Equation 37, the data accurately fit the relationship, and Knudsen's results below describe the fracture behavior of ThO_2 sintered at 1800°C:

Room Temperature Flexural Strength, MPa

$$S = 542\ G^{-0.40} e^{-4.2p}$$

1000°C Flexural Strength, MPa

$$S = 782\ G^{-0.46} e^{-6.6p}$$

Room Temperature Compressive Strength, MPa

$$S = 1149\ G^{-0.50} e^{-6.6p}$$

As expected, strength decreases with increasing porosity and grain size. The 1000°C strength was lower than the room-temperature strength. Lang and Knudsen (1956) and Curtis and Johnson (1957) published some fracture strength data for ThO_2 containing CaO, and the results are reasonably consistent with pure ThO_2 but not complete enough to establish any trends. Lang and Knudsen noted that flexural strength of small specimens was significantly greater than for large specimens. This is due to the decreased probability of finding a large critical flaw and must always be considered when comparing fracture strength data of ceramic materials.

Both Ryshkewitch (1960) and Yust and Poteat (1965) noted a decrease in ThO_2 compressive strength with temperature from 1500 MPa at 20°C to 100 MPa at 1900°C, and a transformation from brittle to ductile failure occurred at 1500°C (Yust and Poteat 1965). Gilbert (1965) observed extensive plastic

deformation in ThO_2 at 1600°C and suggested that slip occurs on (111) planes at high temperatures.

3.3.4 Mechanical Properties of ThO_2 - Summary and Evaluation

With the exception of elastic moduli and flexural strength, the mechanical properties of ThO_2 have not been completely characterized. The limited creep data indicate close similarities with UO_2 behavior, and a few more well defined studies might be sufficient to allow ThO_2 creep equations to be based on those developed for UO_2. Only limited information is available on high-temperature fracture and plastic deformation in ThO_2, and the important area of fracture mechanics and cracking behavior is virtually unexplored.

Limited data show that CaO additions to ThO_2 do not significantly change room temperature strength but can modify creep properties at elevated temperatures. If additives are needed to enhance dissolution rates of ThO_2-based fuels, the influence of these additives on mechanical properties should be understood.

The effect of UO_2 on the mechanical properties of ThO_2 is unknown. The few creep tests with ThO_2-10 wt% UO_2 could not be compared directly with similar ThO_2 tests. Since the properties and structure of ThO_2 and UO_2 are similar, it is tempting to predict that the mechanical properties of mixed oxides will be similar to those of the pure oxides. This might be a good assumption if homogeneous mixing and complete solid solution after sintering could be guaranteed. However, fabrication experience suggests that a homogeneous structure might be difficult to achieve with high UO_2 loadings, and the grain size and porosity will probably be modified by UO_2 additions.

Finally, the influence of neutron irradiation on the mechanical properties of ThO_2 is unknown. Creep results on UO_2 indicate that fission effects can completely swamp other factors such as temperature.

4.0 IRRADIATION BEHAVIOR OF ThO_2-UO_2 FUELS

4.1 IRRADIATION EXPERIENCE

Early studies of the irradiation behavior of ThO_2-UO_2 fuels were initiated because of expected advantages of ThO_2-UO_2 fuels over UO_2 fuels. Thorium dioxide crystallizes in the same stable cubic fluorite lattice as uranium dioxide, but has a melting point about 500°C higher. The higher melting point indicates the potential for higher-temperature operation, increased power ratings, and good structural stability of the thoria-based fuels. Another advantage of the ThO_2-UO_2 fuels is that thorium atoms in the fuel can improve the conversion ratio of thermal reactors by converting natural thorium to fissionable ^{233}U.

Although several isolated irradiation experiments on ThO_2 and ThO_2-UO_2 materials have been conducted, the bulk of the irradiation data generated in the U.S. has come from four goal-oriented programs:

1) the Boiling Water Reactor (BWR) Program, which culminated in the irradiations performed in the BORAX-IV and Elk River reactors
2) the Thorium Utilization Program, which included the irradiation of vibratorily compacted and pelletized fuels
3) the Babcock and Wilcox developmental work on pressurized water reactor (PWR) fuels, which led to the first core loading of the Indian Point Reactor owned by Consolidated Edison
4) the Light Water Breeder Reactor (LWBR) Program at Bettis Atomic Laboratory, which resulted in the core loading of the Shippingport Reactor.

Other countries that have conducted research in ThO_2-UO_2 fuels include Canada, India, and Italy. Irradiation experiments in Canada and India were carried out in CANDU-type (Canadian Deuterium-Uranium) heavy water reactors, while those carried out by Italian researchers were conducted mainly in the Halden Boiling Water Reactor at Halden, Norway.

4.1.1 BORAX-IV BWR Program

Early irradiation experiments of ThO_2-UO_2 fuels were performed at Argonne National Laboratory (Handwerk and Noland 1957, 1959; Hoenig et al. 1958; Kittel and Paine 1958, 1959, 1961; Kittel and Handwerk 1958; Neimark and Kittel 1959). These experiments were carried out in the Chicago Pile No. 5 (CP-5), located at Lemont, Illinois, and the Materials Test Reactor (MTR), located in Idaho Falls, Idaho. Fuel samples in both reactors contained 2.5 and 10.0 wt% UO_2. Data from the CP-5 and MTR irradiation tests were used to determine the fuel design for the later BORAX-IV reactor tests.

Irradiation tests in CP-5 (Hoenig et al. 1958) were performed on 5 pellets (0.64 cm diameter and 1.27 cm long). The uranium was 93% enriched in ^{235}U, and various types of bonding and cladding materials were used. The irradiation periods ranged from 1100 to 1190 h; during this time the specimens received mild irradiation (10^{13} n/cm^2-s) with little resulting damage. The bare specimen did not crack, and the remaining specimens with 2.5 wt% UO_2 showed little reaction between the oxide and cladding. Specimens containing 10 wt% UO_2 did not receive postirradiation examination. A summary of the fuel characteristics and test conditions for the CP-5 experiments is given in Table 16.

TABLE 16. Fuel Characteristics and Irradiation Data From CP-5 Experiments

UO_2 Content, wt%	Cladding Type	Bonding Type	Burnup, at.%	Fuel Temperature, °C		Linear Heat Rate, kW/m
				Surface	Centerline	
2.5	None	Air	0.02	270	435	1.8
2.5	304 SS	Air	0.05	270	465	2.1
2.5	Zircaloy-2	Air	0.05	270	465	2.1
10.0	Al-Ni	Lead	0.31	270	955	9.2
10.0	Al-Ni	Lead	0.32	270	955	9.2

The same types of specimens were irradiated in the MTR during the same period (Kittel and Handwerk 1958). A summary of the MTR irradiations is shown in Table 17. The major differences between the two experiments were in

- maximum neutron flux (CP-5: 10^{13} n/cm^2-s; MTR: 4×10^{14} n/cm^2-s)
- thermal shock caused by reactor scrams (CP-5: 250 scrams; MTR: 50 scrams)
- burnup (CP-5: ≤ 0.32 at.%; MTR: ≤ 1.25 at.%).

Results from the MTR experiment indicated that although no dimensional changes in the specimens outside of experimental error resulted from irradiation, lead-bonded specimens appeared to outperform gas-bonded ones: assemblies of fuel pellets lead-bonded to aluminum alloy cladding experienced higher heat fluxes without damage than similar assemblies with helium-argon bonding. This led to the decision to use lead-bonded, aluminum-alloy-clad fuel pellets for the BORAX-IV experiment. BORAX-IV was the fourth in a series of boiling water reactor experiments conducted at the National Reactor Testing Station at Idaho Falls (Walker et al. 1958; Handwerk and Noland 1959; Simnad 1971a). Table 18 describes the BORAX-IV reactor.

Experiments conducted at the BORAX-IV reactor (Maxon et al. 1959) included control blade ejection (to obtain information on the self-limiting capabilities of the reactor), steady-state boiling (at 0.1 to 2.2 MPa) and reactor stability (obtained from rod oscillator measurement). As a result of intermittent experimental operation for one year, about 300 MWd of energy was generated, and an estimated 71 g of ^{233}U were produced. Because of the successful operating experience, the core was expanded from 59 to 69 fuel elements. Some fuel elements were found to be defective after restart at higher power, but the defects were attributed to a weakness in the mechanical design of the cladding (Robertson and Hall 1959; Reinke et al. 1961); furthermore, the increase in activity in the reactor water was not substantially above that obtained during normal operating conditions.

To determine the burnup limitations of the BORAX-IV fuel assembly and gather more irradiation data on the ThO_2-UO_2 fuel, investigators at Argonne National Laboratory (Neimark and Kittel 1964) took small sections of the

TABLE 17. Fuel Characteristics and Irradiation Data from the Materials Test Reactor (MTR) Experiment

UO_2 Content, wt%	Number of Specimens	Cladding Type	Bonding Type	Burnup, at.%	Fuel Temperature, °C		Linear Heat Rate, kW/m	Pellet Dimensional Changes, %	
					Surface	Centerline		Length	Diameter
2.5	2	None	None	0.16 to 0.75	80 to 220	110 to 480	3 to 18	0.0	0.0
2.5	4	Zircaloy-2	NaK	0.30 to 0.69	120 to 230	290 to 480	8 to 20	0.0 to -0.1	0.0 to -0.7
2.5	4	Zircaloy-2	Air	0.25 to 0.74	380 to 820	470 to 1210	7 to 22	0.0 to 0.3	0.0 to -0.1
2.5	1	304 SS	NaK	0.57	200	380	16	-0.1	0.0
2.5	1	304 SS	Air	0.74	810	1200	21	-0.1	-0.2
10.0	4	Al-1 wt% Ni	Lead	0.34 to 1.25	150 to 440	310 to 2200	7 to 25	-0.2 to -0.3	0.3 to 0.9
10.0	4	Al-1 wt% Ni	Gas[a]	0.34 to 1.25	260 to 860	420 to 2740	6 to 24	0.3 to 2.2	0.3 to 0.2

(a) A welding gas mixture of 80% helium and 20% argon

TABLE 18. Description of the BORAX-IV Reactor and Experimental Conditions

Owner	U.S. Atomic Energy Commission
Designer/operator	Argonne National Laboratory
Location	National Reactor Testing Station, Idaho
Reactor type	BWR, natural circulation, direct cycle
Moderator and coolant	Water
Power	2.4 MWe; 14.5 MWt (initial); 20 MWt (final)
Power density	36 kW/liter
Neutron flux (thermal)	5×10^{13} n/cm^2-s
Fuel composition	93.64 wt% ThO_2; 6.36 wt% UO_2
Enrichment	7% ^{235}U
Pellet diameter	0.58 cm
Pellet length	0.95 - 1.91 cm
Cladding type	Al-Ni
Bonding type	Lead
Core diameter	100 cm
Core height	60 cm
Coolant temperature	215°C
Coolant pressure	2 MPa

standard aluminum alloy BORAX-IV tube plate containing fuel pellets and irradiated them directly in the MTR and the Engineering Test Reactor (ETR). The chosen UO_2 content for use in the BORAX-IV experiment was 6.36 wt%; however, samples of 12.7 and 25.6 wt% UO_2 were also tested because they allowed higher heat ratings and burnups. Results of the irradiation tests in the MTR and ETR, summarized in Table 19, indicated higher burnup and fractional fission gas release from the 25.6 wt% UO_2 specimens than from specimens with lower UO_2 content. The two specimens containing 25.6 wt% UO_2 also experienced cladding failure, which was attributed to excessive internal pressure (presumably caused by fuel thermal expansion and fission gas release) in areas of weak cladding. During postirradiation examination,

TABLE 19. MTR-ETR Irradiation Data

UO_2 Content wt%	Number of Specimens	Effective Full Power Days	Burnup, at.%	Fuel Surface Temperature, °C	Linear Heat Rate, kW/m	Diameter Change, %	Volume Change, %	Fission Gas Release, %
6.36	14	121 to 266	0.7 to 3.7	60 to 200	10 to 67	-7 to +6	0 to 2	0 to 51
12.7	2	143 to 266	3.1 to 3.2	145 to 240	24 to 85	0 to 4	1 to 2	22 to 49
25.6	2	143 to 266	3.7 to 4.4	190 to 240	64 to 85	1 to 8	--	48 to 81

Neimark and Kittel (1964) found the specimens that received a high heat flux (>200 W/cm^2 at cladding surface) during their last reactor cycle released abnormally large amounts of fission gas. Burnup in these specimens was in the range from 3.7 to 4.4 at.%. Metallographic examination of these specimens showed extensive columnar recrystallization below the melting point. Because this type of recrystallization was accompanied by oxygen release (through oxide sublimation and condensation), the fuel thermal conductivity was reduced. Consequently, an increase in fission gas release occurred.

Some additional tests (Robertson 1960; Simnad 1971b) were carried out in the Experimental Boiling Water Reactor (EBWR), with defected fuel rods in order to confirm the low leachability of fission products from ThO_2-UO_2. During these tests, no increase in gross activity of the reactor water was observed. However, analysis of the air ejector gases did show that the quantity of fission product gases had increased and that the fractional gas releases were consistent with calculated results obtained from models that describe fission gas release from oxide fuels by a diffusion-controlled release mechanism.

In an attempt to improve the thermal conductivity and thermal shock resistance of ThO_2-UO_2 fuels, investigators at ANL (Neimark et al. 1961) irradiated ThO_2-UO_2 fuels containing fibers of molybdenum or niobium in the Engineering Test Reactor (ETR). Fuel samples containing 10 to 50 wt% UO_2 were examined. Although the test results showed several advantages for the metal-fiber-reinforced fuels (increased thermal conductivity and heat rating of the fuel, reduced central void formation, and maintained integrity of the pellets), no further research was done after the conclusion of these initial tests.

4.1.2 Elk River BWR Program

The Elk River Reactor (ERR), described in Table 20, was an indirect-cycle, natural-circulation boiling water reactor owned by the U.S. Atomic Energy Commission (AEC). It pioneered the use of ThO_2-UO_2 fuel with 0.06% boron-304SS cladding to demonstrate the thorium fuel cycle (Simnad 1971c). The reactor was started up in 1963. At the end of the first cycle, the core achieved an average burnup of 0.7 at.%. Examination of the rod positions as a function of

irradiation time indicated excellent agreement between predicted and observed fuel performance throughout the core life (Fisher and Kendrick 1968).

Because data on the thorium fuel cycle had been of interest to the AEC and the reactor industry, some of the prototype ERR fuel elements were also irradiated in the Experimental Boiling Water Reactor (EBWR). Neimark (1961) examined a prototype ERR fuel assembly irradiated in the EBWR to a maximum burnup of 0.1 at.%. This assembly, consisting of an array of Type 304 stainless steel tubes with pellets containing 3 wt% UO_2, showed insignificant thermal effects and cracking. Within the ranges of heat rating and burnup, the ThO_2-UO_2 fuel pellets showed no signs of central melting, recrystallization, or heat-affected zones. They also exhibited good gas retention characteristics and excellent dimensional stability. A summary of the irradiation experiment is presented in Table 21.

TABLE 20. Description of the Elk River Reactor (ERR) and Initial Operating Characteristics

Owner	U.S. Atomic Energy Commission
Designer/operator	Allis-Chalmers Rural Cooperative Power Assoc.
Location	Elk River, Minnesota
Reactor type	BWR, natural circulation, indirect cycle
Moderator and coolant	Water
Power	22 MWe; 64 MWt; efficiency 34%
Specific power	341 kW/kg ^{235}U
Power density	25.6 kW/liter
Neutron flux	Thermal average: 1.55×10^{13} n/cm^2-s; Fast average: 4.8×10^{13} n/cm^2-s
Heat flux	27 kW/cm^2
Coolant temperatures	Inlet 230°C; outlet 280°C
Coolant pressure	6 MPa

TABLE 21. Irradiation Experiment on an ERR Fuel Assembly

Design Parameter or Experimental Characteristic	Data
Number of fuel rods	25
Fuel composition	97 wt% ThO_2; 3 wt% UO_2
Fuel density	94% TD
Pellet diameter	1.0 cm
Pellet length	1.3 cm
Enrichment	93% ^{235}U
Cladding type	304 SS
Cladding outside diameter	1.15 cm
Cladding thickness	0.05 cm
Maximum burnup	0.1 at.%
Maximum increase in assembly width	1.2%
Maximum increase in corner rod diameter	2.0%
Fission gas release[(a)]	0.3% and 0.7%

(a) Fission gas release was measured for two rods only. Burnup levels in these rods were 0.04 and 0.05% at.%, respectively.

4.1.3 Thorium Utilization Program

In order to study the potential application of thorium-based compounds (oxide and carbides) in power reactors, the Atomic Energy Commission sponsored a Thorium Utilization Program to investigate the irradiation behavior of thorium-uranium alloys and compounds. The objectives of this irradiation program were to compare the characteristics of the chemically produced sol-gel ThO_2-UO_2 fuel with those of arc-fused material, and to compare the performance of vibratorily compacted rods with rods containing pressed and sintered pellets. Olsen et al. (1965, 1966) at the Oak Ridge

National Laboratory conducted a series of tests (Wymer and Douglas, 1965, 1966a, 1966b; Wymer and Lotts, 1969a, 1969b) in the Materials Test Reactor (MTR). Engineering Test Reactor (ETR), the Chalk River National Research Experimental Reactor (NRX), and the Oak Ridge Research Reactor (ORR). Fifty-eight arc-fused and sol-gel rods, having smear densities of 74 to 90% TD, were irradiated at linear heat rates of 16 to 96 kW/m to various burnup levels (maximum 10 at.%). Among the test rods, 18 sol-gel rods had Zircaloy-2 cladding, while the remainders were clad in Type 304 stainless steel.

To compare test results, Olsen et al. (1966) selected a group of tests conducted at linear heat rates (30 to 46 kW/m) that are similar to those of current water-reactor elements using UO_2 as a fuel. Over 80% of the rods selected for comparision had experienced high burnups ($\geq$5 at.%). The operating conditions of these tests are shown in Table 22. Upon examination of the irradiated rods, Olsen et al. (1966) concluded that sol-gel and sintered pellet ThO_2-UO_2 behaved nearly the same under similar experimental conditions, and that both pellet and sol-gel fuel had the basic performance characteristics for a power reactor fuel up to 10 at.% burnup. In addition, they found that for all three fuel forms (arc-fused, sol-gel and sintered) at up to 10 at.% burnup:

- The fractional fission gas release was generally less than 20%.
- The change in volume was less than 0.5% for each atom percent of burnup.
- There was very little difference in macroscopic appearance of the cross sections between vibratorily compacted and pellet fuels.

One of the earliest attempts to extensively analyze irradiation behavior of ThO_2-UO_2 fuels at high burnup was made by researchers at ORNL (Rabin et al. 1965). A series of unencapsulated fuel rods, ThO_2-4.45 wt% UO_2 pellets clad with Type 304 stainless steel, were successfully irradiated in MTR or ETR. The fuel rods achieved burnups that ranged from 4 to 10 at.% at linear heat rates up to 46 kW/m. Three fuel rods were selected from this series of irradiation tests and given a thorough postirradiation examination.

TABLE 22. Irradiation Conditions for ThO_2-UO_2 Fuels Examined in the Thorium Utilization Program

Form	UO_2 Content, wt%	Fuel Type	Number of Rods	Fuel Density, % TD	Maximum Burnup, at.%	Time Averaged Peak Linear Heat Rate, kW/m	^{85}Kr Release, %
Arc Fused	4.45	Vibratorily Compacted	11	85 to 87	1.5	30	2.4
					5.2	30	7.2
					8.6	27	6.4
Sol-Gel	4.45	Vibratorily Compacted	47	85 to 87	1.7	34	0.5
					4.9	29	13.2
					10.0	31	17.0
Pressed and Sintered	4.45	Pellet	4	93	15.8	42	22.8
					12.7	46	12.4
					4.9	27	- -
					6.6	39	- -

Basic design parameters for the fission gas release experiment are summarized in Table 23, and irradiation data are presented in Table 24.

Although the dimensional data were not completely documented for the individual rods before irradiation, Rabin et al. (1965) deduced from the limited data that no appreciable fuel rod swelling occurred. Stress analyses also indicatedthat fuel pellet swelling was limited to about 0.8% change in volume for each atom percent of burnup. The dimensional stability exhibited in these experiments is shown in Table 25.

Fission gas release data are available only for the rod that experienced the highest burnup (10 at%). The release was 14%, which indicated that fission-gas retention in the ThO_2-UO_2 system was comparable to other oxide fuel systems when irradiated under similar conditions (Rabin et al. 1965). There were no major changes reported in the microstructural details of the fuel pellets or the cladding after irradiation. Analysis of the fuel by x-ray diffraction showed evidence of lattice strain, but a relatively crystalline structure was maintained.

TABLE 23. Design Parameters for High-Burnup Fission Gas Release Experiment

Design Parameters	Data
Fuel Composition	95.55 wt% ThO_2; 4.45 wt% UO_2
Fuel density	93% TD
Enrichment	93.2% ^{235}U
Pellets per tube	7
Pellet diameter	0.65 cm
Pellet length	1.25 cm
Weight of fuel material per tube	31 g oxide
Active length of tube (less ceramic end spacers, if required)	8.90 cm
Cladding type	304 SS
Cladding outside diameter	0.80 cm
Cladding thickness	0.064 cm
End spacer length (each of two)	1.10 cm

TABLE 24. Irradiation Data for High-Burnup Fission Gas Release Experiment

Fuel Rod Number	Irradiation Period, Days	Reactor Power, MWd	Full Power Days	Cladding Surface Temperature, °C	Maximum Burnup, at.%	Peak Linear Heat Rate,(a) kW/m	Peak Surface Heat Flux,(a) kW/m	Fuel Centerline Temperature,(a) °C
1	855	26,400	660	~95	10	46	1850	1410
2	650	19,874	497	~95	4	27	1080	850
3	900	71,078	406	~95	5	39	1580	1190

(a) Calculated, time-averaged value (peak refers to maximum burnup area); gamma heating not included.

TABLE 25. Comparison of Dimensional Data on Unirradiated and Irradiated ThO_2-UO_2 Pellet Rods

Fuel Rod Number	Diameter, cm			Length, cm	
	Preirradiation (Specification)	Postirradiation (Average)	(Max)	Preirradiation (Specification)	Postirradiation
1	0.80 ± 0.0025	0.77	0.78	11.43 ± 0.04	11.41
2	0.80 ± 0.0025	0.80	0.81	11.43 ± 0.04	11.38
3	0.80 ± 0.0025	0.77	0.78	11.43 ± 0.04	11.63

4.1.4 Indian Point PWR Program

The Indian Point Nuclear Power Station, located north of New York City on the Hudson River, has been producing power for the Consolidated Edison system since September 1962 (Ward 1958; Simnad 1971d). This PWR pioneered the use of fertile ThO_2 and highly enriched (93% ^{235}U) fissile UO_2 mixtures for the conversion of ^{232}Th to ^{233}U. A description of the initial characteristics of the Indian Point Reactor is given in Table 26.

To study the effects of irradiation on the design, fabrication techniques, and materials used for the Indian Point Reactor, Babcock & Wilcox (the designer) carried out the Indian Point Reactor Irradiation Program, which consisted of a series of in-pile tests. The mixed-oxide fuels, ThO_2 with 6.5 wt% or 9.1 wt% UO_2, were irradiated under conditions that equalled or exceeded the initial design conditions indicated in Table 26. Specimens were irradiated at linear heat ratings ranging from 7 to 41 kW/m and burnups up to 3 at.% with little change observed except for cracking of the fuel (DeBoskey 1963).

Core 1 (the initial core) of the Indian Point Reactor operated satisfactorily for over 3 years (442 effective full-power days) and attained a burnup of 4 at.% (Deddens and Freyberg 1965; Prestile and Edlund 1966; Baroch and Bishop 1968). After the discharge of Core 1, 13 fuel rods were selected for detailed examination (Baroch et al. 1969). The lack of pellet distortion and cladding strains indicated that irradiation-induced fuel swelling was minimal.

The release of fission gas was also analyzed for four of the fuel rods (Table 27). Results indicated that the amount of fission gas release was less

TABLE 26. Description of the Indian Point Reactor and Core-1 Design

Owner	Consolidated Edison Company
Designer	Babcock and Wilcox
Operator	Consolidated Edison Company
Location	Buchanan, Indian Point, New York
Reactor type	PWR, thorium-uranium converter
Moderator and coolant	Water
Power	151 MWe; 585 MWt; efficiency 26%
Power density	76 kW/liter
Neutron flux	Thermal average: 2×10^{13} n/cm^2-s Fast average: 1.5×10^{14} n/cm^2-s
Heat flux	390 kW/m^2
Fuel composition	94.7 wt% ThO_2; 5.3 wt% UO_2
Enrichment	93% ^{235}U
Pellet diameter	0.66 cm
Pellet length	1.91 cm
Cladding type	304 ss
Cladding outside diameter	0.76 cm
Cladding thickness	0.05 cm
Maximum burnup	4 at.%
Coolant temperatures	Inlet 250^o; outlet 300^{o}C
Coolant pressure	10 MPa

than 2%, regardless of fuel enrichment or burnup. Baroch et al. (1969) pointed out that approximately the same amount would be released from UO_2 operated under similar conditions.

4.1.5 LWBR Development Program

The Atomic Energy Commission in 1965 undertook a research and development program to design and build a Light Water Breeder Reactor (LWBR) core for operation in the Shippingport Station. A large amount of technical information has been generated under the LWBR program since the late 1960s. The majority of

TABLE 27. Analysis of Fission Gas Release from Indian Point Core 1 (Baroch et al. 1969)

Experimental Characteristic		Data
Number of rods examined		4
Gas content in rod		5.5 to 9.5 cm^3
Calculated rod pressure		185 to 315 kPa
Measured composition of fission gases	Xe	18 to 52%
	Kr	5 to 25%
	Xe/Kr	5.1 to 7.2
Average rod burnup		0.66 to 2.03 at.%
Total amount of fission gas released		1.0 to 2.4%

experiments were carried out at the Bettis Atomic Power Laboratory in Pittsburgh, Pennsylvania. These experiments include in-pile studies of thermal conductivity (Jacobs 1969 and 1970), creep behavior (Germann 1967), fission product distribution (Berman 1976), dimensional changes (Giovengo 1970), and fission gas release (Goldberg et al. 1977 and 1978) of ThO_2-UO_2 fuel rods with various UO_2 contents.

Results obtained from thermal conductivity studies of ThO_2-UO_2 fuels containing up to 10 wt% UO_2 irradiated at a low burnup (<1 at.%) indicated that the thermal stability of ThO_2-UO_2 fuels are superior to UO_2 fuels. Within the same irradiation temperature range (600 to 1000°C), there was no significant difference between the thermal conductivities of irradiated and unirradiated UO_2 fuels up to a burnup of 0.03 at.%. This same characteristic was observed for ThO_2-10 wt% UO_2 fuels up to a burnup of 0.1 at.% (Jacobs 1969).

Germann (1967) examined the in-pile creep properties of zircaloy-clad ceramic fuels including UO_2, ThO_2-2 wt% UO_2 and ThO_2-10 wt% UO_2. These fuel samples were irradiated at low temperature (315-760°C) under compressive load for one test reactor cycle to determine the fission-dependent creep. The data

indicated that UO_2 fuel had lower fission induced creep than ThO_2-UO_2 fuels. Increasing the UO_2 content in ThO_2-UO_2 fuels from 2 to 10 wt% reduced the creep by 20%.

Giovengo (1970) evaluated the data on in-pile dimensional changes of ThO_2-UO_2 fuel rods obtained at Bettis Atomic Power Laboratory. The major emphasis of this study was to assess the effects of geometric and environmental test variables on observed axial ratcheting, which is the progressive elongation of a fuel rod resulting from irradiation.

Three irradiation test series (identified as C7, NRX, and B1) comprising 29 fuel rods (2 to 30 wt% UO_2) with non-free-standing cladding were performed with the following test variables:

- Fuel burnup: up to 2.1 at.%
- Zircaloy cladding heat treatment: stress-relieved for 4 h at 510°C and recrystallization annealed for 4 h at 680°C
- Fast flux environment: 0.1×10^{14} to 1.2×10^{14} n/cm^2-s, >1 MeV
- Pellet configuration: flat and dished end
- Fuel centerline temperature: 815 to 2205°C
- Cladding diameter to thickness ratio: 20 to 25
- Fuel-cladding diametral gap: 0.005 to 0.03 cm
- Accelerated power cycling: 20 to 100% power at 2.5%/min
- Number of pressure cycles: maximum of 36.

Tables 28 and 29 provide a physical description of the test specimens and a summary of the operation and test results. Giovengo (1970) concluded that

- Cladding heat treatment and the fast flux environment produce the greatest effect on axial ratcheting of fuel rods.
- Test specimens fabricated with flat-ended pellets elongated substantially more than comparable specimens with dished-end pellets.
- An increase in fuel centerline temperature from less than 1100°C to above 1370°C caused the rod elongation to increase by two to three times.

- Pressure cycling appeared to be the predominant mechanism that induced rod elongation from fuel-cladding interaction.
- Accelerated power cycling showed no effect on the observed ratcheting: Four fuel rods with various cladding gap sizes (0.004 to 0.03 cm) were cycled from 20 to 100% power at a rate of 2.5% per minute. Comparison between the length and diameter changes of these rods indicated essentially equivalent values.

TABLE 28. Description of Test Rods in the LWBR Experiment on Dimensional Changes

Test Series	Number of Rods	UO_2 Content, wt%	Density, % TD	Fuel-Cladding Diametral Gap, μm	Cladding OD, mm	Cladding OD to Thickness Ratio
C7	14	6 to 30	93 to 95	50 to 300	17.9 to 18.2	20.7 to 28.2
NRX	6	3.10 to 3.42	95 to 98	100 to 280	15.2 to 15.5	20.4 to 25.0
B1	9	1.98 to 2.84	93 to 98	100 to 250	14.5 to 15.5	19.6 to 25.0

TABLE 29. Irradiation Test Data from the LWBR Experiment on Dimensional Changes

Test Series	Burnup, at.%	Fuel Centerline Temperature, ^{o}C	Peak Linear Heat Rate, kW/m	Elongation, %	Diameter Change, %
C7	0.03 to 0.77	720 to 2480	4 to 23	0.04 to 0.99	-0.53 to +0.50
NRX	0.01 to 1.37	1160 to 2425	13 to 33	0.07 to 0.88	-0.95 to +0.28
B1	0.07 to 0.48	1200 to 2050	13 to 17	0.09 to 0.57	-0.63 to -0.03

The mechanism of fuel swelling and fission gas release in oxide fuel rods was studied earlier in the LWBR Development Program by Nichols and Warner (1970). They reviewed the various concepts describing the fission gas release mechanism, and developed a model that took into account the recoil and knock-out mechanisms at low temperatures ($<1200^{o}C$ for UO_2), and the bubble migration mechanism at higher temperatures ($\geq 1200^{o}C$ for UO_2). Based on this model, a computer code (BUBL) was developed to predict fission gas release behavior in oxide fuels. Following the study of Nichols and Warner, Goldberg et al. (1978) investigated the fission gas release from ThO_2 and ThO_2-UO_2 fuels. The purpose of

Goldberg's fission gas release study was to collect experimental data from 51 irradiated fuel rods and to compare them to calculated results from a model used in performance assessment. This model combined the high-temperature model of Warner (1969) and a modified low-temperature model derived from that of Bellamy and Rich (1969). The major mechanisms of fission gas release described in this model included gas bubble coalescence and release from grain boundaries and dislocations.

A summary of the design data for the experiment is given in Table 30. Fuel rod operating parameters and fission gas release measurements are presented in Table 31. Because of the scatter in the fission gas release data, fractional gas release was calculated by the use of a correction factor which accounted for the effect of pellet density on fission gas release. Measured gas release and initial pellet density were used to determine the magnitude of the normalized (corrected) gas release.

To compare experimental data with calculated results, Goldberg et al. (1978) plotted the measured and normalized fission gas release data against rod average burnup for two fuel centerline temperature regimes--temperatures above and below the ThO_2 dislocation release region (1440 to 1610^{o}C), where fission gas bubbles were released from dislocations. The authors concluded that, within the range of parameters tested for the 51 fuel rods,

- Fission gas release was higher at higher temperatures and burnups.
- Higher initial fuel density resulted in significantly less fission gas release.
- No sensitivity to UO_2 content or fuel rod diameter was observed.
- Calculated results bound experimental data; hence the model was conservative for use in performance assessments.

4.1.6 Canadian Experience

The known thorium resources in Canada are quite significant: the recoverable ThO_2 was estimated to be 1000 tons (Griffith and Roscoe 1964). To evaluate the potential of ThO_2-UO_2 as a nuclear fuel, experiments have been carried out by Chalk River Nuclear Laboratories, Chalk River, Canada, in their reactors NRU and NRX. Initially the irradiation experiments were carried out

TABLE 30. Summary of Fuel Rod Design Data for the LWBR Fission Gas Analysis

Design Parameter	Data
Number of rods examined	51
Fuel type	ThO_2, ThO_2-UO_2
Fuel composition	ThO_2, ThO_2-2 wt% UO_2 to ThO_2-24.7 wt% UO_2
Pellet density	77.8 to 98.7% TD
Pellet diameter	0.5 to 1.7 cm
Pellet length/diameter	1.0 to 3.0
Active pellet stack length	7.6 to 17.8 cm (short)
	76.2 to 213.4 cm (long)
Cladding type	Zircaloy-4
Cladding outside diameter	0.6 to 1.8 cm
Cladding OD/thickness	12 to 25
Gap size	0.01 to 0.06 cm
Pressurized	No
Coolant temperature	288°C
Coolant pressure	67 MPa

TABLE 31. Summary of Irradiation Test Data from the LWBR Experiment on Fission Gas Release

Fuel Type	Number of Rods	UO_2 Content, wt%	Linear Heat Rate, kW/m		Burnup, at.%		Measured Fission Gas Release, %
			Peak	Average	Peak	Average	
ThO_2	7	0	7 to 37	7 to 37	0.1 to 3.5	0.1 to 3.5	0.1 to 1.2
ThO_2 - $^{233}UO_2$	7	6.6 to 8.5	27 to 34	23 to 27	2.2 to 4.7	1.5 to 4.7	0.4 to 2.8
ThO_2 - $^{235}UO_2$	37	2.0 to 24.7	19 to 74	16 to 54	0.4 to 5.1	0.3 to 4.6	<0.1 to 5.2

at low linear heat rates (≤3 kW/m) and low burnups (<0.4 at.%). Bain (1960) conducted irradiation tests on three ThO_2-UO_2 pellet specimens containing 8.8 to 9.0 wt% UO_2 in the NRX reactor, and reported that at up to 3 kW/m and 0.4 at.% burnup, the performance of zircaloy-clad ThO_2-UO_2 pellets was

similar to that of the UO_2 pellets. In a later irradiation experiment on seven ThO_2-2 wt% UO_2 pellets containing pre-formed cracks and holes, Bain (1967) observed that at up to 6 kW/m, the crack healing and void movement behavior mechanism in these pellets were similar to those of UO_2 fuels. At similar power ratings, however, structural changes and fission product relocation were less in ThO_2-2 wt% UO_2 pellets than in UO_2 pellets.

Rao (1964) examined the thermal properties of ThO_2-UO_2 pellet fuel specimens containing up to 20 wt% UO_2 as a function of composition. By measuring the power output necessary to produce central melting in the fuel pellets, he derived the fuel thermal conductivity during irradiation. Calculated thermal conductivities for fuels containing up to 20 wt% UO_2 were then compared to that of UO_2 to investigate the limitations of ThO_2-UO_2 as a nuclear fuel. Rao's results indicated that up to 10 wt% UO_2 the thermal expansion behaviors of ThO_2-UO_2 and UO_2 fuels were essentially the same. As the UO_2 content was raised from 10 to 20 wt%, the thermal conductivity of ThO_2-UO_2 decreased. He attributed this behavior to the increase in pore fraction of the fuel caused by the increasing UO_2 content.

MacEwan and Stoute (1969) studied the irradiation induced thermal conductivity changes in ThO_2-1.3 wt% UO_2 pellets at low temperatures ($<156^{o}C$) and burnups ($<3 \times 10^{-3}$ at.%), and the annealing behavior of the irradiated fuel. Sixteen irradiated pellets having densities of 93.2 to 94 %TD and enrichment of 93% ^{235}U were examined. MacEwan and Stoute reported that irradiation at low temperatures caused a significant reduction in fuel thermal conductivity for burnups above 7×10^{-6} at.%. As burnup proceeded to above 5×10^{-4} at.%, this reduction in thermal conductivity tended to "saturate" and to remain constant at about 50%. Increasing the irradiation temperature into the range of 330 to $420^{o}C$ reduced the change in thermal conductivity by 10%. This result indicated the annealing of damage during irradiation at higher temperatures.

More recently Bain et al. (1977) conducted an experiment on ThO_2-UO_2 fuels irradiated in the NRU reactor. The fuel elements again contained

1.3 wt% UO_2. Two types of assemblies (a "fast-flux peaking" assembly and a "fast-neutron" assembly) were irradiated to maximum burnups of 4 and 6 at.% to study the ThO_2-UO_2 fuel performance under fast-flux conditions. A description of the experiment is given in Table 32.

As a result of the fast-flux irradiation, failures occurred in five "fast-flux peaking" assemblies and ten "fast-neutron" assemblies. Examination of both the intact and failed elements indicated that the causes of failure could include excessive localized strain, preferential cracking in the cladding at the location of the brittle hydrides, and pitting on the cladding inner surfaces caused by corrosive fission products.

TABLE 32. Irradiation Experiment of ThO_2-1.3 wt% UO_2 Fuel Elements in the NRU Reactor

Design Parameter or Experimental Characteristic	"Fast Flux Peaking" Assembly	"Fast Neutron" Assembly
Number of assemblies	13	>10
Number of fuel elements per assembly	19	15
Enrichment	93% ^{235}U	93% ^{235}U
Fuel length	300 cm	50 cm
Cladding type	zircaloy	zircaloy
Cladding outside diameter	1.25 cm	1.52 cm
Cladding thickness	0.04 cm	0.035 cm
Fuel grain size	5 μm	5 μm
Maximum burnup	6 at.%	4 at.%
Maximum linear heat rate	37 kW/m	68 kW/m
Number of assemblies failed	5	10
Number of assemblies examined	6 (3 intact, 3 failed)	5 (failed)
Fission gas release	<1%	≤ 25%

Twenty zircaloy-clad UO_2 rods were also irradiated in the fast neutron assembly to 1 at.% burnup. No failure of the UO_2 rods was observed. Bain et al. examined the difference in irradiation behavior between the ThO_2-1.3 wt% UO_2 and UO_2 fuels, and concluded that the observed differences between ThO_2-UO_2 and UO_2 were due to:

1) Burnup level - the ThO_2-UO_2 rods were irradiated to relatively high burnup levels (4 to 6 at.%), while the UO_2 rods were irradiated to 1 at.%. At 1 at.%, no ThO_2-UO_2 rod would have failed either.

2) Hydriding - Hydrogen present in the ThO_2-UO_2 rods formed brittle hydrides at low operating temperatures ($<100^{o}C$). When the cladding was under excessive localized strain (caused by cyclic loading, fuel swelling, etc.), preferential cracking occurred at the locations of the hydrides. The UO_2 rods, operated at lower burnups, contained no moisture and experienced negligible swelling. Consequently, no excessive localized strain or cracking in the cladding was expected to occur.

The Chalk River and Whiteshell Research Laboratories conducted irradiation tests on over 30 bundles of ThO_2-UO_2 fuels containing 1.5 to 4.7 wt% UO_2 (Jones et al. 1977). At low burnups ($\leq$0.4 at.%) the fission gas release rate was 1 to 2 orders of magnitude lower than that of the UO_2 fuel at the same power rating (30 kW/m). As burnup levels increased to about 1 at.%, fission gas release from both types of fuel were of the same order of magnitude.

Large-scale nuclear energy production from the thorium fuel cycle using CANDU-type reactors has also been considered (Lewis et al. 1971). Economic analysis and conceptual designs have been made (Banerjee et al. 1975). Recent developments in the thorium cycle include the economic analysis of CANDU reactors cooled by pressurized heavy water (PHW) (Critoph et al. 1975), boiling light water (Hatcher et al. 1975), and organic liquids (Hatcher et al. 1975). The effect of various design parameters, such as channel power and lattice pitch, was studied.

4.1.7 Indian Experience

Thorium reserves in India are substantially larger than uranium reserves. Most of the published literature on ThO_2-UO_2 fuels was related to the analysis of fission gas release from pellet or powder fuels having low UO_2

contents (< 1 wt% UO_2), low temperatures (<1000°C) and burnups (<0.01 at.%) (Chawla et al. 1971; Naik et al. 1972 and 1974).

In an analysis of the release behavior of ^{133}Xe as a function of pellet density, Naik et al. (1974) studied two parameters (the apparent diffusity D' and the initial burst release f_0) for sintered ThO_2-0.1 wt% $^{235}UO_2$ and ThO_2-0.1 wt% $^{233}UO_2$ pellets at various fuel densities and operating temperatures. These pellets were irradiated at a flux of $10^{13}n/cm^2$-s for 10 to 15 minutes. A comparison of the results is shown in Table 33. As indicated in this table, the parameters D' and f_0 are of the same order of magnitude for both ^{235}U and ^{233}U containing pellet fuels. Moreover, D' and f_0 decrease with increasing fuel density at varying rates. This phenomenon was explained by an increase in the number of closed pores and a sharp decrease in the number of open pores with increasing fuel density. Naik et al. (1977) also studied the effect of Y_2O_3 doping (0.25 mole %) on ^{133}Xe release from the same ThO_2-0.1 wt% UO_2 pellets, and attributed the decrease in D' (50 to 75%) in doped pellets to the absence of gas atom migration through cation or anion vacancies in the fuel lattice.

Release of ^{133}Xe at low burnups ($\leq$0.02 at.%) from ThO_2-1 wt% UO_2 pellets and powders were compared by Naik et al. (1975). Again the comparison was made in terms of D' and f_0: Both parameters were dose independent below 10^{-5} at.%. As burnup increased, both D' and f_0 decreased sharply. This effect was more pronounced in powder than pellet fuel. For example, at 10^{-5} at.% the D's for both powder and pellet were the same and f_0 for powder was one third that for pellet. As burnup increased to 0.02 at.%, D' for powder decreased to one-twelfth that for the pellet fuel and f_0 for powder decreased to one-eighth that for pellet fuel.

4.1.8 Italian Experience

The Italian uranium-thorium fuel cycle program began in 1960 with the design and construction of the ITREC pilot plant for remote reprocessing and refabrication of irradiated fuel elements for water reactors. Aiming at the effective use of available energy resources, economic evaluations were made on several reactor systems that use thorium as the fertile material (Cardosi et al. 1968). As a result of this study, a comparison of the economic costs of

TABLE 33. Comparison of Release Behavior of ^{133}Xe from ThO_2-0.1% $^{233}UO_2$ and ThO_2-0.1% $^{235}UO_2$ Sintered Pellets

Density, % TD	Fuel Temperature, °C	ThO -0.1 wt% $^{233}UO_2$		ThO -0.1 wt% $^{235}UO_2$		Variation in D', %
		Initial Burst Release (f_o), %	Apparent Diffusivity (D'), s^{-1}	Initial Burst Release (f_o), %	Apparent Diffusivity (D'), s^{-1}	
67	850	-	-	10.00	8.73×10^{-9}	-
66	850	10.21	1×10^{-8}	-	-	-
79	1000	3.95	7.2×10^{-9}	4.08	6.82×10^{-9}	+5.3
79	1000	4.1	7.1×10^{-9}	4.08	6.82×10^{-9}	+3.9
90	1000	8.5×10^{-2}	7.44×10^{-12}	8.7×10^{-2}	7.75×10^{-12}	-4.2

uranium-thorium, enriched uranium, and natural uranium cycles was made. Cardosi et al. (1968) concluded that "although the enriched uranium cycle is the cheapest one, the uranium-thorium cycle offers the biggest saving in fuel reserves." The Comitato Nazionale per l'Energia Nucleare (CNEN) therefore decided to undertake an experimental program (Baldetti et al. 1971) to verify the design hypotheses and the results of the economic evaluation.

A series of irradiation experiments on zircaloy-clad fuel rods containing ThO_2-UO_2 pellets were carried out in the Halden Boiling Water Reactor in Halden, Norway. Test fuels in these experiments were divided into two groups. The first group, consisting of 7 fuel rods (ThO_2-2.4 wt% UO_2), was irradiated in the central zone of the reactor. These fuel rods were produced by the extrusion and sintering methods adopted in the ITREC pilot plant. The objective of the experiment was to test the in-pile behavior of ThO_2-UO_2 fuels made with the ITREC fabrication process. The fuel rods, irradiated at linear heat rates less than 30 kW/m, reached an average burnup of 0.55 at.% without any detectable failure (Baldetti et al. 1971).

A second group, consisting of five test assemblies that contained cold pressed and sintered ThO_2-UO_2 pellets, was irradiated at high linear heat rates and to high burnups to obtain information on the behavior of the test fuel and the effects of certain parameters, such as pellet length and pellet fabrication method. A description of the irradiation tests on the second group is given in Table 34 (Baldetti et al. 1971). Fission gas release data for four test assemblies (Doria 1971) are presented in Table 35.

Some observations made during the above experiments were:

- No significant structural changes took place below a fuel centerline temperature of 1400°C.
- Columnar grain growth in the fuel did not occur below 1800°C, but was evident around 2800°C.

These observations led to the conclusion that the fuel performance of ThO_2-UO_2 was superior to UO_2.

TABLE 34. Summary of CNEN Thorium Fuel Cycle Program: Irradiation of Cold-Pressed and Sintered Pellet Zircaloy-2-Clad Rods (Baldetti et al. 1971)

Test Assembly Number	Number of Rods	UO_2 Content, wt%	Fuel Density, % TD	Fuel Rod Dimensions, cm				Bundle Average Burn-up, at.%	Objective
				Length	OD	Cladding Thickness	Gap Size		
IFA 125	6	10[a]	94	77	1.4	0.06	0.018 to 0.030	0.2[c]	Obtain high heat rating and examine the influence of diametral clearance on fuel centerline temperature and cladding elongation
IFA 126	3	10[a]	94	77	1.4	0.06	0.018 to 0.030	2.5[d]	Study ThO_2-UO_2 at high heat rating and high burnup
IFA 127	3	10[a]	94	77	1.4	0.06	0.018 to 0.030	1.4	Same as for IFA 126; unloaded because of instrumentation failure
IFA 175	8	3.3[b]	90 to 95	30	2.5	0.10	0.016 to 0.024	0.1[c]	Study thorium fuel material for the Cirene reactor
IFA 176	8	3.3[b]	90 to 95	30	2.5	0.10	0.016 to 0.024	0.1[c]	Same as for IFA 175

(a) Uranium enriched in ^{235}U to 93 wt%
(b) Uranium enriched in ^{235}U to 90 wt%
(c) Based on post-irradiation examinations (Nd-method) and on 200 MeV/fission
(d) Based on calorimentry

TABLE 35. Fission Gas Analysis on Four Halden Test Assemblies

Assembly Number	Number of Rods	Fuel Density, % TD	Fission Gas Release, %	
			Xe	Kr
IFA 125	3	94	2.4 to 4.5	2.1 to 3.6
IFA 127	2	94	4.1 to 4.2	2.5 to 3.7
IFA 175	2	90 and 95	1	1
IFA 176	2	90 and 95	1	1

4.1.9 Irradiation Experience Summary

Since the ANL irradiation experiments in the late 1950s, various aspects of the behavior and performance of ThO_2-UO_2 fuels have been investigated. These include thermal conductivity, fuel swelling, fission gas release, dimensional stability, corrosion resistance, and burnup and fuel composition effects. Analyses of experimental results have enhanced both the understanding of ThO_2-UO_2 fuel behavior and the possibility of correlating the existing UO_2 data with ThO_2-UO_2 data by direct comparison.

To provide a general overview and a quick comparison of ThO_2-UO_2 irradiation experience, Table 36 reviews the various experimental programs.

This review allows the following observations:

- The majority of experiments (86%) were performed on fuels with less than 10 wt% UO_2. On the basis of the number of samples (rods, pellets, or specimens) examined, only 3% of the fuels had UO_2 contents above 20 wt%.
- The burnup ranges of the experiments were generally low.
- Zircaloy replaced stainless steel as the cladding material in recent experiments.

Upon reviewing the irradiation experience, an evaluation of the performance of ThO_2-UO_2 is made in terms of the following properties:

1) Fission gas release behavior

The magnitude of release from ThO_2-UO_2 fuel is comparable to that from UO_2 fuels within the range of burnup (3 to 6 at.%) and heat rating (25 to 45 kW/m) that are typical of commercial reactors using UO_2 fuels

TABLE 36. Summary of Irradiation Experience

Program	Reactor Name(s)	Number of Rods (R)/ Pellets (P)/ Specimens (S)/ Examined	Fuel Composition, wt% UO2	Bonding Material	Cladding Type	Burnup Range, at.%
United States						
BWR	Borax IV	14S	6	Lead	Al-1 wt% Ni	0.7 to 3.7
	Elk River	25R	3	--	304 SS	≤0.15
Thorium Utilization	MTR, ETR, NRX	62R	3 to 5	--	304 SS and Zircaloy-2	1.5 to 15.8
PWR	Indian Point	13R	0 to 9	--	304 SS	≤4.0
LWBR						
Fission Gas Release Experiment	ETR, ATR, NRX	51R	2 to 25	--	Zircaloy-4	≤5.1
Dimensional Change Experiment	ETR, ATR, NRX	29R	2 to 30	--	Zircaloy-4	0.01 to 1.4
Canada, HWR	NRU	189R	1.3	--	Zircaloy-2	4.0 to 6.0
	NRX	31P	9	--	--	≤0.4
India, HWR	CIRUS	16P	0.1 and 1	--	--	(a)
Italy, BWR	Halden	28R	3 to 10	--	Zircaloy-2	0.2 to 3.6

(a) Thermal neutron flux of 10^{13} n/cm^2-s for 10-15 minutes for the ThO_2-0.1 wt% UO_2 fuel, and 0.02 at.% for the ThO_2-1 wt% UO_2 fuel.

(Rabin et al. 1965; Baroch et al. 1969; Jones et al. 1977). Increasing the UO_2 content has little or no effect on the release behavior (Neimark and Kittel 1964; Goldberg et al. 1978).

2) Dimensional Stability

Very little irradiation-induced swelling occurs in ThO_2-UO_2 fuels up to 4 at.% burnup (Baroch et al. 1969; Giovengo 1970). In general the volume change is less than 1% for each at.% burnup (Rabin et al. 1965; Olsen et al. 1966). This relationship holds up to 10 at.% (Olsen et al. 1966).

3) Thermal Properties

The thermal conductivity of ThO_2-UO_2 fuel remains unchanged under irradiation to 0.1 at.% burnup, as compared to UO_2 at 0.03 at.% (Jacobs 1969). As UO_2 content increases to above 10 wt%,the thermal conductivity of ThO_2-UO_2 fuel decreases (Rao 1964). Thermal expansion behavior of both UO_2 and ThO_2-UO_2 are essentially the same at low UO_2 contents.

4) Structural Stability

ThO_2-UO_2 fuel has good structural stability at low burnups. For burnup range 0.1 to 3 at.% and UO_2 content range from 2 to 9 wt%, the structural changes of ThO_2-UO_2 fuel are minimal (Bain 1960 and 1967; Neimark 1961; Deboskey 1963). Several investigators (Bain 1967; Doria 1971; Baldetti 1977) showed that at similar power ratings and fuel temperatures, ThO_2-UO_2 fuel experienced less structural changes and fission product relocation than UO_2 fuel.

In summary, evidence indicates that the performance of ThO_2-UO_2 fuel is comparable to, or in some cases better than, that of the UO_2 fuel.

4.2 NEEDS FOR FURTHER DATA

In order to qualify denatured ThO_2-UO_2 fuels for commercial LWR utilization, a comprehensive data base is required. As summarized in the previous

sections, there are indications of superior irradiation performance in ThO_2-UO_2 fuel when compared to UO_2 fuels. However, the currently available results are hardly comprehensive when compared to the information required for the licensing of commercial fuels.

In addition to data on cracking, swelling, microstructural changes, and densification, ThO_2-UO_2 data are needed for the following fuel characteristics during normal or steady-state operations:

- fission gas (product) release to predict internal rod pressure and gas conductivity, and propensity for stress-corrosion cracking of the cladding
- stored energy and fuel temperature distributions to define differential thermal expansion and mechanical interaction with the cladding, as well as, the starting point for areas of concern during off-normal operation, e.g., margin to fuel melting,
- propensity for rod failure during normal operating conditions.

Information for both pressurized- and boiling-water reactor types at selected points over the normal range of steady-state operating conditions will be required. Due to the similarities between ThO_2-UO_2 and UO_2 fuels, spot-check irradiations of the alternative fuel with correlation to the extensive UO_2 data base may be all that is needed to generate a normalized operational data base for the licensing of ThO_2-UO_2.

Data are also required for off-normal and safety-related operations. Information on the comparative behavior of ThO_2-UO_2 to UO_2 fuel during reactivity insertion accidents, departure from nucleate boiling, transient overpower operation and loss-of-coolant conditions will be necessary for the licensing of reload quantities of alternative fuels.

In conclusion, a comprehensive data base for denatured ThO_2-UO_2 which is similar to the existing extensive data base for UO_2 needs to be generated. Due to the similarities between ThO_2-UO_2 and UO_2, significantly fewer data points than those for UO_2 need to be generated for ThO_2-UO_2, because a "normalized" UO_2 data base may be all that is required for licensing of ThO_2-UO_2 fuels.

5.0 REFERENCES

Ackermann, R. J., E. G. Rauh, R. J. Thorn and M. C. Cannon. 1963. "A Thermodynamic Study of the Thorium-Oxygen System at High Temperature." J. Phy. Chem. 67:762-769.

Adler, H. H. 1962. "The Economic Mineralogy and Geology of Thorium." In Book I of Proceedings of the Thorium Fuel Cycle Symposium, TID-7650, pp. 19-28. U. S. Atomic Energy Commission. Available from National Technical Information Service, Springfield, Virginia.

Aitken E. A., J. A. Edwards and R. A. Josephs. 1966. "Thermodynamics Study of Solid Solutions of Uranium Dioxide. I. Uranium Oxide-Thorium Oxide." J. Phy. Chem. 70:1084-1090.

Alcock, C. B., R. J. Hawkins, A. W. D. Hills and P. McNamara. 1966. "A Study of Cation Diffusion in Stoichiometric UO_2 Using X-Ray Spectroscopy." In Volume 2 of Thermodynamics, pp. 57-72, International Atomic Energy Agency, Vienna, Austria.

Alexander, C. A., J. S. Ogden and G. W. Cunningham. 1967. Thermal Stability of Zirconia- and Thoria-Base Fuels. BMI-1789, Battelle Memorial Institute, Columbus, Ohio.

Allis-Chalmers Manufacturing Co. 1960. Fuel Element Report - Elk River Reactor. NP-14272, Washington, D.C.

Allred, V. D., S. R. Buxton and J. P. McBride. 1957. "Characteristic Properties of Thorium Oxide Particles." J. Phys. Chem. 61 117-20.

Anderson, J. G., D. H. Edgington, L. E. J. Roberts, and E. Wait. 1954. "The Oxides of Uranium, Part IV. The System UO_2-ThO_2-O_2." J. Chem. Soc. pp. 3324-31.

Ando, K., Y. Oishi and Y. Hidaka. 1976. "Self-Diffusion of Oxygen in Single Crystal Thorium Oxide." J. Chem. Phys. 65:2751-2755.

Aronson, S., and J. Belle. 1958. "Nonstoichiometry of Uranium Dioxide," J. Chem. Phys. 29:151-158.

Aronson, S., E. Cisney and K. A. Gingerich. 1967. "Thermal Expansion of Some Cubic Refractory Compounds of Thorium." J. Am. Ceram. Soc. 50:248-252.

Aronson, S., and J. C. Clayton. 1960. "Thermodynamic Properties of Nonstoichiometric Urania-Thoria Solid Solutions." J. Chem. Phys. 32:749-752.

Baldetti, S., F. Doria, M. Gabaglio and S. Grifoni. 1971. "CNEN Work on the Uranium-Thorium Cycle Applied to Water Reactors." In Proceedings of the 4th International Conference on the Peaceful Uses of Atomic Energy, A/CONF. 49/P/186. Internation Atomic Energy Agency, Vienna, Austria.

Banerjee, S., E. Critoph and R. G. Hart. 1975. "Thorium as a Nuclear Fuel for CANDU Reactors." Can. J. Chem. Eng. 53:291-296.

Baroch, C. J., and W. N. Bishop. 1968. "Performance of ThO_2-UO_2 Fuel in Indian Point Reactor." Trans. Am. Nucl. Soc. 11:494.

Baroch, C. J., E. N. Harbison and A. V. Munim. 1969. Examination of Stainless-Steel-Clad ThO_2-UO_2 Fuel Rods and Zircaloy-2 Can after Operation for 442 EFPD in the Indian Point Reactor. BAW-3809-6, Babcock and Wilcox Company, New York, New York.

Bearse, A. E., G. D. Calkins, J. W. Clegg and R. B. Filbert. 1954. "Thorium and Rare Earths from Monazite." Chem. Eng. Prog. 50:338.

Becket, R., and M. E. Winfield. 1951. "The Thermal Decomposition of Thorium Oxalate. Austr. J. Sci. Res. 4:644-50.

Bellamy, R. G., and J. B. Rich. 1969. "Grain Boundary Gas Release and Swelling in High Burnup Uranium Dioxide." J. Nucl. Mater. 33:64-78.

Belle, J., R. M. Berman, W. F. Bourgeois, I. Cohen and R. C. Daniel. 1967. Thermal Conductivity of Bulk Oxide Fuels. WAPD-TM-586 (Rev), Bettis Atomic Power Laboratory, West Mifflin, Pennsylvania.

Beltram, C., F. Forscher and B. L. Vondra. 1965. "Development of ThO_2 Pellet Fabrication." Paper presented at ANS Winter Meeting, Washington, D. C., November 1965.

Benz, R. 1969. "Thorium-Thorium Dioxide Phase Equilibria." J. Nucl. Mater. 29:43-49.

Berman, R. M. 1972. The Homogenization of ThO_2-UO_2. WAPD-TM-1051, Bettis Atomic Power Laboratory, West Mifflin, Pennsylvania.

Berman, R. M. 1976. Fission Product Distribution in Oxide Fuels. WAPD-TM-1236, Bettis Atomic Power Laboratory, West Mifflin, Pennsylvania.

Berman, R. M., T. S. Tully, J. Belle and I. Goldberg. 1972. Thermal Conductivity of Polycrystalline Thoria and Thoria-Urania Solid Solutions. WAPD-TM-908, Bettis Atomic Power Laboratory, West Mifflin, Pennsylvania.

Bonner, W. F., H. T. Blair, and L. S. Romero. 1976. Spray Solidification of Nuclear Waste. BNWL-2059, Battelle, Pacific Northwest Laboratories, Richland, Washington.

Breysse, M., B. Claudel and Y. Trambouze. 1965. Effect of Conditions for Precipitating a Salt on the Texture of Its Thermal Decomposition Product: the Case of Thorium Oxalate. WAPD-Tr-64, Bettis Atomic Power Laboratory, West Mifflin, Pennsylvania.

Brown, A., and A. Chitty. 1960. "Thoria as a Fertile Component for a Liquid Metal Breeder Blanket." J. Nucl. Energy Part B. 1:145-152.

Brown, K. B., D. J. Crouse, F. J. Hurst and W. D. Arnold. 1962. "Thorium Reserves in Granitic Rock and Processing of Thorium Ores." In Book I of Proceedings of the Thorium Fuel Cycle Symposium, TID-7650, pp. 30-56. U.S. Atomic Energy Commission. Available from National Technical Information Service, Springfield, Virginia.

Burke, T. J. 1969. Effect of Carbowax Binder and Dextrose Additive on the Microstructure, Density, and Open Porosity of Thoria-Urania Fuel Pellets. WAPD-TM-880, Bettis Atomic Power Laboratory, West Mifflin, Pennsylvania.

Burkhardt, W., G. G. Briggs, A. L. Clavel and J. F. White. 1969. Production of Dense Thoria. NLCO-1029, National Lead Company of Ohio, Cincinnati, Ohio.

Busby, C. C., and J. C. Clayton. 1976. Thorium Oxide Granule and Compact Properties Which are Important to ThO_2 and ThO_2-UO_2 Fuel Fabrication. WAPD-1231, Bettis Atomic Power Laboratory, West Mifflin, Pennsylvania.

Chawla, O. P., M. C. Naik and M. D. Karkhanavala. 1971. Post-Irradiation Thermal Release Study of Fission Gases from Fuel Pellets. BARC-538, Bhabha Atomic Research Center, India.

Christensen, J. A. 1963. UO_2-ThO_2 Phases Studies. HW-76559, General Electric Company, Richland, Washington.

Clayton, J. C. 1976. Thorium Oxide Powder Properties Which are Important to ThO_2 and ThO_2-UO_2 Fuel Pellet Fabrication. WAPD-TM-1230, Bettis Atomic Power Laboratory, West Mifflin, Pennsylvania.

Cohen, I., and R. M. Berman. 1966. "A Metallographic and X-ray Study of the Limits of Oxygen Solubility in the UO_2-ThO_2 System." J. Nucl. Mater. 18:77-107.

Cardosi, G., A. Mazzanti and P. Venditti. 1968. Analisi Comparativa di vari cicli di Combustibile in un Reattore Tipo Cirene. RT/FI (68) 39, Comitato Nazionale per l'Energia Nucleare, Rome, Italy.

Crain, H. H., and C. R. Hutchison. 1966. Fabrication of Fuel Pellets from Sol-Gel Powders. WAPD-TM-581, Bettis Atomic Power Laboratory, West Mifflin, Pennsylvania.

Critoph, E., S. Banergee, F. W. Barclay, D. Hamel, M. S. Milgram and J. I. Veeder. 1975. "Prospects for Self-Sufficient Equilibrium Thorium Cycles in CANDU Reactors." Trans. Am. Nucl. Soc. 22:706-707.

Crocker, H. W. and H. H. Hopkins, Jr. 1963. Conversion of Plutonium Nitrate to Plutonium Tetrafluoride via the Continuous Oxide-Fluoride Method. HW-SA-2880, General Electric Company, Richland, Washington.

Curtis, C. E., and J. R. Johnson. 1957. "Properties of Thorium Oxide Ceramics." J. Am. Ceram. Soc. 40:63-68.

Cuthbert, F. L. 1958. Thorium Production Technology. Addison-Wesley, Reading, Massachusetts.

D'Eye, R. W. M., and P. G. Sellman. 1955. "The Thermal Decomposition of Thorium Oxalate." J. Inorg. Nucl. Chem. 1:143-48.

Davis, H. H., and L. J. Ferrell. 1977. "Microstructures of As-Fabricated UO_2 Fuel Pellets." In Ceramic Microstructures '76, eds. Richard Fulrath and Joseph A. Pask. Westview Press, Boulder, Colorado.

DeBoskey, W. R. 1963. "Irradiation Testing of Thoria-Urania Fuel for the Indian Point Reactor." In Proceedings of the Thorium Fuel Cycle Symposium, TID-7650, pp. 630-642. Available from National Technical Information Service, Springfield, Virginia.

Deddens, J. C., and R. H. Freyberg. 1965. "Indian Point Nuclear Power Station - The First Two Years' Operation." J. Brit. Nucl. Energy Soc. 4:45-55.

Doria, F. 1971. "Thorium Programme: IFA 125, 126, 127, 175, 176. Current Status Evaluation Summary." Paper presented at the Symposium on Irradiation Experience from HBWR, March 1971, Ustaoset, Norway.

Edwards, H. S., A. F. Rosenberg and J. T. Bittel. 1963. Thorium Oxide-Diffusion of Oxygen Compatibility with Borides and Feasibility of Coating Borides by Pyrohydrolysis of Metal Halides. ASD-TDR-63-635, General Electric Company, Cincinnati, Ohio.

Eisenstein, A. 1946. "A Study of Oxide Cathodes by X-Ray Diffraction Methods Part I. Methods, Conversion Studies and Thermal Expansion Coefficients." J. Appl. Phys. 17:434-443.

Enderlin, W. I. 1978. An Assessment of U.S. Domestic Capacity for Producing Reactor-Grade Thorium Oxide and Controlling Associated Wastes and Effluents. PNL-2593, Pacific Northwest Laboratory, Richland, Washington.

Ferro, C., C. Patimo and C. Piconi. 1972. "Thermal Diffusivity of Mixed ($Th_{1-x}U_x$) Oxides and Some Materials to be Used as Reference in the Range 650-2700 K." J. Nucl. Mater. 43:273-276.

Ferro, C., S. Moretti and C. Patimo. 1969. "Thermal Diffusivity and Conductivity of Sintered Uranium-Thorium Mixed Oxides." In Thermal Conductivity Proceedings of the Eighth Conference. eds. C. Y. Ho and R. E. Taylor, pp. 815-822. Plenum Press, New York.

Fink, J. K., M. G. Chasanov and L. Leibowitz. 1977. Thermophysical Properties of Thorium and Uranium Systems for Use in Reactor Safety Analysis. ANL-CEN-RSP-77-1, Argonne National Laboratory, Argonne, Illinois.

Fisher, J. R. and E. D. Kendrick. 1968. "Comparison of Measured and Predicted Characteristics of the Elk River Reactor." In Proceedings of the Second International Thorium Fuel Cycle Symposium, pp. 681-694, U. S. Atomic Energy Commission. Available from National Technical Information Service, Springfield, Virginia.

Fitts, R. B., H. G. Moore, A. P. Olsen and J. D. Sease. 1968. Sol-Gel Thoria Extrusion. ORNL-4311, Oak Ridge National Laboratory, Oak Ridge, Tennessee.

Foex, M. 1949. "Study of the Change of the Apparent Density of Crude Oxides: Application of Thorium Oxide." AEC-tr-1990, Translated from Bull. Soc. Chim. Fr. D231-7.

Foster, J. S. et al. 1978. Nuclear Resources. Report to the Conservation Commission of the World Energy Conference, IPC Science and Technology Press, New York, New York.

Freshley, M. D., D. W. Brite, J. L. Daniel and P. E. Hart. 1976. "Irradiation-Induced Densification of UO_2 Pellet Fuel." J. Nucl. Mater. 62:138-166.

Fricke, H. 1924. "A Mathematical Treatment of the Electrical Conductivity and Capacity of Disperse Systems. I. The Electrical Conductivity of a Suspension of Homogeneous Spheroids." Phys. Rev. 24:575-587.

Frondel, C. 1956. "Mineralogy of Thorium." Professional Paper 300, U.S. Geological Survey, pp. 567-79.

Furuya, H. 1968. "Lattice and Grain Boundary Diffusion of Uranium in ThO_2 and ThO_2-UO_2 Solid Solution." J. Nucl. Mater. 26:123-128.

Geller, R. F., and P. J. Yavorsky. 1945. "Effects of Some Oxide Additions on the Thermal Length Changes of Zirconia." J. Res. Nat. Bur. Stand. 35:87-110.

Germann, J. D. 1967. Analysis of In-Pile Creep Measurements of Bulk Oxide Fuels. WAPD-TM-687, Bettis Atomic Power Laboratory, West Mifflin, Pennsylvania.

Gilbert, A. 1965. "Deformation and Fracture of Thoria." Phil. Mag. 13:139-144.

Gilpatrick, L. O., and C. H. Secoy. 1966. Status and Progress Report for Thorium Fuel Cycle Development, December 31, 1965. ORNL-4001, Oak Ridge National Laboratory, Oak Ridge, Tennessee.

Giovengo, J. F. 1970. In-Pile Dimensional Changes of ThO_2-UO_2 Fuel Rods with Non-Free Standing Cladding. WAPD-TM-986, Bettis Atomic Power Laboratory, West Mifflin, Pennsylvania.

Godfrey, T. G., J. A. Woolley and J. M. Leitnaker. 1966. Thermodynamic Functions of Nuclear Materials UC, UC_2, UO_2, ThO_2, and UN. ORNL-TM-1596 (Revised), Oak Ridge National Laboratory, Oak Ridge, Tennessee.

Goldberg, I., G. L. Spahr, J. E. Giovengo and L. A. Waldman. 1977. "Fission Gas Release from ThO_2-UO_2 Fuels." Trans. Am. Nucl. Soc. 27:308-310.

Goldberg, I., G. L. Spahr, L. S. White, et al. 1978. Fission Gas Release from ThO_2 and ThO_2-UO_2 Fuels. WAPD-TM-1350, Bettis Atomic Power Laboratory, West Mifflin, Pennsylvania.

Grain, C. F., and W. J. Campbell. 1976. Thermal Expansion and Phase Inversion of Six Refractory Oxides. BM-RI-5982, U.S. Bureau of Mines, Washington, D.C.

Griffith, J. W., and S. M. Roscoe. 1964. "Canadian Resources of Uranium and Thorium" Paper Number 64 in Proceedings of the Third International Conference on the Peaceful Uses of Atomic Energy.

Handwerk, J. H., L. L. Abernathy and R. A. Bach. 1957. "Thoria and Urania Bodies." Am. Ceram. Soc. Bull. 36:99-100.

Handwerk, J. H., and R. A. Noland. 1957. "Oxide Fuel Elements for High Temperatures." Chem. Eng. Progress, 53:60-F-62-F.

Handwerk, J. H., and R. A. Noland. 1959. "Fabrication of Fuel Elements for the BORAX-IV Reactor." In Volume 2 of Metallurgy and Fuels. Series V of Progress in Nuclear Energy. pp. 234-260. Pergamon Press, New York, New York.

Harada, Y., Y. Baskin and J. H. Handwerk. 1962. "Calcination and Sintering Study of Thoria." J. Am. Ceram. Soc. 45:253-7.

Hart, P. E., R. B. Matthews, G. D. White and N. C. Davis. 1979. "ThO_2-Based Pellet Fabrication Development for Proliferation-Resistant Fuels." Paper presented at American Ceramic Society Annual Meeting, May 1979, Cincinnati, Ohio.

Hatcher, S. R., S. Banerjee, A. D. Lane, H. Tamm and J. I. Veeder. 1975. "Thorium Cycle in Heavy Water Moderated Pressure Tube (CANDU) Reactions. Trans. Am. Nucl. Soc. 22:334-336.

Hawkins, R. J., and C. B. Alcock. 1968. "A Study of Cation Diffusion in UO_{2+x} and ThO_2 Using X-Ray Spectrometry." J. Nucl. Mater. 26:112-122.

Hill, R. 1952. "Elastic Behavior of a Crystalline Aggregate." Proc. Phys. Soc. (London), 65A:349-54.

Hirata, K., K. Moriya and Y. Waseda. 1977. "High Temperature Thermal Expansions of ThO_2, MgO, and Y_2O_3 by X-ray Diffraction." J. Mater. Sci. 12:838-839.

Hock, M., and H. L. Johnston. 1954. "The Reaction Occurring on Thoriated Cathodes." J. Am. Chem. Soc. 76:4833-4835.

Hock, M., and H. L. Johnston. 1961. "The Heat Capacity of Aluminum Oxide from 1000 to 2000° and of Thorium Dioxide from 1000 to 2500°." J. Phys. Chem. 65:1184-1185.

Hock, M., and A. C. Momin. 1969. "High Temperature Thermal Expansion of UO_2 and ThO_2." High Temp. High Pressures. 1:401-407.

Hoenig, C. L., J. H. Handwerk, J. H. Kittel and C. R. Breden. 1958. "Thoria-Urania Bodies and Irradiation Studies." J. Am. Ceramic Soc. 41:117-123.

Huber, E. J., C. E. Holley, Jr. and E. H. Meierkoid. 1952. "The Heats of Combustion of Thorium and Uranium." J. Am. Chem. Soc. 74:3406-3408.

Hultgren, R., R. L. Orr, P. D. Anderson and K. K. Kelley. 1963. Selected Values of Thermodynamic Properties of Metals and Alloys. John Wiley and Sons Inc., New York.

Hutchison, C. R., and R. G. R. Johnson. 1966. Fabrication of High and Low Density ThO_2 Pellets. WAPD-TM-576, Bettis Atomic Power Laboratory, West Mifflin, Pennsylvania.

Jacobs, D. C. 1969. The In-Pile Thermal Conductivity of Selected ThO_2-UO_2 Fuels at Low Depletions. WAPD-TM-758, Bettis Atomic Power Laboratory, West Mifflin, Pennsylvania.

Jacobs, D. C. 1970. In-Pile and Unirradiated Thermal Conductivity of a Single-Fired ThO_2 + 10 wt% UO_2. WAPD-TM-901, Bettis Atomic Power Laboratory, West Mifflin, Pennsylvania.

Jaeger, R. E., and T. J. Miller. 1974. Particulate Material by Freeze Drying. U.S. Patent 3,916,532, U.S. Patent Office, Washington D.C.

Johnson, D. W. and F. J. Schnettler. 1970. "Characterization of Freeze-Dried Al_2O_3 and Fe_2O_3." J. Amer. Ceram. Soc. 53:440-44.

Johnson, R. G. R. 1966. Fabrication of Fuel Pellets from Pot Process Denitrated ThO_2 Powder. WAPD-TM-577, Bettis Atomic Power Laboratory, West Mifflin, Pennsylvania.

Jones, J. R., H. R. Lee, H. Hahn, J. F. Walker and A. Celli. 1977. "Thoria Fuel Technology for CANDU-PHW Reactors." Trans. Am. Nucl. Soc. 27:303-304.

Kantan, S. K., R. V. Raghavan and G. S. Tendolkar. 1958. "Sintering of Thorium and Thoria." In Volume 6 of Proceedings of the Second United Nations International Conference on the Peaceful Uses of Atomic Energy, pp. 132-138, United Nations, Geneva.

Kempter, C. P., and R. O. Elliott. 1959. "Thermal Expansion of UN, UO_2, UO_2-ThO_2, and ThO_2." J. Chem. Phys. 30:1524-1526.

Kerr, J. M., H. M. Jones, C. J. Baroch and E. J. Silk. 1978. "Indian Point I-A ThO_2-UO_2 Fueled Reactor." Paper presented at AICHE Annual Meeting, February 28, 1978, Atlanta, Georgia.

Kim, Y. S., and F. R. Monforte. 1971. "Theoretically Dense (99.9%) Polycrystalline Alumina prepared from Cryochemically Processed Powders." Am. Ceram. Soc. Bull. 50:532-35.

King, A. D. 1971. "Thorium Diffusion in Single Crystal ThO_2." J. Nucl. Mater. 38:347-349.

Kingery, W. D. 1959a. Property Measurements at High Temperature. John Wiley and Sons, Inc., New York.

Kingery, W. D. 1959b. "Thermal Conductivity: XIV, Conductivity of Multicomponent Systems." J. Am. Ceram. Soc. 42:617-627.

Kittel, J. H., et al. 1977. Properties of Fuels for Alternate Breeder Fuel Cycles. ANL-AFP-38, Argonne National Laboratory, Argonne, Illinois.

Kittel, J. H., and J. H. Handwerk. 1958. Preliminary Irradiations of the Ceramic Fuels UO_2, UO_2-Zr and ThO_2-UO_2. ANL-5675, Argonne National Laboratory, Argonne, Illinois.

Kittel, J. H. and S. H. Paine. 1958. "Effect of Irradiation on Fuel Material." In Proceedings of the Second U.N. International Conference on the Peaceful Uses of Atomic Energy, 5:500-509, United Nations, Geneva.

Kittel, J. H., and S. H. Paine. 1959. "Engineering Decisions Based on Irradiation Experiments." Metal Progress 76:119.

Kittel, J. H., and S. H. Paine. 1961. "Effect of Irradiation on Fuel Material." In Volume 3 of Metallurgy and Fuels. Series V of Progress in Nuclear Energy. Pergamon Press, Inc., New York, New York.

Knudsen, F. P. 1959. "Dependence of Mechanical Strength of Brittle Poly-Crystalline Specimens on Porosity and Grain Size." J. Am. Ceram. Soc. 42:379-387.

Kubaschewski, O., E. L. Evans and C. B. Alock. 1967. Metallurgical Thermochemistry. Pergamon Press, New York.

Lackey, W. J., and J. E. Selle. 1978. Assessment of Gel-Sphere-Pac Fuel for Fast Breeder Reactors. ORNL-5468, Oak Ridge National Laboratory, Oak Ridge, Tennessee.

Lambertson, W. A., M. H. Mueller and F. H. Gunzel Jr. 1953. "Uranium Oxide Phase Equilibrium Systems, IV. UO_2-ThO_2." J. Am. Ceram. Soc. 36:397-399.

Lane, A. D., A. Celli, R. W. Jones and R. B. Matthews. 1978. "Fabrication of Recycle Thoria Fuels for CANDU Reactors." Paper presented at the American Chemical Society Meeting, September 1978, Miami Beach, Florida.

Lane, A. D., R. W. Jones and D. Hamel. 1977. "Fuel Technology for Denatured Thorium Cycles in CANDU Reactors. Trans. Am. Nucl. Soc. 27:304-305.

Lang, S. J., and F. P. Knudsen. 1956. "Some Physical Properties of High Thorium Dioxide." J. Am. Ceram. Soc. 39:415-424.

Lee, H. M., and C. B. Alcock. 1971. "Cation Diffusion in UO_2-Based Solid Solutions As a Function of Stoichiometry." Proc. Br. Ceram. Soc. 19:85-93.

Lee, H. R., A. Krawczyk and R. W. Jones. 1978. "A Method of Manufacturing Denatured Thoria Fuel." Paper presented at the Annual Meeting of the American Ceramic Society, May 1978, Detroit, Michigan.

Leitnaker, J. M., M. L. Smith and C. M. Fitzpatrick. 1972. Conversion of Uranium Nitrate to Ceramic-Grade Oxide for the Light Water Breeder Reactor: Process Development. ORNL-4755, Oak Ridge National Laboratory, Oak Ridge, Tennessee.

Lewis, W. B., et al. 1971. "Large Scale Nuclear Energy from the Thorium Cycle." In Proceedings of the Fourth International Conference on the Peaceful Uses of Atomic Energy. A/CONF/49/P/157, United Nations, Geneva.

Loeb, A. L. 1954. "Thermal Conductivity: VII, A Theory of Thermal Conductivity of Porous Materials." J. Am. Ceram. Soc. 37:96-99.

Lynch, E. D. 1965. Studies of Stoichiometric and Hyperstoichiometric solid Solutions in the Thoria-Urania System. ANL-6894, Argonne National Laboratory, Argonne, Illinois.

Macedo, P. M., W. Capps and J. B.Watchman, Jr. 1964. "Elastic Constants of Single Crystal ThO_2 at 25°C." J. Am. Ceram. Soc. 47:651.

MacEwan, J. R., and R. L. Stoute. 1969. "Annealing of Irradiation-Induced Thermal Conductivity Changes in ThO_2-1.3 wt% UO_2." J. Amer. Ceram. Soc. 52:160-165.

Margrave, J. L. 1959. "Vapor Pressure." In Physicochemical Measurements at High Temperatures. eds. J. O'M. Brockris, J. L. White and J. D. Mackenzie, pp. 225-246. Academic Press Inc., New York.

Marino, G. P. 1970. The Porosity Correction Factor for the Thermal conductivity of Porous Materials. WAPD-TM-807, Bettis Atomic Power Laboratory, West Mifflin, Pennsylvania.

Marino, G. P. 1971. "The Porosity Correction Factor for the Thermal Conductivity of Ceramic Fuels." J. Nucl. Mater. 38:178-190.

Marlowe, M. O., and A. I. Kaznoff. 1969. "Elastic Behavior of Uranium Dioxide." In Proceedings of the International Symposium on Nuclear Fuels. eds. O. L. Kruger and A. I. Kaznoff, pp. 90-99. American Ceramic Society, Columbus, Ohio.

Matolich, J., Jr. and V. W. Storhok. 1970. Thermal Diffusivity Measurements of Irradiated Oxide Fuels. BMI-X-10274, Battelle Memorial Institute, Columbus, Ohio.

Matzke, H. 1967. "Xenon Migration and Trapping in Doped ThO_2." J. Nucl. Mater. 21:190-198.

Mauer, F. A., and L. H. Bolz. 1955. Measurement of Thermal Expansion of Cermet Components by High Temperature X-ray Diffraction. WADC-TR-55-473, Wright Air Defense Command, Dayton, Ohio.

Maxon, B. S., D. A. Schulze, and J. A. Thil. 1959. "Reactiority Transients and Steady-State Operation of a Thoria-Fueled Direct-Cycle Light Water-Boiling Reactor (BORAX-IV)." ANL-5733, Argonne National Laboratory, Argonne, Illinois.

Mohan, A., and V. K. Moorthy. 1971. Studies on Sintering of Nuclear Fuel Materials - Sintering Behavior of Urania - Thoria Mixtures. BARC-568, Bhabha Atomic Research Center, Bombay, India.

Moore, G. E., and K. K. Kelley. 1947. "High Temperature Heat Contents of Uranium, Uranium Dioxide, and Uranium Trioxide." J. Am. Chem. Soc. 69:2105-2107.

Moorehead, D. R. and E. R. McCartney. 1976. "The Formation of Thoria by Decomposition of the Nitrate, Oxalate, and Hydroxide." J. Aust. Ceram. Soc. 12:27-33.

Moorthy, V. K., A. K. Kulkarni and S. V. K. Rao. 1964. "Relation Between the Origin, Powder Characteristics, and Sintering Treatment on the Densification and Microstructures of Urania and Thoria." In Volume 11 of Proceedings of the Third International Conference on the Peaceful Uses of Atomic Energy, pp. 386-392. United Nations. Geneva.

Morgan, C. S., and L. L. Hall. 1966. "The Creep of ThO_2 and ThO_2-CaO Solid Solutions." Proc. Br. Ceram. Soc. 6:233-238.

Murabayashi, M. 1970. "Thermal Conductivity of Ceramic Solid Solutions." J. Nucl. Sci. Technol. 7:559-563.

Murabayashi, M., Y. Takahashi and T. Mukaibo. 1969. "Effect of Porosity on the Thermal Conductivity of ThO_2." J. Nucl. Sci. Technol. 6:657-662.

Naik. M. C., K. N. G. Kaimal and M. D. Karkhanavala. 1972. ^{133}Xe Release from Irradiated Thoria Powders at Low Temperatures. BARC-601, Bhabha Atomic Research Center, India.

Naik, M. C., K. N. G. Kaimal and M. D. Karkhanavala. 1974. Post-Irradiation Thermal Release of Xe^{133} from Sintered (ThO^2-0.1% $U^{233}O_2$ Pellets. BARC-754, Bhabha Atomic Research Center, India.

Naik, M. C., K. N. G. Kaimal and M. D. Karkhanauala. 1977. "Release of Xenon from Low-Dose Irradiated Thoria Pellets." J. Nucl. Mater. 67:239-243.

Naik, M. C., A. R. Paul, K. N. G. Kaimal and M. D. Karkhanavala. 1975. "Effect of Burnup on Release of Xenon from Thoria." Radiation Effects 25:73-77.

Neimark, L. A. 1961. Examination of Irradiated Prototype Fuel Element for the Elk River Reactor. ANL-6160, Argonne National Laboratory, Argonne, Illinois.

Neimark, L. A., and J. H. Kittel. 1959. "Irradiation Behavior of ThO_2-UO_2 Fuels." Nuclear Metallurgy, Effects of Irradiation on Fuel and Fuel Elements. American Institute of Mining, Metallurgical and Petroleum Engineers.

Neimark, L. A., and J. H. Kittel. 1964. The Irradiation of Aluminum Alloy-Clad Thoria-Urania Pellets. ANL-6538, Argonne National Laboratory, Argonne, Illinois.

Neimark, L. A., J. H. Kittel and C. L. Hoenig. 1961. Irradiation Behavior of Metal-Fiber-Reinforced Thoria-Urania. ANL-6397, Argonne National Laboratory, Argonne, Illinois.

Nichols, F. A., and H. R. Warner. 1970. Review of Mechanisms for Swelling and Gas Release of Oxide Fuel Rods. WAPD-TM-980, Bettis Atomic Power Laboratory, West Mifflin, Pennsylvania.

O'Holleran, T. P., R. R. Neurgaonkar, D. M. Roy and R. Roy. 1978. "EDS for the preparation of X-Fe_2O_3." Am. Ceram. Soc. Bull. 57:459-60.

Ohnysty, B., and F. K. Rose. 1964. "Thermal Expansion Measurements on Thoria and Hafnia to 4500°F." J. Am. Ceram. Soc. 47:398-400.

Osborne, D. W., and E. F. Westrum, Jr. 1953. "The Heat Capacity of Thorium Dioxide from 10 to 305°K. The Heat Capacity Anomalies in Uranium Dioxide and Neptunium Dioxide." J. Chem. Phys. 21:1884-1887.

Parker, W. J., R. J. Jenkin, C. P. Butler and G. L. Abbott. 1961. "Flash Method of Determining Thermal Diffusivity Heat Capacity and Thermal Conductivity." J. Appl. Phys. 32:1679-1684.

Pearson, R. L., K. H. McCorkle, C. V. Ellison and P. A. Haas. 1958. Preparation of ThO_2 for Homogeneous Reactor Blanket Use. ORNL-2509, Oak Ridge National Laboratory, Oak Ridge National Laboratory, Oak Ridge, Tennessee.

Peterson, S., and C. E. Curtis. 1970 Thorium Ceramics Data Manual: Volume I-Oxides. ORNL-4503, Oak Ridge National Laboratory, Oak Ridge, Tennessee.

Pickett, J. B., and J. R. Fowler. 1979. "Thoria Pellet Roasting and Dissolution Studies." In Savannah River Laboratory Technical Progress Report--Consolidated Reprocessing Program October 1978 - March 1979. DP-CFRP-79-11, pp. 3-6. Savannah River Laboratory, Aiken, South Carolina.

Pope, J. M., and K. C. Radford. 1974. "Physical Properties of Some Thoria Powders and Their Influence on Sinterability." J. Nucl. Mater. 52:241-54.

Poteat, L. E., and C. S. Morgan. 1968. Metals and Ceramic Div. Annual Report, June 30, 1968. ORNL-4370, Oak Ridge National laboratory, Oak Ridge, Tennessee.

Poteat, L. E., and C. S. Yust. 1966. "Creep of Polycrystalline Thorium Dioxide." J. Am. Ceram. Soc. 49:410-414.

Prestile, J. A., and M. C. Edlund. 1966. "Indian Point Unit No. 1 Core A Performance Summary." In Volume XXVIII of Proceedings of the American Power Conference, pp. 200-207. Illinois Institute of Technology, Chicago, Illinois.

Rao, S. U. K. 1964. "Investigation of ThO_2-UO_2 as a Nuclear Fuel." J. Nucl. Mater. 12:323-329.

Reinke, C. F., L. A. Neimark, R. Carlander and J. H. Kittel. 1961. Metallurgical Evaluation of Failed BORAX-IV Reactor Fuel Elements. ANL-6083, Argonne National Laboratory, Argonne, Illinois.

Reuss, A. 1929. "Calculation of Flow Limits of Mixed Crystals on the Basis of Plasticity of Single Crystals." Z. Angew. Math. Mech. 9:49-58.

Richardson, H. K. 1935. "Small Cast Thorium Oxide Crucibles." J. Am. Ceram. Soc. 18:65-69.

Robbins, J. M., and J. G. Stradley. 1969. Fabrication of Sol-Gel Derived Thoria-Urania by Cold Pressing and Sintering. ORNL-4426, Oak Ridge National Laboratory, Oak Ridge, Tennessee.

Roberts, L. E. J., L. E. Russel, A. G. Adwick, A. J. Walter and M. H. Rand. 1958. "The Actinide Oxide." In Proceedings of the International Conference on the Peaceful Uses of Atomic Energy. pp. 215-222. International Atomic Energy Agency, Geneva.

Robertson, R. F. S., and V. C. Hall, Jr. 1959. Fuel Defect Test - BORAX-IV. ANL-5862, Argonne National Laboratory, Argonne, Illinois.

Robertson, R. F. S. 1960. Tests of Defected Thoria-Urania Fuel Specimens in EBWR. ANL-6022, Argonne National Laboratory, Argonne, Illinois.

Roy, D. M., R. R. Neurgaonkar, T. P. O'Holleran and R. Roy. 1977. "Preparation of Fine Oxide Powders by Evaporative Decomposition of Solutions." Am. Ceram. Soc. Bull. 56:1023-24.

Russell, E. R., M. L. Hyder, W. E. Prout and C. B. Goodlett. 1967a. "A Sol-Gel Thorium Oxide with Improved Dissolving Characteristics." Nucl. Sci. and Engr. 30:20-24.

Russell, E. R., W. E. Prout, H. J. Groh and G. W. Watt. 1967b. Thorium Oxide or Thorium-Uranium Oxide with Magnesium Oxide. U.S. Patent 3,309,323, U.S. Patent Office, Washington, DC.

Ruthner, J. J. 1973. "Preparation and Sintering Characteristics of MgO, Al_2O_3, $MgAl_2O_4$, and $MgCr_2O_4$." Paper presented at the Third Round Table Meeting, International Team for Studying Sintering, Herceg-Novi, Yugoslavia, September 1973.

Ryshkewitch, E. 1960. "Thoria." Chapter 7 in Oxide Ceramics. Academic Press, New York, New York.

Seltzer, M. S., J. S. Perrin, A. H. Clauer and B. A. Wilcox. 1971. "A Review of Creep Behavior of Ceramic Nuclear Fuels." React. Technol. 14:99-135.

Shapiro, E. 1952. "Vapor Pressure of Thorium Oxide from 2050 to 2250°K." J. Am. Chem. Soc. 74:5233-5235.

Simnad, M. T. 1971a. "BORAX." In Fuel Element Experience in Nuclear Power Reactors. pp. 383-390. Gordon and Breach Science Publishers, New York, New York.

Simnad, M. T. 1971b. "EBWR." In Fuel Element Experience in Nuclear Power Reactors. pp. 334-348. Gordon and Breach Science Publishers, New York, New York.

Simnad, M. T. 1971c. "Elk River." In Fuel Element Experience in Nuclear Power Reactors. pp. 378-382. Gordon and Breach Science Publishers, New York, New York.

Simnad, M. T. 1971d. "Indian Point." In Fuel Element Experience in Nuclear Power Reactors. pp. 288-292. Gordon and Breach Science Publishers, New York, New York.

Smid, R. J. 1976. Grain Growth in Thoria and Thoria-Based Fuel Pellets. WAPD-TM-1311, Bettis Atomic Power Laboratory, West Mifflin, Pennsylvania.

Southard, J. C. 1941. "A Modified Calorimeter for High Temperatures. The Heat Content of Silica, Wollastonite and Thorium Dioxide Above 25°." J. Am. Chem. Soc. 63:3142-3146.

Spinner, S., F. P. Knudsen and L. Stone. 1962. "Elastic Constant-Porosity Relations for Polycrystalline Thoria." J. Res. Nat. Bur. Stand. Sect. C 67C:39-46.

Spinner, S., L. Stone and F. P. Knudsen. 1963. "Temperature Dependence of the Elastic Constants of Thoria Specimens of Varying Porosity." J. Res. Nat. Bur. Stand. Sect. C 67C::93-100.

Springer, J. R. and J. F. Lagedrost. 1968. Thermal Properties of Bettis-Fabricated ThO_2-UO_2 Fuel Materials. BMI-X-10231, Battelle Memorial Institute, Columbus, Ohio.

Springer, J. R., E. A. Eldridge, M. U.Goodyear, T. R. Wright and J. F. Lagedrost. 1967. Fabrication, Characterization, and Thermal Property Measurements of ThO_2-UO_2 Fuel Materials. BMI-X-10210, Battelle Memorial Institute, Columbus, Ohio.

Staatz, M. H. 1978. Proceedings of the Uranium Industry Seminar, 1978. GJO-108(78), U.S. Department of Energy, Grand Junction, Colorado.

Stull, D. R., and G. C. Sinke. 1956. Thermodynamic Properties of the Elements, p. 143. American Chemical Society, Washington, D.C.

Swanson, H. E., and E. Tatge. 1953. National Bureau of Standards Circulation No. 539. U.S. National Burea of Standards, Washington D.C.

Tiegs, S. M. 1978. "Fabrication of UO_2 Fuel Pellets from Gel Microspheres." Paper presented at the American Ceramic Society Paciofic Coast Regional Meeting, October 1978, San Diego, California.

Touloukian, Y. S., R. K. Kirby, R. E. Taylor and T. Y. R. Lee. 1977. "Thermal Expansion--Non Metallic Materials." Thermophysical Properties of Matter Vol. 13. ed. Y., S. Touloukian, pp. 413-420, IFI/Plenum Press, New York, New York.

Turnbull, J. A. 1974. "The Effect of Grain Size on the Swelling and Gas Release Properties of UO_2 During Irradiation." J. Nucl. Mater. 50:62-68.

Valentich, J. 1969. "Thermal Expansion Measurement." Instr. Control Sys. 42:91-94.

Victor, A. C., and T. B. Douglas. 1961. "Thermodynamic Properties of Thorium Dioxide from 298 to 1200°K." J. Res. Nat. Bur. Stand. Sect. A. 65:106-111.

Voigt, W. 1910. "Lehrbuch der Krystallphysck." (Mit Ausschluss der Krystalloptik) Teubner, Leipzig.

Wachtman, J. B., Jr. and D. G. Lam, Jr. 1959. "Young's Modulus of Various Refractory Materials as a Function of Temperature." J. Am. Ceram. Soc. 42:254-260.

Wachtman, J. B., Jr., T. G. Scuderi and G. W. Cleek. 1962. "Linear Thermal Expansion of Al_2O_3 and ThO_2 from 100 to 1100°K." J. Am. Ceram. Soc. 45:319-323.

Wachtman, J. B.,Jr., W. E. Tefft, D. G. Lam, Jr. and C. S. Apstein. 1961. "Exponential Temperature Dependence of Young's Modulus for Several Oxides." Phys. Rev. 122:1754-1759.

Walker, D. E., et al. 1958. BORAX-IV Reactor: Manufacture of Fuel and Blanket Elements. ANL-5721, Argonne National Laboratory, Argonne, Illinois.

Ward, F. 1958. "The Consolidated Edison Thorium Reactor." Thorium-^{233}U Symposium. BNL-483. 23-25. Brookhaven National Laboratory, Upton, New York.

Warner, H. R. 1969. Release of Fission Gases from Oxide Fuels. WAPD-TM-805, Bettis Atomic Power Laboratory, West Mifflin, Pennsylvania.

Weinreich, W. A., W. H. Britton, C. R. Hutchison, R. G. R. Johnson and T. J. Burke. 1977. "Fabrication of High-Density, High-Integrity Thoria-Based Fuel Pellets." Trans. Am. Nucl. Soc. 27:305.

Wendlandt, W. W., T. D. George and G. R. Horton. 1961. "The Thermal Decomposition of Thorium (IV), Uranium (IV), and the Rare Earth Metal (III) Oxalate Hydrates. Differential Thermal Analysis and Weight-Loss Studies." J. Inorg. Nucl. Chem. 17:273-80.

Whittemore, O. J., Jr., and N. N. Ault. 1956. "Thermal Expansion of Various Ceramic Materials to 1500°C." J. Am. Ceram. Soc. 39:443-444.

Williams, G. H., M. K. Rodriquez and R. G. R. Johnson. 1968. Fabrication of Low Density Urania-Thoria Pellets. WAPD-TM-721, Bettis Atomic Power Laboratory, West Mifflin, Pennsylvania.

Wolfe, R. A. 1970. High Temperature Creep of Oxide Fuels. ORNL-4503, Oak Ridge National Laboratory, Oak Ridge, Tennessee.

Wolfe, R. A., and S. F. Kaufman. 1967. Mechanical Properties of Oxide Fuels. WAPD-TM-587, Bettis Atomic Power Laboratory, West Mifflin, Pennsylvania

Wolff E. G., and C. B. Alcock. 1962. "The Volatilization of High-Temperature Materials in Vacuo." Trans. Br. Ceram. Soc. 61:667-687.

Wymer, R. G., and D. A. Douglas (compilers). 1965. Status and Progress Report for Thorium Fuel Cycle Development for Period Ending December 31, 1963. ORNL-3611, Oak Ridge National Laboratory, Oak Ridge, Tennessee.

Wymer, R. G., and D. A. Douglas (compilers). 1966a. Status and Progress Report for Thorium Fuel Cycle Development For Period Ending December 31, 1964. ORNL-3831, Oak Ridge National Laboratory, Oak Ridge, Tennessee.

Wymer, R. G., and D. A. Douglas, Jr. 1966b. Status and Progress Report for Thorium Fuel Cycle Development for Period Ending December 31, 1965. ORNL-4001. Oak Ridge National Laboratory, Oak Ridge, Tennessee.

Wymer, R. G., and A. L. Lotts. 1969a. Status and Progress Report for Thorium Fuel Cycle Development for Period Ending December 31, 1966. ORNL-4275, Oak Ridge National Laboratory, Oak Ridge, Tennessee.

Wymer, R. G., and A. L. Lotts. 1969b. Status and Progress Report for Thorium Fuel Cycle Development for 1967 and 1968. ORNL-4429, Oak Ridge National Laboratory, Oak Ridge, Tennessee.

Young, J. K. et al. 1980. Economics of Large-Scale Thorium Production: Assessment of Domestic Resources. PNL-3150, Pacific Northwest Laboratory, Richland, Washington.

Yust, C. S., and L. E. Poteat. 1965. Metals and Ceramics Division Annual Progress Report, June 30, 1965. ORNL-3870, Oak Ridge National Laboratory, Oak Ridge, Tennessee.

PNL-3064
UC-78

DISTRIBUTION

No. of Copies

OFFSITE

A. A. Churm
DOE Chicago Patent Division
9800 South Cass Avenue
Argonne, IL 60439

S. W. Ahrends
U.S. Department of Energy
Oak Ridge Operations Office
P.O. Box E
Oak Ridge, TN 37830

D. E. Bailey
U.S. Department of Energy
HQ/RRT
Washington, DC 20545

2 W. W. Ballard
U.S. Department of Energy
HQ/FCD
Washington, DC 20545

2 P. R. Clark, R. H. Steele
U.S. Department of Energy
HQ/DNR
Washington, DC 20545

T. Hindman
U.S. Department of Energy
Savannah River Operations Office
P.O. Box A
Aiken, SC 29801

S. McDowell
U.S. Department of Energy
HQ/OSS
Washington, DC 20545

A. Mravca
U.S. Department of Energy
Chicago Operations Office
9800 South Cass Avenue
Chicago, IL 60439

No. of Copies

27 Technical Information Center

M. J. Steindler
Argonne National Laboratory
9700 South Cass AVenue
Argonne, IL 60439

C. Youell
Babcock & Wilcox
Lynchburg, VA 24505

W. A. Weinreich
Bettis Atomic Power Laboratory
Westinghouse Electric Corp.
P.O. Box 79
West Mifflin, PA 15122

E. Zebroski
Electric Power Research Inst.
3412 Hillview Avenue
P.O. Box 10412
Palo Alto, CA 94304

E. W. Neben
Fluor Engineers & Contractors, Inc.
3333 Michelson Drive
Irvin, CA 92730

K. L. Kighfill
Gas Cooled Reactor Associates
3344 N. Torrey Pines Ct.
Suite 300
La Jolla, CA 92037

W. V. Goeddel
General Atomic Company
P.O. Box 81608
San Diego, CA 92138

P. Miller
General Electric Company
175 Curtner Avenue
San Jose, CA 95125

No. of
Copies

D. J. Groetch
Knolls Atomic Power Laboratory
P.O. Box 1072
Schenectady, NY 12301

G. R. Keepin
Los Alamos Scientific Laboratory
P.O. Box 1663
Los Alamos, NM 37545

A. L. Lotts
Oak Ridge National Laboratory
P.O. Box X
Oak Ridge, TN 37830

J. D. Spencer
Savannah River laboratory
E. I. du Pont de Nemours & Co.
Aiken, SC 29801

A. Camp
Sandia Laboratory
Albuquerque, NM 87185

C. Palmer
Westinghouse NFD
Westinghouse Electric Company
P.O. Box 355
Pittsburgh, PA 15230

ONSITE

DOE Richland Operations

P. A. Craig
H. E. Ransom

Exxon Nuclear Company

O. Kruger

No. of
Copies

Hanford Engineering Development Laboratory

T. T. Claudson
E. A. Evans

FFTF Project Office

J. J. Keating

100 Pacific Northwest Laboratory

J. O. Barner
D. W. Brite
J. R. Carrell
T. D. Chikalla (2)
N. C. Davis
R. M. Fleischman
S. Goldsmith
C. W. Griffin
C. M. Hagen
C. R. Hann
P. E. Hart (20)
K. A. Hsieh
R. K. Johnson (50)
R. S. Kemper
L. R. Lambert
R. C. Liikala
R. P. Marshall
R. B. Matthews
T. I. McSweeney
J. R. Nesbitt
D. R. Newman
R. E. Schreiber
R. E. Sharp
G. D. White
Technical Information (5)
Publishing Coordinaton YO (2)